



RETURNING MATERIALS:

Place in book drop to
remove this checkout from
your record. FINES will
be charged if book is
returned after the date
stamped below.

--	--	--

ON THE TRANSPORT PROPERTIES AND
DYNAMICS OF DISORDERED SYSTEMS

By

Weizhu Xia

A DISSERTATION

Submitted to
Michigan State University
in partial fulfillment of the requirements
for the degree of

DOCTOR OF PHILOSOPHY

Department of Physics and Astronomy

1988

ABSTRACT

ON THE TRANSPORT PROPERTIES AND DYNAMICS OF DISORDERED SYSTEMS

By

Weizhu Xia

This thesis presents recent studies of the disordered systems in condensed matter physics. It addresses the problems of effective steady-state transport properties, such as electric conductivity and elastic moduli, and dynamic responses of strongly disordered systems. In Part I, the continuum percolation of a system containing random ellipses is studied. The percolation thresholds are obtained, for various elliptical aspect ratios, from computer simulations. The macroscopic effective steady-state conductivity for this system is studied by incorporating the properties of effective conductivity at low and critical concentrations of inclusions. A set of semi-phenomenological interpolation formulas is derived and agrees very well with the experimental data

over the whole range of concentrations. In Part II, the elastic percolation problem of a stretched spring model on the dilute honeycomb lattice is studied. While we find the similar second order rigid \rightarrow floppy phase transition studied before on the triangular lattice, an additional first order rigid \rightarrow floppy phase transition is found above a tricritical point. The bulk modulus, as well as some other elastic constants, behave differently when the two different phase transitions occur. A Landau type phase transition theory is applied to draw an analogy between the two types of phase transitions. A self-consistent effective medium theory is also developed for the phase boundary and the tricritical point observed in the computer simulations. In Part III, the density of states (DOS) of vibrational excitation spectra of percolation networks at thresholds are obtained by computer simulations using the equation of motion method. A careful study of the low frequency part of the density of states shows that the spectral dimensionalities, extracted from DOS, agree well with the predictions of the scaling hypothesis which takes into account the critical scaling behaviour of both mass and elastic moduli. This direct method of obtaining spectral dimensionalities is superior to the random walk method in the superconducting-normal network.

Part I and Part III are the expanded versions of the following published papers:

I. W. Xia and M. F. Thorpe, "Continuum Percolation of Ellipses", Phys. Rev. A. (1988) (in press)

III. R. A. Day, W. Xia and M. F. Thorpe, "Spectral Dimensionality of Random Superconducting-normal network", Phys. Rev. B, 37, 1339, (1988). This is contained in the appendix.

ACKNOWLEDGEMENTS

First of all I would like to thank my thesis advisor Professor M. F. Thorpe for his careful and patient guidance over the last four years. His knowledge of solid state physics and his approach to research have been a real inspiration to me. I would also like to express my appreciation to Professor S. D. Mahanti for valuable lectures in statistical mechanics, solid state physics and many helpful conversations, to Professor W. Repko for interesting lectures in quantum field theory and high energy physics, to all of the three above and Professor J. Cowen for serving on my guidance committee. I gratefully acknowledge Dr. A. R. Day for his enlightening collaboration on the work described in Part II and III and for stimulating discussions. I also benefit a great deal from useful conversations with Dr. S. de Leeuw and Dr. P. Sen.

Dr. E. Garboczi, Dr. H. He, Dr. W. Tang, Mr. Y. Li, J. Gales, W. Jin and H. Yan have been good friends and a source of much help and relaxed discussions throughout my graduate career. I would like to thank Dr. J. S. Kovacs and Mrs. J. King for additional assistance.

I would also like to express my gratitude to my dear wife Lihua for all her patience, encouragement and assistance over last three years.

Financial support from the Office of Naval Research, the Michigan State University Center for Fundamental Materials Research and the National Science Foundation is gratefully acknowledged.

TABLE OF CONTENTS

List of Tables	viii
List of Figures	ix
General Introduction	1
Part I. Continuum Percolation and Macroscopic Conductivity of Random Composite Systems	14
I. Introduction	15
II. Continuum Percolation	17
III. Computer Simulations and Results	29
IV. Critique of Effective Medium Theories	36
V. Interpolation Formulae	40
VI. Summary of Results	50
VII. References	51
Part II. Elastic Percolation of Stretched Spring Model on Honeycomb Lattice	54
I. Introduction	55
II. Elasticity of Pure Honeycomb Lattice and Percolation Thresholds	60
III. Computer Simulations and Effective Medium Theory Approach	81
IV. Tricritical Point and Effective Medium Theory	101
V. Conclusions	120

VI. References	121
Part III. The Vibrational Spectra of Random Superconducting-	
Normal network	123
I. Introduction	124
II. Density of States	129
III. Scaling Arguments	144
IV. One Dimensional Case	152
V. Conclusions	158
VI. References	159
Appendix I. Elasticity of Pure Honeycomb Lattice	162
Appendix II. Percolation Thresholds of Stretched	
Spring Model on Honeycomb Lattice	168
Appendix III. Published Paper	174

LIST OF FIGURES

Fig. 1.1	An example of randomly oriented ellipses with aspect ratio $b/a = 0.5$.	19
Fig. 1.2	(a) A prolate with $a > b$ and $b = c$; (b) A oblate with $a > b$ and $a = c$.	26
Fig. 1.3	Percolation thresholds p_c for various b/a .	32
Fig. 1.4	$f_2 = 1 - \exp(-\pi a b n_c)$ and $f_1 = \pi a b n_c$ vs. b/a .	35
Fig. 1.5	p_c 's from EMT and computer simulations.	39
Fig. 1.6	Conductance from the interpolation formula.	44
Fig. 1.7	A comparison between interpolation formulae and Experiments.	49
Fig. 2.1	Bulk moduli vs. p for central force model.	57
Fig. 2.2	Honeycomb lattice.	65
Fig. 2.3	Extrapolated intercepts.	70
Fig. 2.4	Extrapolated intercepts $P(E)$, $p(T)$ and $p(B)$ vs. L_0/L for honeycomb lattice and triangular lattice.	75
Fig. 2.5	Equilibrium positions and the corresponding elastic potential.	78
Fig. 2.6	Simulation results of elastic potentials.	79
Fig. 2.7	K_{eff} and K_{eff}^b vs. L_0/L .	80
Fig. 2.8	E_0 , T and B are plotted vs. p for various L_0/L .	82
Fig. 2.9	Equivalence relations are checked.	84
Fig. 2.10	Quantities with sudden discontinuity at percolation threshold.	86

LIST OF TABLES

Table 1.1	Values of p_c , n_c , k , and $\langle A_{ex} \rangle$ for randomly oriented ellipses for various aspect ratios b/a .	33
Table 1.2	Values of p_c , n_c , k , and $\langle A_{ex} \rangle$ for ellipses with two allowed orientations.	34
Table 3.1	Comparing the spectral dimensionality \tilde{d} obtained directly in this work with the scaling relation.	150

Fig. 2.11	Phase diagram.	87
Fig. 2.12	Configuration with zero B for $L_0/L = 1$.	89
Fig. 2.13	$L_{\text{eff}}^0/L_{\text{eff}}$ from simulations.	94
Fig. 2.14	Various elastic constants from simulations.	96
Fig. 2.15	C_{44}/C_{11} are plotted vs. p for various L_0/L .	99
Fig. 2.16	Critical values of C_{44}/C_{11} vs. L_0/L .	100
Fig. 2.17	Phase diagram and the tricritical point.	106
Fig. 2.18	Phase boundary and the tricritical point.	117
Fig. 2.19	η^a plotted against p .	118
Fig. 2.20	E , T and B plotted against p .	119
Fig. 3.1	Diagrams of monomer, dimers, trimers.	133
Fig. 3.2	A bond percolation network on square lattice.	136
Fig. 3.3	The DOS for a random square lattice of superconducting and normal bonds at $p_c = \frac{1}{2}$.	137
Fig. 3.4	The DOS for a simple cubic lattice at $p_c = .249$.	138
Fig. 3.5	Diagrams of 'pockets' in 2D.	141
Fig. 3.6	Diagrams of 'pockets' in 3D.	143
Fig. 3.7	$r(E/E_{co})$ vs. E/E_{co} for $p = 0.475, 0.480,$ $0.485, 0.490$ and 0.495 .	151
Fig. 3.8	The DOS for a random linear chain.	156
Fig. 3.9	The linear chain results for $p = 0.999$ and the two limiting forms.	157

GENERAL INTRODUCTION

The study of macroscopic transport properties of inhomogeneous systems has been a subject of great interest for more than a century. A good historical review on the subject is given by Landauer¹. When studying the macroscopic properties, solids are classified, at a relatively coarse level, into two categories: homogeneous materials and inhomogeneous ones. Inhomogeneous materials (particularly composite materials) can be treated as a mixture of different constituent grains. The constituents at some typical scale, for example less than grain size, can be treated as homogeneous. Mineral rocks, sandstones, concrete, cast-iron and conductor-insulator alloys are just a few examples. These composite materials are characterized by the so called effective transport properties such as electrical and thermal conductivities, which reflect the average behavior of the bulk materials. As the applications of composite materials become more and more specialized, accurate predictions of the overall bulk transport properties are required in order to make effective use of these materials.

While the macroscopic transport properties such as the electrical and thermal conductivity of homogeneous materials are well understood and can be found in many handbooks, their counterparts in the inhomogeneous case are not. As a matter of fact, these transport

properties are very difficult to calculate except for some special cases where the microscopic geometric structures of composite systems are simple. Maxwell, Clausius, Mossotti, Lorenz and Lorentz are the names associated with early attempts to solve this problem.¹ Modern theories started when Bruggeman published an extensive treatment of dielectric properties of two phase materials in 1935.¹ Since then, there have been many theoretical approaches to the problems¹⁻⁴. Among the various approaches, Effective Medium Theory (EMT)^{1,5,9} and absolute bounds^{6,7,8} (i.e. upper and lower bounds) are two major ones. The absolute bounds are derived from the variational methods and are useful when a real calculation is impossible. There are many versions of EMT which can be regarded as perturbation expansions where calculations can only be made for relative simple weak inhomogeneous systems (also called weakly disordered systems). Simple refers to the shape of the geometric boundaries between the phases and weak means that the transport properties, (e.g. electric conductivities) of the different phases are similar. The effective conductivity is calculated by expanding the difference of conductivities (a small parameter) in a power series⁹. The results agree well with experiments in most cases. For strong inhomogeneous systems (also called strongly disordered systems) in which the ratios of conductivities of the phases are infinite (i.e. mixture of conductors-insulators or superconductors-conductors), however, the above perturbation theories fail because the expansion parameters are no longer small. Absolute bounds (i.e. upper and lower bounds) in this

case turn out to be very large and practically useless. Computer modeling of the transport properties has also been impossible, because even the largest available machines cannot store enough information to meaningfully discretize the composite systems for complicated geometric structures. Therefore a semi-phenomenological description for transport properties of strongly disordered continuum systems is needed in order to make overall predictions for systems with certain geometric distributions. To show the underlying physics and simplicity of our approach, we only consider two phase composite systems in this thesis.

The equations describing the transport properties of processes such as electric conductivity, thermal conductivity, dielectric displacement, magnetic induction and diffusion all have the same mathematical structure. Therefore one only needs to study one of these and then generalize the results to all cases. We choose electric conductivity for convenience. The bulk effective conductivity, denoted by Σ , is in general a function of both the conductivity and geometric distribution of the constituent phases. It can be written as

$$\langle \vec{J} \rangle = \langle \sigma \vec{E} \rangle = \Sigma_{\text{eff}} \langle \vec{E} \rangle \quad (1)$$

where $\langle \vec{J} \rangle$ and $\langle \vec{E} \rangle$ are macroscopic current and applied electric field which can be measured experimentally. $\langle \rangle$ denotes the average over samples with the same constituents and statistical geometric distributions. In a continuum conductor-insulator composite system, when the fraction of conductor is below a certain threshold, no current

is able to flow across the system. This threshold can be well described by a continuum percolation theory¹⁰. Unlike the lattice percolation problem^{11,12}, there is no underlying lattice in continuum percolation problem. In the case of the conductor-insulator disk continuum percolation problem, one can imagine that on an uniform background of conducting matrix (with finite conductivity σ_0) identical circular holes are punched out randomly (overlaps are allowed). As more and more holes are punched out, the system will not carry any current below a critical threshold (called percolation threshold) even if a voltage is applied. Although there is no underlying lattice in continuum percolation problem concepts such as percolation threshold, correlation length and cluster size etc. are still similar to those of lattice percolation¹³. The conductivity vanishes at percolation threshold according to an exponent depending on the dimensionality of the problem¹⁴. Of course the determination of the percolation threshold is more difficult in continuum percolation problems than in lattice percolation especially when the objects are irregular. As a matter of fact, the continuum percolation thresholds even for many regular objects were still unknown. Prior to this work the percolation thresholds are known only for circles and parallel ellipses in 2D¹⁵. In Part I, we consider the continuum percolation of identical random elliptical holes with various aspect ratios ranging from disk-like objects to needle-like ones. We obtain the percolation threshold from computer simulations. Then we develop a set of semi-phenomenological interpolation formulas for overall bulk behaviors for composite systems consisting of random identical elliptical holes.

The interpolation formulas are based on the percolation threshold and the single defect effective medium theory which is exact in the low concentration limit.

The transport properties such as electric conductivity, thermal conductivity, dielectric constant, magnetic permeability and diffusion coefficient are scalar quantities. Materials also possess elastic properties. Elastic constants, however, are fourth rank tensors and therefore elastic composite systems in general are more complicated and difficult to treat. Due to the nature of the problems we only consider solids with covalent chemical bondings. In studying elastic properties, chemical bonds can be thought of as springs with certain elastic energy potentials depending on the nature of the problems and the atoms serve as nodes linking up the springs. de Gennes and Stauffer were the first¹⁶ to study the sol → gel phase transition defined below using the site elastic percolation model on a lattice. In the process of the sol → gel phase transition some monomer molecules are initially dissolved in a liquid solution. As the chemical reactions continue, monomers form finite polymer molecules (sol molecules) through covalent chemical bondings. In the sol phase the sol molecules (finite molecules) are separated by liquid which does not resist any shear deformation, so that the system in sol phase has zero shear modulus. As the sol molecules become larger and larger, a micromolecule crossing the whole system (gel molecule) will eventually appear. Because the gel molecule can resist the shear deformation, the shear modulus for the system is no longer

zero. Of course the shear modulus will increase as more and more cross links in gel molecule are built up. The following process



is an example of above mentioned sol → gel process¹⁰. The molecules of H_4SiO_4 are monomers and will stick together to form sol molecules and eventually gel molecule through covalent chemical bondings. By using an idealized elastic percolation model, de Gennes and Stauffer were able to capture the major features of the above sol → gel phase transition¹⁶. For example, adding sites and connecting springs correspond to sticking together sol molecules; the percolation threshold corresponds to the sol→gel transition point; elastic shear moduli vanishes below percolation threshold and sol → gel transition point etc. Other elastic percolation models can also be used to study the elastic behavior of compositional chalcogenide glass such as $\text{Se}_{1-x-y}\text{As}_x\text{Ge}_y$ as a function of x and y ¹⁷.

While the model proposed by de Gennes (called isotropic force model) can be used to explain the sol → gel phase transition, it also serves as a primary model among various elastic percolation models. de Gennes pointed out that the elastic percolation problem of this model is identical to the conductivity percolation problem which had been studied in great detail^{11,12}. This is reflected by the fact¹⁶ that the two problems can be mapped into each other and therefore (a) the percolation thresholds of elastic and conductivity percolation problems are the

same; (b) the critical exponents describing the vanishing bulk moduli and conductivity near percolation thresholds are identical. Feng and Sen¹⁸ proposed the central force model and pointed out that the elastic percolation described by central force model is different from that of isotropic force model. In fact they belong to different class of the problems^{18,19}. For example, in two dimensions the percolation thresholds, according to Thorpe's constraint counting method²⁰, are $p_c = \frac{2}{z}$ for isotropic force model and $p_{cen} = \frac{4}{z}$ for central force model. Here z is the number of nearest neighbors of a site. In the above two models, the elastic energies are expressed in quadratic forms of small displacements. Tang and Thorpe recently²¹ introduced a rotationally invariant stretched spring model which leads to a more natural way of expressing the elastic energy for Hooke springs. It turns out that the isotropic force model and the central force model are the two extreme limits of the stretched spring model. Tang and Thorpe pointed out that, by continuously changing a parameter, the stretched spring model can serve as a bridging model between the isotropic force model and central force model. In general there is a lot of stress associated with stretched or compressed springs in this model. Most computer simulations have been done on triangular lattice in the stretched region where initially every spring is stretched. In second part of this thesis we study the elastic percolation of stretched spring model on honeycomb lattice. The motivation of this study is as follows.

Both the constraint counting method¹⁷ and effective medium theory²⁰ predict that the percolation threshold for the central force model on

honeycomb lattice is $p_{\text{cen}} = \frac{4}{3}$. This result is unphysical because p must always equal or less than one. This tells us that the central force model on a honeycomb lattice is not stable. One may find that the shear modulus is zero for the honeycomb lattice with the central forces. There is no such instability on the triangular lattice. Therefore, by studying the honeycomb lattice with the stretched spring model, we expect to see some new phenomena associated with the instability not observed on the triangular lattice. Indeed we have found that the usual second order rigid \rightarrow floppy phase transition becomes a first order phase transition above a tricritical point. We also want to determine the percolation threshold for the stretched spring model in the central force limit.

The properties we have just discussed above are the static properties of the disordered systems. It is also very interesting to study the dynamic properties of the disordered systems particularly in the low frequency (or energy) limits. The quantity that concerns us here is the density of states of vibrational excitations which gives the number of excitational modes per unit frequency interval. In a homogeneous system, in the very long wavelength or low frequency limit, the density of states denoted by $g(E)$ has the Debye form²²

$$g(\omega) d\omega \sim \omega^{d-1} d\omega \quad (2)$$

where ω is the frequency of the excitation modes and d is the dimensionality of the problem. The simplest way to obtain the density of states $g(\omega)$ is to calculate the excitational dispersion relation (phonon dispersion relation) on a perfect crystal lattice and consequently obtain $g(\omega)$. In the long wavelength limit, i.e., the wavelength of excitation is much larger than the lattice spacing, the lattice is regarded as a homogeneous continuum and (2) is obtained²². One can ask the question of how the density of states changes when disorder is introduced. A good review article concerning the general aspects of this question is given by Elliott et al.²³ Here we only discuss the low frequency limit. From one's physical intuition, it can be expected that when the wavelength of excitation is comparable to the length scale on which the system is disordered the density of states should have different form than (2) because the system is no longer homogeneous. On the other hand, however, (2) should still be observed in the very long wavelength limit because then even disordered systems are homogeneous. Alexander et al.²⁴ pointed out that in dilute disordered system (or inhomogeneous system) (i) the density of states should have the following form

$$g(\omega)d\omega \sim \omega^{\tilde{d}-1} d\omega \quad (3)$$

where \tilde{d} is called the spectral dimensionality which is different from d for the homogeneous case; (ii) the density of states has a cross-over

from the homogeneous region to the inhomogeneous region at frequency ω_{co} ; and (iii) \tilde{d} is an universal quantity for d greater than two. While it is still controversial whether the results should be applied to some real amorphous systems at low temperature²⁹, there have been considerable theoretical studies²⁵⁻²⁸ concerning the spectral dimensionality \tilde{d} .

The studies are done on fractal systems²⁵⁻²⁸. A random fractal network is inhomogeneous on a length scale less than a certain length and homogeneous at a scale larger than the length. Therefore it is an ideal system to observe the cross-over³⁰. Of course there are many random fractal networks¹⁷. The fractal network chosen in this thesis, as well as in many other studies, is a percolation network. The length scale on which the cross-over happens is now simply the percolation correlation length. Many other methods can also be used to obtain \tilde{d} . The transfer matrix method³¹ and the random walker method³² are the ones used most frequently. It should be pointed out that, when considering the density of states, the random walker (RW) method is an indirect one to obtain \tilde{d} . In dilute systems, the RW method gives results as good as any other method. But this method is not useful for the model³³ discussed in this thesis. In part III of this thesis, we study the low frequency vibrational density of states of a superconducting-normal networks. In this model the density of states, in the low frequency limit, has the same form as (3) but with a different spectral dimensionality \tilde{d} due to the different scaling relations. These scaling relations are supported by the computer simulations.

REFERENCES

1. R. Landauer in AIP Conference Proceedings No.40, Ed. by J. Garland and D. Tanner (1978).
2. G. Deutscher, A. Kapitulnik and M. Rappaport, Ann. Israel Phys. Soc. 5, 207 (1983).
3. L. K. H. van Beek in Progress in Dielectrics 7, Ed. by J. B. Birks (1967).
4. J. C. Garland and D. B. Tanner, Electrical Transport and Optical Properties of Inhomogeneous Media, AIP Conference Proceedings No 40 (1978).
5. R. Landauer, J. Appl. Phys. 23, 779 (1952).
6. Z. Hashin and S. Shtrikman, Phys. Rev. 130, 129 (1963).
7. G. W. Milton, Appl. Phys. Lett. 37, 300 (1980).
8. D. J. Bergman, Annals of Phys. 138, 78 (1982).
9. S. Torquato, J. Appl. Phys. 58(10), 3790 (1985).
10. R. Zallen, The Physics of Amorphous Solids, (John Wiley & Sons, New York, 1983).
11. S. Kirkpatrick in Ill-Condensed Matter-Les Houches 1978, Ed. by R. Balian, R. Maynard, and G. Toulouse,(North-Holland, Amsterdam, (1979).
12. D. Stauffer, Introduction to Percolation Theory, (Taylor and Francis, London, 1985).
13. I. Balberg, Phys. Rev. B 37, 2391 (1988).

14. B. I. Halperin, S. Feng, and P. N. Sen, Phys. Rev. Lett. 54, 2391,(1985).
15. I. Balberg, Phys. Rev. B 31, 4053 (1985).
16. P. G. de Gennes, J. Phys. (Paris) 37, L-1,(1976); D. J. Stauffer, J. Chem. Soc. Faraday Trans. II 72, 1354 (1976).
17. M. F. Thorpe, J. Non-Crys. Sol. 57, 355 (1983); H. He and M. F. Thorpe, Phys. Rev. Lett. 54, 2107 (1985).
18. S. Feng and P. N. Sen, Phys. Rev. Lett. 52, 216 (1984).
19. A. R. Day, R. R. Tremblay and A. -M. S. Tremblay, Phys. Rev. Lett. 56, 2501 (1986).
20. S. Feng, M. F. Thorpe and E. Garboczi, Phys. Rev. B 31, 276 (1985).
21. W. Tang and M. F. Thorpe, Phys. Rev. B 37, 5539 (1988); W. Tang, Ph. D. Thesis, Michigan State Univ (unpublished).
22. C. Kittel, Introduction to Solid State Physics (J. Wiley & Sons, Inc. New York, 4th Edition, 1971).
23. R. J. Elliott, J. A. Krumhansl and P. L. Leath, Rev. Mod. Phys. 46, 465 (1974).
24. S. Alexander and R. Orbach, J. de Physique Letters 43, L625, (1982).
25. R. Rammal and G. Toulouse, J. de Physique Lettres, 44, L13 (1983).
26. Y. Gefen, A. Aharony and S. Alexander, Phys. Rev. Lett. 50, 77 (1983).

27. S. Alexander, C. Laermans, R. Orbach and H.M. Rosenberg, Phys. Rev. B 28, 4615 (1983).
28. A. Aharony, S. Alexander, O. Entin-Wohlman and R. Orbach, Phys. Rev. B 31, 2565 (1985).
29. R. Orbach, Science, Vol. 231, 814 (1986).
30. B. B. Mandelbrot, The Fractal Geometry of Nature, (Freeman, New York, 1983); Ann. Israel Phys. Soc., 5, 59 (1983); J. Stat. Phys., 34, 895 (1984).
31. M. A. Lemieux, P. Breton, A.-M. S. Tremblay, J. Phys. (Paris) Lett 46 L1 (1985).
32. D. C. Hong, H. E. Stanley, A. Coniglio and A. Bunde, Phys. Rev B 33, 4564 (1986).
33. A. R. Day, W. Xia and M. F. Thorpe, Phys. Rev. B 37, 1339 (1988).

Part I

**Continuum Percolation and Effective Macroscopic
Conductivity of Random Composite Systems**

I Introduction

The universal behaviour of the critical exponents that describe transport quantities such as electrical conductivity, thermal conductivity, the diffusion constant and elastic moduli of a composite system near the percolation threshold can be understood by continuum percolation theory.¹ Experimental results agree well with the theoretical predictions of such quantities.² In designing composite materials it is more important to know the overall behaviour of the properties of these materials which are governed by non-universal quantities away from the critical region. The location of the critical point is also non-universal. When the concentration of one of the components (for simplicity, we will consider only two component composite systems) is extremely low, the behaviour of quantities like the electrical conductance can be adequately described by the Clausius-Mossotti equation.³ Inbetween these two extremes, an exact microscopic theory or detailed computer modeling of the transport properties would be very difficult and neither is currently available. Some progress has been made recently in studying two elliptical holes in a homogeneous medium.⁴ However, even here there are still unresolved problems associated with overlapping inclusions that have prevented a useful generalisation of the Clausius-Mosotti equations. Computer simulations have also not been possible because even the largest available machines cannot store enough information to meaningfully discretise such continuum systems. Thus a major reasearch tool, that has led to so much of our understanding of

the response of discrete lattice systems⁵, has not been available or exploited yet in continuum systems.

The purpose of this paper is to develop a semi-phenomenological description of the behaviour of the transport properties of these systems. Many effective medium theories (EMT) have been developed^{3,6-11} but are of dubious validity away from the dilute limit, where all these theories agree. In order to ascertain which of these theories are good for all concentrations, we have located the critical concentration of ellipses at percolation. These results are new except for the special case of circles and provide a most stringent test of effective medium theories. We find that there are no reasonable EMT for electrical conductance; all fail to predict the correct critical concentration for circles. On the other hand, we find one such existing theory to be clearly superior and adequate for elastic inclusions. This is the asymmetric reinforced model (also called SCA-A, reinforced problem in section II B of Thorpe and Sen⁷). This was originally derived for circular inclusions by Hill, Budiansky, Wu and Berryman⁸⁻¹⁰ using different self-consistent methods. In the circular limit symmetric and asymmetric theories are identical. Those results were generalised by Thorpe and Sen⁷ to ellipses for which symmetric and asymmetric theories are no longer identical. Note however that this theory applies to the case when the circular inclusions are infinitely hard so that the elastic compliance and not the elastic modulus vanishes at the critical concentration. We would expect that this effective medium theory should also be superior for mixtures where the elliptical inclusions are hard.

The SCA-A for holes does not give a good value for the critical concentration.

The interpolation formula we develop incorporates the behaviour at the two extremes (i.e. low concentrations and near the percolation threshold) for a system containing randomly distributed insulating elliptical laminae (i.e. holes) embedded in the uniform background of a conducting matrix.

The layout of this paper is as follows. In section II we discuss the geometric aspects of continuum percolation for a system containing random elliptical laminae in 2D and spheroids in 3D and in section III we present our computer simulations of the percolation thresholds in 2D and compare with the results of previous work. In section IV we use our results to critique effective medium theories by examining their predictions for the percolation concentrations. In section V an interpolation formula for the electrical conductance is developed and in section VI a comparison is made between the effective conductivity predicted from our interpolation formulae and that of experiments.

II Continuum Percolation

(1) Continuum Percolation of Elliptical Laminae in 2D.

In the continuum percolation problem, as well as in percolation on a lattice, an important quantity to describe the onset of percolation is the percolation threshold p_c .¹² There exist extensive studies¹³ in the literature of p_c for percolation on various lattices, where p_c is the

fraction of bonds or sites remaining, depending on the type of percolation being studied. In the continuum percolation problem, p_c is defined to be the fractional area occupied by one phase which, in our case is the area remaining after the elliptical holes are removed. Fig.1.1 shows an example of the system under study and the area covered by ellipses has fractional area $1 - p$ (at the percolation threshold $p = p_c$). Imagine that a constant voltage is applied across a conducting sheet and randomly oriented elliptical holes with random centers are punched out. As more and more material is removed, electric current flow through the sheet is restricted and vanishes at p_c . We are interested in how p_c changes as the geometry (i.e. aspect ratio) of one phase changes^{14,15} or more precisely how p_c changes as the inclusions change from circles to needles.

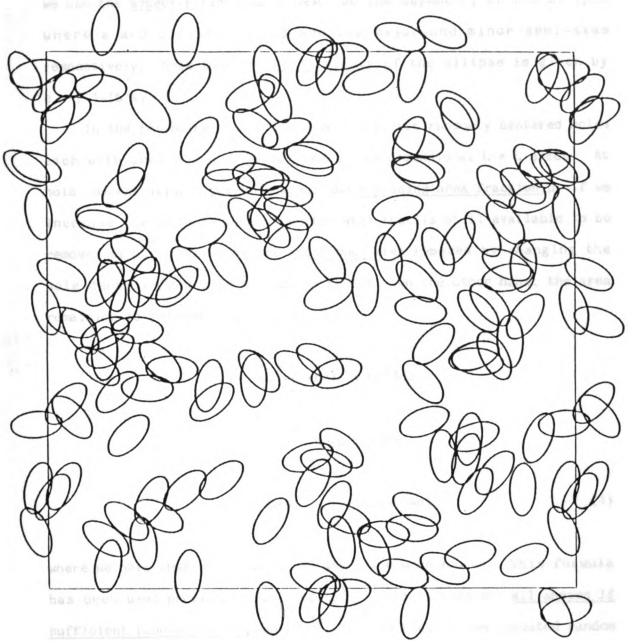


Fig. 1.1 An example of randomly oriented ellipses with aspect ratio $b/a = 0.5$. The periodic boundaries can clearly be seen. Actual samples used were much larger.

We use the aspect ratio b/a to describe the asymmetry of the ellipse where a and b (with $a > b$) are the major and minor semi-axes respectively. Note that the eccentricity of the ellipse is given by $e = [1 - (b/a)^2]^{1/2}$.

In the following discussion, identical, but randomly centered holes each with area A are removed from a two dimensional $L \times L$ sheet. At hole concentration n per unit area, and remaining area fraction p , if we increase the hole density, then the area that is still available to be removed is pL^2 . Therefore the additional area removed by changing the hole density from n to $n + dn$ is $pL^2 Adn$. On the other hand, the area remaining is reduced to $pL^2 - (p+dp)L^2$, so

$$pL^2 - (p+dp)L^2 = pL^2 Adn$$

$$\text{i.e.} \quad dp/p = -Adn$$

$$\text{so that} \quad p = \exp(-An) \quad (1)$$

where we note that $p = 1$, when $n=0$ and $p = 0$ when $n = \infty$. This formula has been used previously for circles^{16,17} but is true for all shapes if sufficient randomness is present.¹⁸ This is because the repeated random placement of an additional object or hole serves as a measure of the remaining area. We are of course always thinking of the thermodynamic limit when the system size is very large. Eq. (1) can be generalized to three dimensions where A is replaced by the volume of each individual

hole and n is the hole density per unit volume (this can be visualized as Swiss Cheese). In the two dimensional case we are studying, $A = \pi ab$ and at the percolation threshold $n = n_c$, therefore

$$p_c = \exp(-\pi ab n_c) \quad (2)$$

Eq. (2) allows an immediate determination of the percolation threshold p_c for a given a and b once n_c is known or vice versa. This equation is very convenient to use in practice as it only involves counting; no area evaluation is involved. For circles we find from our simulations that

$$p_c = \exp(-\pi a^2 n_c) = 0.33 \pm 0.02 \quad (3)$$

where a is circle radius and n_c is density of circles per unit area at percolation. We have given generous error bars on (3). Our result (3) agrees well with other results for circles.¹⁹ We also notice that a careful finite size scaling study gives better results,¹⁹ but this would need huge amounts of computer time if it was to be done for all aspect ratios. Our purpose here is to look at the general trend of how p_c changes with b/a . The percolation threshold for ellipses aligned in one direction but with random centers is the same as that for random circles. The reason is as follows. A conformal transformation can always be performed in one direction on the aligned elliptical system in order to obtain the random circular case. Obviously the change in the area A , due to the conformal transformation, exactly cancels the change

in the ellipse density per unit area. Therefore there is no change in $p = \exp(-An)$ and the percolation threshold is the same as that for the circular case. This is checked by computer simulations in this work.

In 2D, the background ceases to percolate when the inclusions percolate. This is because there is no way around the infinite cluster. Therefore, there is a single percolation concentration. In higher dimensions, this is obviously not the case and there are two separate percolation concentrations for the inclusions and the backgrounds.

In continuum percolation involving identical objects, it is useful to introduce the average excluded area denoted as $\langle a_{ex} \rangle$.^{20,21} For given relative orientations of two identical objects the excluded area is defined as the area that if the center of one is outside it, the two objects have no overlap at all. Average means over all allowed relative orientations. The excluded area at percolation is defined as

$$\langle A_{ex} \rangle = n_c \langle a_{ex} \rangle \quad (4)$$

Although the mean coordination number and the critical area or volume fraction are essentially invariant²² in bond and site lattice percolation respectively, $\langle A_{ex} \rangle$ is not quite such a quasi-universal invariant quantity and it has a small range.¹² Our results will be discussed in detail in the next section, but we see from Table 1 that for randomly oriented ellipses,

$$3.4 \leq \langle A_{ex} \rangle \leq 4.5 \quad (5a)$$

For ellipses that can only lie in two directions, we see from Table 2 that,

$$2.8 \leq \langle A_{ex} \rangle \leq 4.4 \quad (5b)$$

Taking account of the error bars noted in the table captions, both these sets of results for $\langle A_{ex} \rangle$ are probably monotonic in the aspect ratio.

The excluded area of two identical ellipses can be defined as

$$\langle a_{ex} \rangle = 4\pi abk \quad (6)$$

where k is a geometric factor that is chosen as above so that $k = 1$ for circles. For randomly centered and oriented ellipses,²³

$$k = 1/2 + s^2/8\pi^2 ab \quad (7)$$

where s is the perimeter of an ellipse (this involves an elliptical integral which can be evaluated numerically). For randomly centered ellipses that can only lie in the two principal directions the k factor is different from (7) and not available in a closed form for general b/a . For parallel ellipses $k = 1$ but must be computed (using for example the contact function described in the next section) for ellipses at right angles. These two results are then averaged. The values of k for both these cases have been calculated and are given in Tables 1 and 2 for various aspect ratios.

From Eqs. (2), (4) and (6), we notice that

$$p_c = \exp(-\langle A_{ex} \rangle / 4k) \quad (8)$$

which reduces to $p_c = \exp(-\langle A_{ex} \rangle / 4)$ for circles when $k = 1$.¹⁶⁻¹⁸ In the needle limit where b/a is small, and the ellipses are randomly oriented, using (7) we have $s = 4a$ and $k = 2a/(\pi^2 b)$ so that from Eq. (8)

$$\begin{aligned} p_c &= \exp[-3.4/(4k)] = \exp(-0.425\pi^2 b/a) \\ &\approx 1 - 4.2 b/a \end{aligned} \quad (9)$$

where we have used $\langle A_{ex} \rangle \approx 3.4$ from Table 1. We note that in this limit, the result (9) is independent of the precise shape of the needles. For example they can be elliptical or rectangular. As b/a becomes very small, only a few needles are needed to cross the sample and these have essentially no area so that $p_c \rightarrow 1$ as given by (1). A similar limit is obtained for needles that can only point horizontally or vertically for which $k = a/(2\pi b)$. Using Eq. (8), with $\langle A_{ex} \rangle \approx 2.8$ from Table 2, we find that

$$\begin{aligned} p_c &= \exp[-2.8/(4k)] = \exp(-1.4\pi b/a) \\ &\approx 1 - 4.4 b/a \end{aligned} \quad (10)$$

which we notice is close to the result for randomly oriented ellipses given in (9). Indeed because the values of $\langle A_{ex} \rangle$ are only known numerically; the error bars are sufficiently large that Eqs. (9) and (10) could be identical.

(2) Continuum Percolation of Spheriods in 3D

Various concepts, just described above, for two dimensional percolation can be easily generalized to three dimensional case. As we mentioned earlier, in 2D the background ceases to percolate when the inclusions percolate. This is because there is no way around the infinite cluster and therefore there is a single percolation concentration. In higher dimensions (e.g. three dimensions), this is obviously not the case and there are two separate percolation concentrations for the inclusions and the background. For percolation involving identical insulating spheres the percolation thresholds are $p_c = .31$ for inclusions¹² to percolate and $p_c = .968$ for background cease to percolate²⁷. Here, of course, p_c refers to volume fraction. It is also known that the excluded volume $\langle V_{ex} \rangle$ in 3D is bounded by¹²

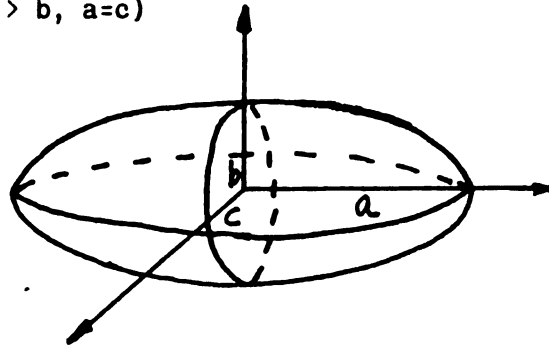
$$0.7 \leq \langle V_{ex} \rangle \leq 2.8 \quad (5c)$$

where 2.8 refers to spherical inclusions and 0.7 to very long thin rods.

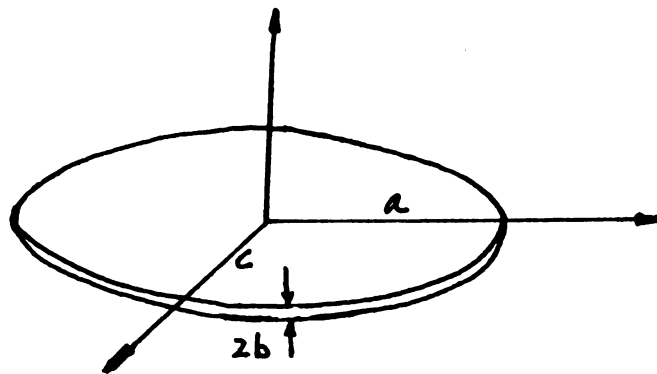
Now we consider the following two cases of inclusion percolation for spheroids of revolution. [see Fig. 1.2]

Prolate ($a > b, b=c$)

Oblate ($a > b, a=c$)



(a)



(b)

Fig. 1.2 (a) A prolate with $a > b$ and $b=c$; (b) A oblate with $a > b$ and $a=c$.

We can also make predictions on the dependence of the percolation threshold on b/a for small b/a by using the fact that $\langle V_{ex} \rangle = n_c \langle v_{ex} \rangle$ approaches a constant as $b/a \rightarrow 0$ shown in Eq. (5c).

In the prolate case, we assume $\langle V_{ex} \rangle \rightarrow V_1'$ (constant) as $b/a \rightarrow 0$. By the same definition of Eq. (6)

$$\langle v_{ex} \rangle = \frac{32}{3} \pi a b^2 k \quad (8a)$$

and

$$\langle v_{ex} \rangle \sim (2a)^3. \quad (8b)$$

In Eq. (8b) the fact that $\langle v_{ex} \rangle$ is proportional to $(2a)^3$ is the result of averaging over various positions of two very long prolates and it can be easily seen that the major contribution is from a sphere with radius $2a$. So $k \sim (a/b)^2$. Using Eq. (8) we have

$$p_c = \exp(-V_1'/4k) \quad (8c)$$

$$\sim \exp(-V_1'(b/a)^2)$$

$$\sim 1.0 - V_1'(b/a)^2 \quad (9a)$$

An appropriate constant is absorbed into V_1 in Eq. (9a).

In the oblate case, we can also assume that $\langle V_{ex} \rangle \rightarrow V_2'$ (constant) as $b/a \rightarrow 0$. In this case, however, $\langle v_{ex} \rangle = \frac{32}{3} \pi a^2 b k$, and $\langle v_{ex} \rangle \sim (2a)^3$. So $k \sim (a/b)$. Using Eq. (8) we have

$$p_c = \exp(-V_2'/4k) \quad (8d)$$

$$= \exp(-V_2 a/b)$$

$$\sim 1.0 - V_2 (b/a) \quad (9b)$$

Again we notice that an appropriate constant is absorbed into V_2 in Eq. (9b).

From Eq. (9a) and (9b) we can see that the dependence of p_c on b/a are different for prolate case and oblate case in the small b/a limit. In the above arguments, constants V_1 and V_2 may be determined mathematically or by computer simulations. We perform computer simulations to check various predictions in this section for the two dimensional case. The 3D case can also be checked after modifying the 2D programs.

III Computer simulations and results

In our 2D computer simulations, the whole system has periodic boundary conditions in both the x and y directions. For each fixed aspect ratio b/a about 2000 elliptical laminae are randomly distributed. The relative orientations are also random. An example of the system under study is shown in Fig. 1.1. As b/a becomes smaller fewer ellipses, for a given system size, are needed at percolation. To insure consistent statistics, we expanded the system size, while maintaining about the same number (2000) of ellipses. We determined n_c by keeping a record of whether there are clusters formed by overlapping elliptical laminae which cross the lower and upper boundaries at the same place (because of the periodic boundary condition).

In the course of recording clusters we used a very efficient algorithm involving a contact function²⁴ to determine whether two ellipses with given centers and relative orientation overlap or not. For two identical ellipses one centered at the origin and one centered at (x_0, y_0) with relative orientation θ , the contact function ψ is defined by

$$\psi = 4(g_1^2 - 3g_2)(g_2^2 - 3g_1) - (9 - g_1g_2)^2 \quad (11)$$

where

$$g_1 = 3 + (a/b - b/a)^2 \sin^2 \theta - (x_0/a)^2 - (y_0/b)^2 \quad (12)$$

$$g_2 = 3 + (a/b - b/a)^2 \sin^2 \theta - (x_0 \cos \theta + y_0 \sin \theta)^2 / a^2$$

$$-(y_0 \cos\theta - x_0 \sin\theta)^2 / b^2 \quad (13)$$

If ψ is negative, the two ellipses overlap. If ψ is positive, and both g_1 and g_2 are positive, the two ellipses also overlap; otherwise the two ellipses do not overlap. If $\psi = 0$ the two ellipses just touch. A similar contact function for 3D case can also be found in ref 24. We only test those ellipses whose centers lie within $2a$ of each other. We find the average number of ellipses required for the system to percolate in both the x and y directions if (as invariably happens) one direction percolates before the other. Then we average over 25 to 30 samples for a fixed aspect ratio b/a and use Eq.(2) to evaluate p_c . The errors are due to the statistical averaging over the p_c which have a roughly Gaussian distribution. We repeat the same procedure for different aspect ratios b/a that range from $1/400$ up to 1.0 .

In Fig. 1.3 the percolation threshold p_c is plotted against the aspect ratio b/a . The results for both randomly oriented ellipses and ellipses that are aligned along two perpendicular directions are shown. It can be seen that the two sets of results are indistinguishable within our limits of accuracy.

We have also evaluated $\langle A_{ex} \rangle$ using n_c found from the computer simulation and Eqs. (4) and (6) for both randomly oriented and two direction oriented ellipses. The error bar in our computer simulation in determining n_c is about $\pm 5\%$; therefore the error bar in $\langle A_{ex} \rangle$ is about ± 0.2 . Tables 1 and 2 list p_c , n_c , k , and $\langle A_{ex} \rangle$ for various

aspect ratios b/a for the two cases and they show that in both cases $\langle A_{ex} \rangle$ decreases very slowly as b/a decreases.

In the following discussion, we only consider quantities for the randomly oriented case. The case of only two orientations would give essentially indistinguishable results. Note that although n_c and hence p_c are virtually indistinguishable for a fixed aspect ratio b/a in the two cases, the quantities k and $\langle A_{ex} \rangle$ are different as can be seen by comparing tables 1 and 2.

In Fig. 1.4 we plot $f_1 = \pi ab n_c$ and $f_2 = 1 - f = 1 - \exp(-\pi ab n_c)$. The quantity f_1 is the total area in the ellipses for a sample of unit area, not allowing for the overlap effects, whereas f_2 is less than f_1 because overlap effects are included.

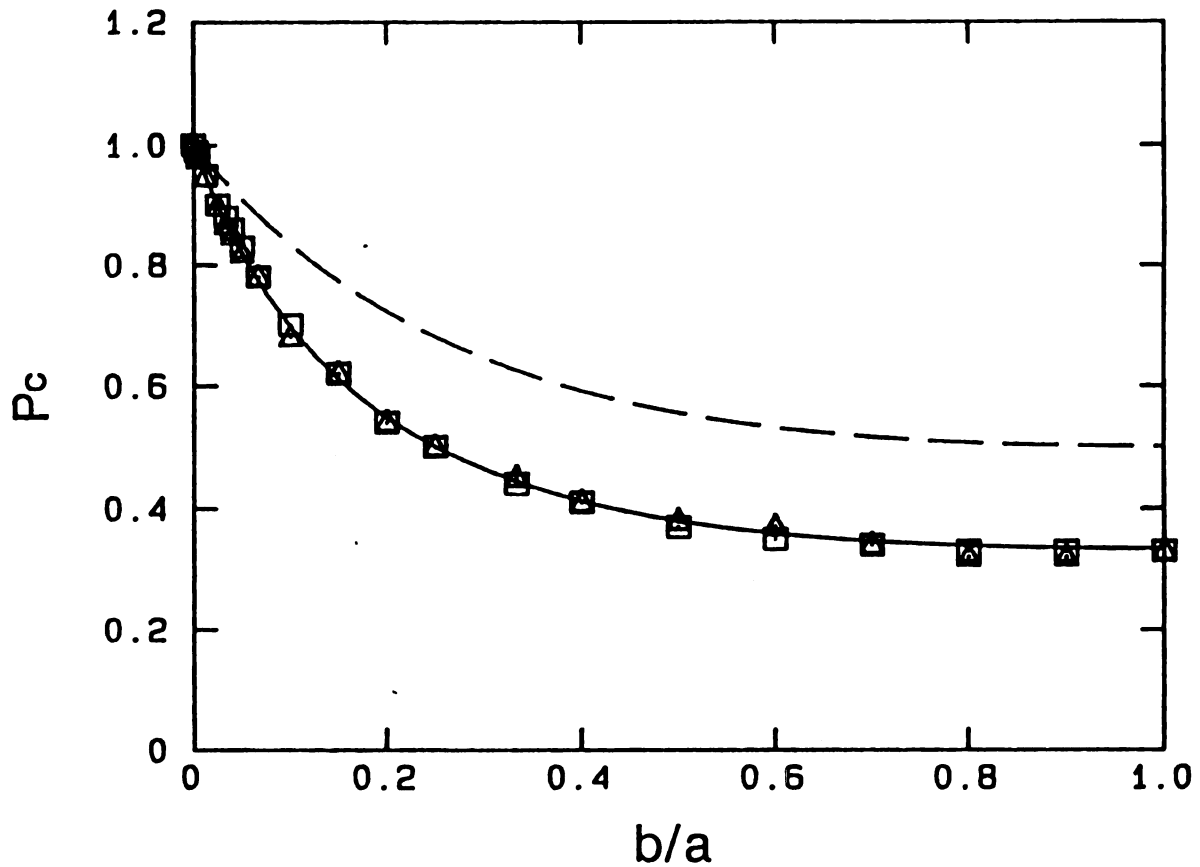


Fig. 1.3 Percolation threshold p_c for various aspect ratios b/a . Squares are for randomly oriented ellipses while triangles are for vertically and horizontally oriented ellipses. Every point is averaged over 25 - 30 samples each containing ~ 2000 ellipses. The solid curve is the interpolation formula (28) for p_c . The dashed curve is p_1 , which gives the initial slope, from Eq. (22).

Table 1.1

b/a	p_c	n_c	k	$\langle A_{ex} \rangle$
1.0000	0.33	2.8	1.000	4.4
0.9000	0.33	2.8	1.002	4.4
0.8000	0.33	2.8	1.009	4.4
0.7000	0.34	2.8	1.024	4.5
0.6000	0.35	2.7	1.050	4.5
0.5000	0.37	2.5	1.094	4.3
0.4000	0.41	2.3	1.171	4.2
0.3333	0.44	2.10	1.254	4.1
0.2500	0.50	1.76	1.432	4.0
0.2000	0.54	1.57	1.618	4.0
0.1500	0.62	1.22	1.937	4.0
0.1000	0.70	0.90	2.592	3.7
0.0667	0.78	0.62	3.589	3.7
0.0500	0.83	0.49	4.592	3.5
0.0400	0.86	0.40	5.599	3.5
0.0333	0.88	0.34	6.609	3.5
0.0250	0.91	0.26	8.629	3.5
0.0125	0.949	0.133	16.74	3.5
0.0050	0.979	0.054	41.06	3.5
0.0025	0.990	0.027	81.12	3.4

Table 1.1 Values of p_c , n_c , k, and $\langle A_{ex} \rangle$ are listed for randomly oriented ellipses for various aspect ratios b/a. The value of k is obtained by evaluating the perimeter s of the ellipse from an elliptic integral and using the formula in the text. The value of n_c is obtained from the simulation with the area of the ellipses fixed at $\pi/8$ and then $\langle A_{ex} \rangle$ is obtained from formulas (4) and (6). The error bar in $\langle A_{ex} \rangle$ is ± 0.2 .

Table 1.2

b/a	p_c	n_c	k	$\langle A_{ex} \rangle$
1.0000	0.33	2.8	1.000	4.4
0.9000	0.33	2.8	1.002	4.4
0.8000	0.33	2.8	1.009	4.4
0.7000	0.34	2.7	1.024	4.3
0.6000	0.36	2.6	1.049	4.3
0.5000	0.37	2.5	1.091	4.3
0.4000	0.41	2.3	1.162	4.2
0.3333	0.45	2.06	1.237	4.0
0.2500	0.50	1.80	1.391	3.9
0.2000	0.54	1.59	1.548	3.9
0.1500	0.62	1.24	1.812	3.5
0.1000	0.68	0.97	2.342	3.6
0.0667	0.78	0.65	3.137	3.2
0.0500	0.82	0.51	3.933	3.2
0.0400	0.85	0.42	4.729	3.1
0.0333	0.87	0.37	5.525	3.2
0.0250	0.90	0.28	7.117	3.1
0.0125	0.947	0.145	13.48	3.1
0.0050	0.976	0.061	32.58	3.1
0.0025	0.989	0.028	64.41	2.8

Table 1.2 Values of p_c , n_c , k, and $\langle A_{ex} \rangle$ are listed for ellipses with two allowed orientations. The values of k is obtain by evaluating the excluded area $\langle a_{ex} \rangle$ numerically and then using Eq. (6). The values of n_c are from simulation with the area of the ellipses fixed at $\pi/8$ and $\langle A_{ex} \rangle$ are obtained by using Eq. (4). The error bar in $\langle A_{ex} \rangle$ is ± 0.2 .

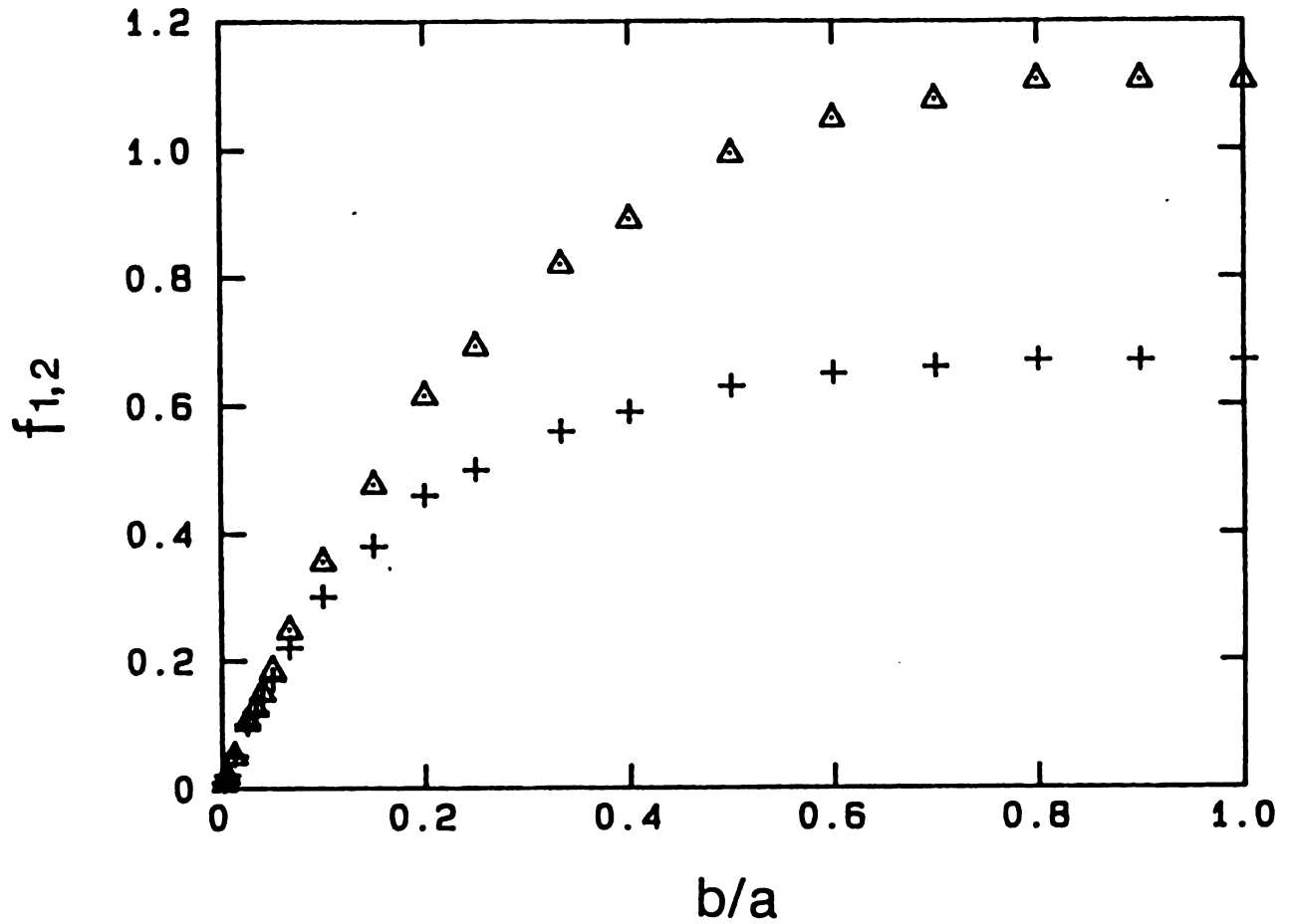


Fig. 1.4 The quantities $f_2 = 1 - \exp(-\pi abn_c)$ and $f_1 = \pi abn_c$ are plotted against the aspect ratio b/a for the case of randomly oriented ellipses. Crosses are for f_2 and triangles are for f_1 .

It can be seen that for small b/a these two quantities are the same as the overlap area for needles is negligibly small. In the circle limit $f_1 = 1.09 \pm 0.02$; that is the area in the circles at percolation, before they are thrown down, is greater than unity. Note that if f_2 is expanded in powers of the density n_c , the first term is f_1 and the corrections for r body overlap are given by the coefficient of the n_c^r term.

IV Critique of Effective Medium Theories

There are extensive discussions in the literature on EMT for dielectric constants³ and elastic moduli¹¹ of composite materials with circular or spherical inclusions. A strong assumption is always required, in deriving these approximations, that the inclusion concentration is sufficiently low that the overlap of inclusions can be neglected. However these approximations are often used over the whole concentration range where they are of dubious validity. In order to judge how good various EMT results are when applied to completely permeable objects, we see how close their predictions of p_c are compared to our exact (numerical) results. Physical properties, like the conductivity and all elastic moduli, should vanish at p_c when holes are punched in the medium. Similarly the resistance and all the elastic compliances should vanish when infinitely hard inclusions are present in the medium. Infinitely hard means superconducting in the electrical case and infinitely rigid or undeformable in the elastic case. All these p_c should be the same as it is a geometrical property of the

material. However different EMT give very different estimates for p_c . These various EMT predictions for p_c can be used as a figure of merit, when compared to our exact results, to judge how good the EMT is away from the dilute limit. In what follows we will examine two versions of EMT for each physical property. Depending on whether we treat the inclusion and background symmetrically or asymmetrically, two versions (i.e. symmetric or asymmetric) of EMT can be derived.³ Thus we have 8 cases to consider, electrical or elastic, symmetric or asymmetric with inclusions that are either holes (Swiss cheese model) or hard inclusions (reinforced model). Sen, Thorpe and Milton⁶ have summarised these results for the electrical case. These results can also be obtained from ref. 3. The critical p_c for the dilute (Swiss cheese) case are

$$p_c^s = 1/2 \quad (14)$$

$$p_c^a = (a^2 + b^2) / (a+b)^2 \quad (15)$$

where the superscripts s and a refer to the symmetric and asymmetric cases respectively. The results for the reinforced case are identical to (14) and (15).

Similar results have been obtained by Thorpe and Sen⁷ for the elastic case. For the dilute (Swiss cheese) model, all the elastic moduli vanish at

$$p_c^s = 2 \left\{ 1 + [2(a+b)^2 / (a^2 + b^2)]^{1/2} \right\}^{-1} \quad (16)$$

$$p_c^a = [1 + ab/(a^2 + b^2)]^{-1} \quad (17)$$

For the reinforced model, all the elastic compliances vanish at

$$p_c^s = 1 - 2 \{ 1 + [2(a+b)^2 / (a^2 + b^2)]^{1/2} \}^{-1} \quad (18)$$

$$(1 - p_c^a)^{-1} = 2 \{ 1 + (1 - \sigma)(a+b)^2 / [2ab(1 + \sigma)] \} / (3 - \sigma) \quad (19a)$$

$$(1 - p_c^a)^{-1} = \{ (a+b)^2 / [ab(3 - \sigma)] + 1 / [1 - ab(1 + \sigma) / (a+b)^2] \} / 2 \quad (19b)$$

where p_c^a is found from Eqs. (19a) and (19b) by eliminating σ , the value of Poisson's ratio at the critical point. If these were exact theories, all the results (14) - (19) would be identical. Note that there is no difference between the symmetric and asymmetric cases in the circle limit for all these results. The above results are shown in Fig. 1.5 as a function of the aspect ratio and we can see that only curve 6 which is the result (19) is reasonable. Indeed all results except for the reinforced elastic model fail to get even the circle limit correct. These two approximations for the reinforced elastic model [Eqs. (18) and (19)] give $p_c = 1/3$ which is the correct result for circles within numerical error as can be seen from Tables 1 and 2. These results show that EMT is inadequate, when strong disorder is present, except in the one special case. In other cases we believe a better procedure is to develop interpolation formulas.

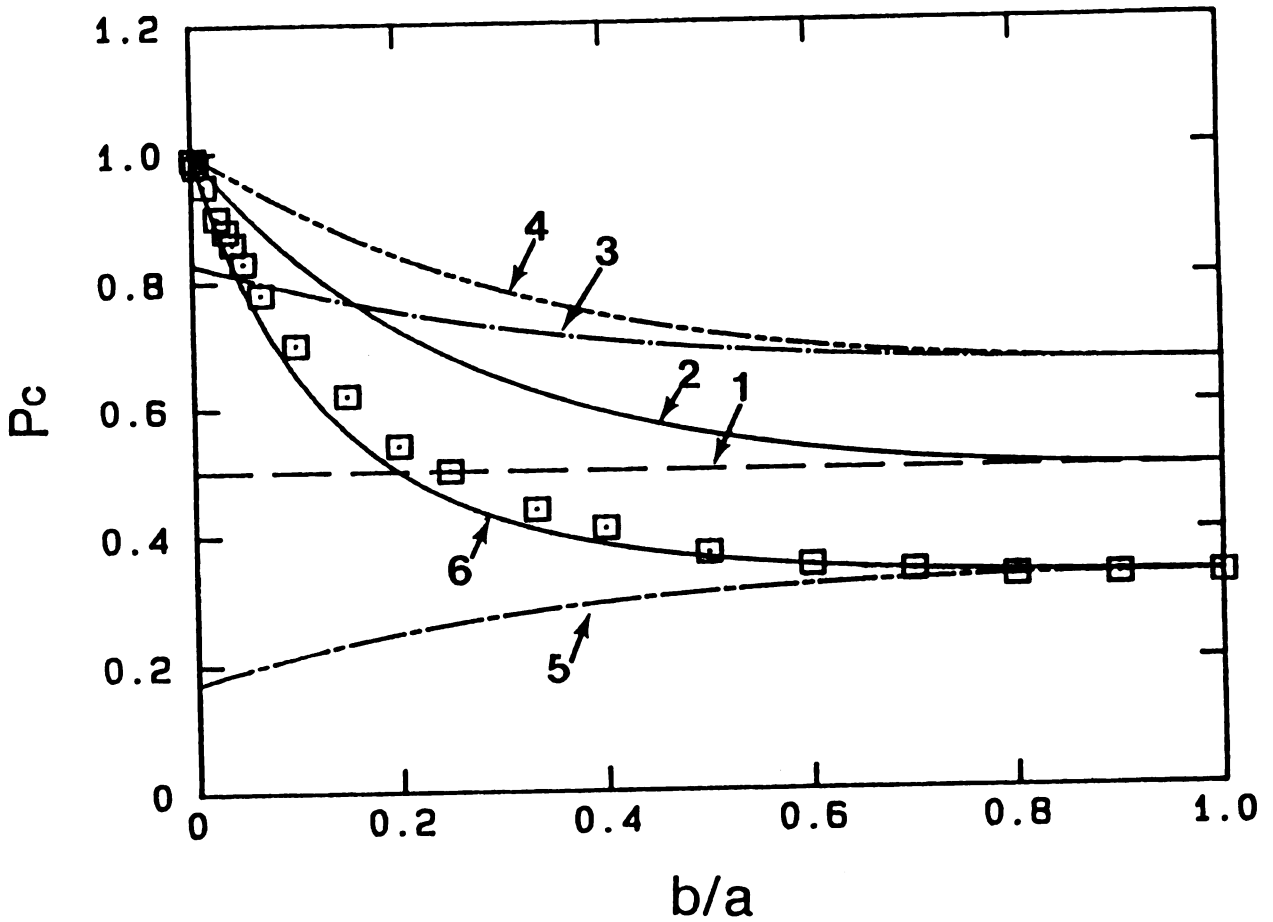


Fig. 1.5 Percolation thresholds p_c predicted from various effective medium theories and our computer simulations from Fig.1.3. The curves are marked 1 for Eqn. (14), 2 for Eqn. (15), 3 for Eqn. (16), 4 for Eqn. (17), 5 Eqn. (18) and 6 for Eqn. (19). The squares indicate the exact percolation thresholds from computer simulations taken from the results for randomly oriented ellipses in Fig. 1.3.

We note that Eqs. (19) could be used as a useful parametric approximation to p_c when required. It gives $p_c = 1/3$ (compared with 0.33 in Tables 1 and 2) in the circle limit and

$$p_c \approx 1 - 16/3 (b/a) \quad (20)$$

in the needle limit. This should be compared with Eqs. (9) and (10)

V Interpolation Formulae

(1) Semi-phenomenological Formulation

As we mentioned in introduction, the Clausius-Mossotti equation for the conductance of a two phase system is exact when one phase has a very low concentration. All attempts to extend these equations beyond this region are rather uncontrolled and many versions exist in the literature. As we discussed in the previous section, all are unsatisfactory for the electrical case. We therefore develop a simple interpolation formula that gets all the known limits for the dilute (Swiss cheese) model correct. We believe that this should be of considerable utilitarian use. Similar formulas can be written down for all other cases.

For a small number of holes in a material with conductance Σ_0 the effective conductance Σ is given by

$$\Sigma = \Sigma_0 [1 - (1-p)/(1-p_1)] \quad (21)$$

where

$$p_I = (a^2 + b^2)/(a + b)^2 \quad (22)$$

The quantity p_I is where the initial slope for a small number of defects^{3,6} would eventually cross the $\Sigma = 0$ axis when extrapolated and is a convenient way to express the initial slope. The relation $\Sigma \sim (p - p_c)^t$ holds only in the small critical region around p_c . Our interpolation formula is designed to link these two limits by assuming the conductivity has the following form

$$\Sigma = \Sigma_0(1.0 + \alpha c + \beta c^2)^\lambda \quad (23)$$

where $c = 1 - p$ and α , β and λ are constants to be determined from the following,

$$\Sigma \sim (p - p_c)^t \quad \text{as } p \rightarrow p_c \quad (24)$$

$$\Sigma = \Sigma_0[1 - c/(1 - p_I) + O(c^2)] \quad \text{as } c \rightarrow 0 \quad (25)$$

and Σ_0 is the conductivity of the sample without any inclusions ($c = 0$). Of course one would like to include higher order terms in c in Eq. (23). but since we have no more information other than (24) and (25) it is not possible to do better. After some simple algebra we find,

$$\Sigma/\Sigma_0 = \{1 - c/[t(1-p_I)] - c^2[t(1-p_I) - (1-p_c)]/[t(1-p_I)(1-p_c)^2]\}^t \quad (26)$$

It is rather inconvenient to use the expressions (19) for p_c and so we make a simpler approximation (27) for p_c that is correct in the two limits $b/a = 1$, when $p_c = 1/3$ and b/a small, when $p_c \approx 1 - 9/2(b/a)$

$$p_c = (1 + 4y)/(19 + 4y) \quad (27)$$

where $y = b/a + a/b$ is symmetric in $a \leftrightarrow b$. The result (27) is virtually indistinguishable from the computer simulations in Fig. 1.3 and is actually superior to (19) as can be seen by comparing Fig. 1.3 and Fig. 1.5. Of course there is no basis for (27) except that it is correct in the two limits and fits the simulation data for all aspect ratios.

By taking $t = 1.3$,¹ and using Eq. (22) for $p_I = y/(2 + y)$ and Eq. (27) for p_c , we can determine the effective conductance Σ ,

$$\begin{aligned} (\Sigma/\Sigma_0)^{1/t} = & 1 - c(2+y)/(2t) + c^2(19 + 4y)[9(2+y) \\ & -(19 + 4y)t]/(324t) \end{aligned} \quad (28)$$

which we recommend for use in practice (with $t = 1.3$) as it reproduces all the known results (i.e. the value of Σ for the pure system, with $p = 1$; the initial slope for small $1 - p$; the value of $p = p_c$ where Σ vanishes with critical exponent t) to within numerical accuracy. Note that the term in c^2 is always small and positive. This is because p_I is always larger than p_c for all aspect ratios ($1 \leq p_I/p_c \leq 1.5$) as can be

seen from Fig. 1.5. In Fig. 1.6, Σ/Σ_0 is plotted against $p = 1 - c$ for various aspect ratios b/a and shown as the solid lines. Also in Fig. 1.6, Σ/Σ_0 is plotted against c but with $t = 1.0$ for the same aspect ratios and shown as the dashed lines. The two plots are very similar and only differ a little in the critical region. Clearly the EMT described in the previous section would give very different results as the p_c are so different.

Because of the equivalence of the problems, the interpolation formula (28) can be used for, the electrical conductivity of sheets containing holes, the thermal conductivity of sheets containing holes or the dielectric constant of a medium with holes. In all cases, $p = 1 - c$ is the fraction of material remaining after the holes have been punched and $y = b/a + a/b$ where b/a is the ratio of the minor to major axis of the ellipses.

If the inclusions are superconducting, rather than insulating (i.e. holes) then the result (28) still holds if we replace Σ/Σ_0 on the left hand side with R/R_0 where R is the resistance of the sample and R_0 is the resistance when there are no inclusions ($c = 0$). These two problems map on to one another and are exactly equivalent.^{25,26} Note that p_I and p_c given in Eqs. (22) and (27) and the critical exponents are the same.¹

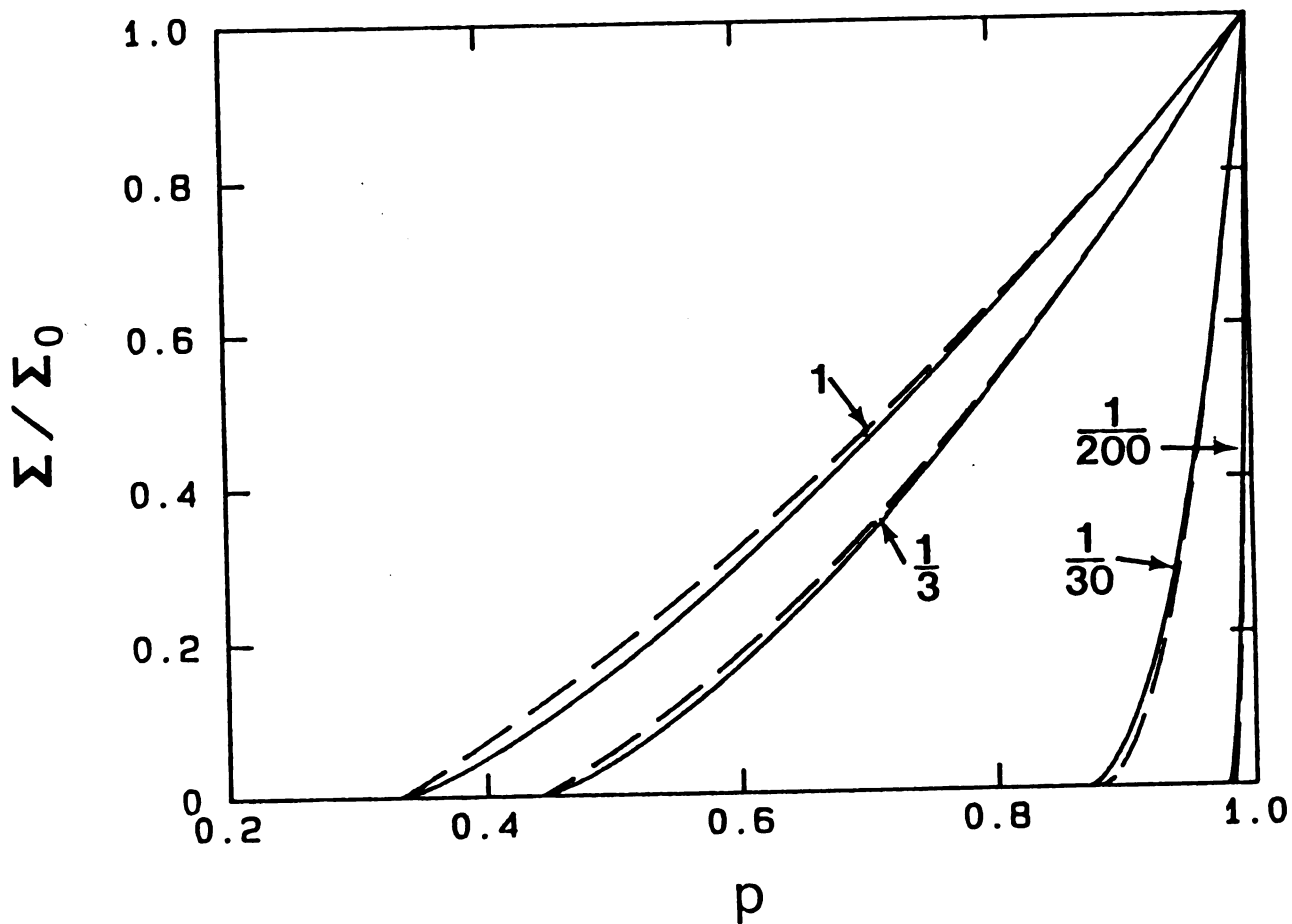


Fig. 1.6 Electrical conductance from the interpolation formula (28) for various aspect ratios as indicated. The solid curves are for $t = 1.3$ and the dashed curves are for $t = 1.0$.

Finally we note that the interpolation formula (28) has two interesting limiting forms. Using the limiting forms for p_I and p_c , we find that for circles,

$$(\Sigma/\Sigma_0)^{1/t} = 1 - 2c/t + 3c^2(4 - 3t)/(4t) \quad (29)$$

and for needles,

$$(\Sigma/\Sigma_0)^{1/t} = 1 - n\pi L^2/(8t) + n^2\pi^2 L^4(9 - 4t)/(1296t) \quad (30)$$

where we have used Eq. (1) with $A = \pi ab$ and put $c = 1 - p = 1 - \exp(-\pi abn) \approx n\pi ab$ and the length of the needles is $L = 2a$. The result (30) is independent of the width b of the needles as would be expected. Here n is the number of inclusions per unit area. A generalization of above interpolation formulae to 3D case is straight forward. One only needs to know p_I (can be easily found from one defect problem), p_c (from computer simulations), and t or s (superconducting diverging exponent near p_c). However p_I , p_c , and λ (i.e. t or s) in the interpolation formulae for conductor-insulator (c-i) system and superconductor-conductor (s-c) system are different now because there is no similar duality, which exists in 2D, exists in 3D. In fact p_c 's for c-i and s-c systems are 0.968 and 0.31 respectively.

(2) Comparison with Experiments

In the previous section we have discussed the formulation of the interpolation formulas. We think these formulas are useful in the predictions of overall electric conductivity for practical applications. The reason is as follows. The actual conductivity of a random composite system, such as the one studied here, in general is a smooth monotonic decreasing function of p . If one can develop a formula which is a smooth monotonic decreasing function with correct limits in the low and critical p , then the overall behavior predicted by the formula cannot be too far away from the real situation. In our case, as we will see later, the agreement between interpolation formulas and experiments are rather good. There have been two recent experiments^{2,28} done on the conductor-insulator system for which our interpolation formulae have been developed. Therefore these experiments are a direct test of how good these interpolation formulae are in predicting the macroscopic conductivity in the whole concentration range. There are no other predictions, to our knowledge, made by any other theory for overall conductivity in the whole concentration range in conductor-insulator systems. In the experiment of ref. 2, which we refer to as experiment I, about 3300 circular holes were drilled on each of two steel and two molybdenum sheets (these materials are used instead of copper or aluminum to avoid deformation of holes during the drill). The size of the sheets are 16cm X 16cm and the radius of the holds is 0.32cm. The thickness of the sheets are 0.13mm, 0.25mm and 0.38mm respectively. Effects due to the thickness of samples are negligible after observing no change among

the samples with different thickness. Also finite size effect only exists when percolation correlation length is comparable to the system size L (in the experiment this happens when $(p-p_c)/p_c \sim 2\%$). The macroscopic conductivity is monitored while holes are drilled. The area fraction is estimated by using the equation

$$p = \exp(-\pi n a^2)$$

which is explained in section II of this thesis. In the experiment of ref. 28, which we refer to as experiment II, about 650 ~ 700 circular holes are cut from an metalized myler foil. The size of system is 10cm X 10cm and the radius of hole is 0.4cm. Effects due to sample thickness can be neglected. The area fraction is measured by weighing the cut fragments on an accurate scale. Also the macroscopic conductivity is monitored as holes are cut. The normalized conductivities from interpolation formula are plotted in Fig. 1.7, using Eq. (28) in section V for circular holds, against area fraction p . We use $t=1.3$ in the solid curve and $t=1.0$ in the dashed curve. The squares and triangles are experimental results from experiment I and experiment II respectively. We can see that apart from some fluctuation the general features of the two sets of experimental data are very close to the two lines in a wide range of concentrations. The data from experiment II have serious deviations near the percolation threshold. Experiments near the percolation threshold need to be done with extreme care because of critical and brittle features of the system. Since the percolation threshold is

wrong in experiment II, we attribute the deviation due to some unexpected failure in the experiment. We have sent our comments to authors in ref. 28. Also we notice that number of holes in experiment II is much less than that in experiment I. While a serious deviation is observed in experiment II near the percolation threshold the rest of data points are not effected because the experiment is performed step by step. The agreement between experiments and our interpolation formulae is very encouraging and it gives us enough confidence in the interpolation formulae. Therefore we believe, with confidence, our interpolation formulae should be very good in predicting the overall features of conductivity in two phase composite systems. Experiments on continuum percolation with randomly distributed elliptical holes are recommended for a further check.

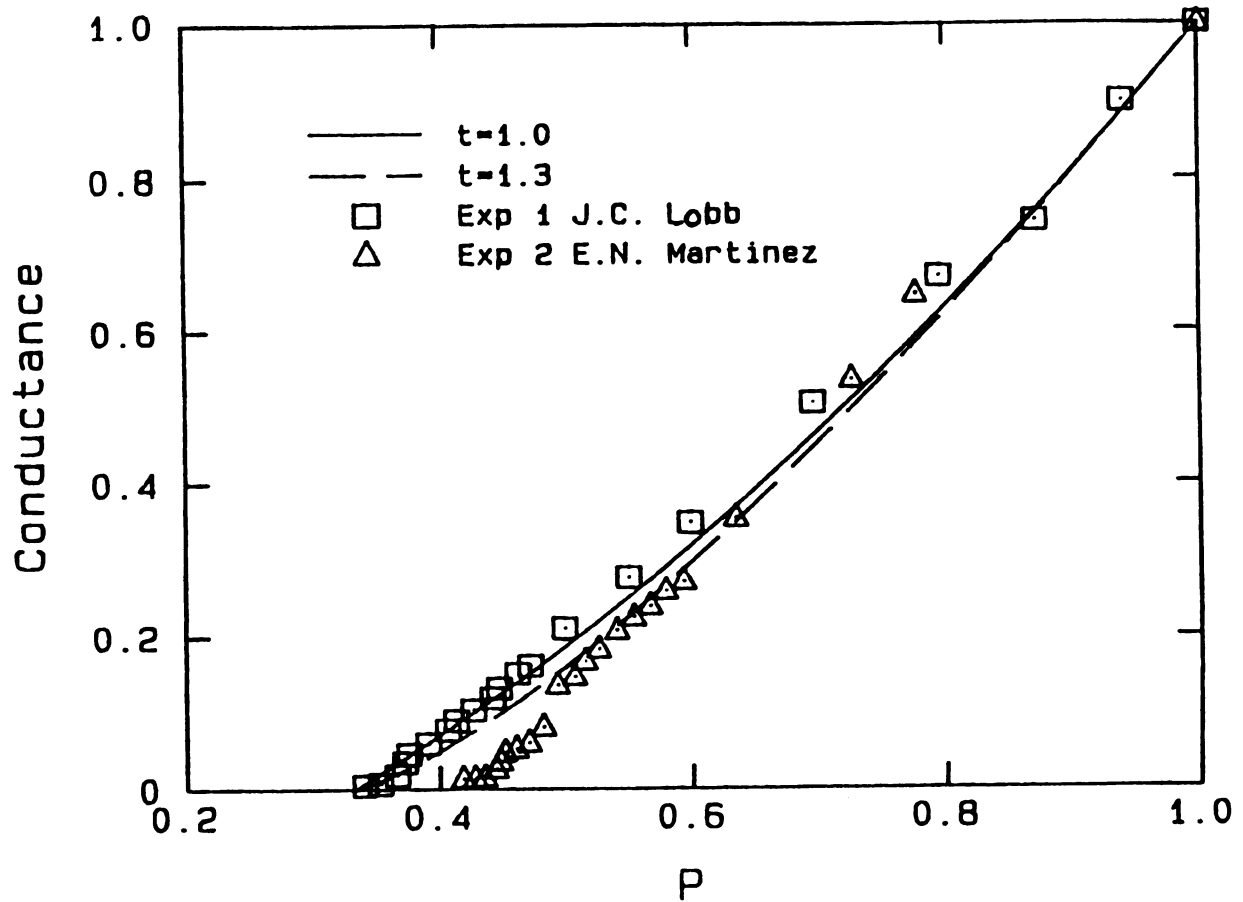


Fig. 1.7 A comparison between interpolation formulae (lines) and Experiments (squares and triangles).

VI Summary of Results

Our main result has been the numerical determination of the percolation concentration of randomly centered and oriented ellipses. This has been done by using a contact function to determine if neighboring ellipses overlap, and constructing a connectivity table. It is not necessary to measure any overlap areas to find the areas at percolation; it is sufficient to merely count the number of ellipses.

We have also determined the percolation concentration of ellipses when the axes are constrained to lie in only two Cartesian directions. The results are indistinguishable, within our numerical accuracy, from the previous case where all orientations are allowed.

We have used these results to critique various effective medium theories that have been developed for the electrical and elastic responses of sheets containing elliptical inclusions. Only one of these approximations is found to give a reasonable percolation threshold while all the others fail to describe the electrical conductivity or elastic properties near the critical point.

We have shown that the percolation concentration is described well by the formula $p_c = (1 + 4y)/(19 + 4y)$ where $y = b/a + a/b$. Here p_c is the amount of material remaining and b/a is the aspect ratio of the ellipses. We have also developed a simple interpolation formula for the electrical conductance that is correct both for a few inclusions and near percolation. The agreements between interpolation formulas and experiments lead us to believe that this kind of formula is superior to effective medium theories and may have useful practical applications.

VII REFERENCES

1. B. I. Halperin, S. Feng, and P. N. Sen, Phys. Rev. Lett. 54, 2391, (1985).
2. C. J. Lobb and M. G. Forrester in preprint (1986).
3. R. Landauer in AIP Conference Proceedings No.40, Ed. by J. Garland and D. Tanner (1978).
4. R. I. Cukier, J. Phys. Chem. 89, 246 (1985)
5. S. Kirkpatrick in Ill-Condensed Matter-Les Houches 1978, Ed. by R. Balian, R. Maynard, and G. Toulouse, (North-Holland, Amsterdam, (1979).
6. P. N. Sen, M. F. Thorpe, and G. Milton, unpublished notes, (1985).
7. M. F. Thorpe and P. N. Sen, J. Acoust. Sco. Am., 77, 1674, (1985).
8. R. Hill, J. Mech. Phys. Solids 13, 213 (1965); B. Budiansky, J. Mech. Phys. Solids 13, 223 (1965).
9. T. T. Wu, Int. J. Solids Struct. 3, 1 (1966).
10. J. Berryman, J. Acoust. Sco. Am. 68, 1820 (1980) and references, therein.
11. J. P. Watt, G. F. Davies, and R. J. O'Connell, Rev. Geophys. and Space Phys. 14 (4), 541 (1976).
12. I. Balberg, Phys. Rev. B 31, 4053 (1985).
13. D. Stauffer, Introduction to Percolation Theory, (Taylor and Francis, London, 1985).
14. L. N. Smith and C. J. Lobb, Phys. Rev. B 20, 3653 (1979).

15. F. Carmona and A El Amarti in preprint (1987).
16. A. S. Skal and B. I. Shklovskii, Fiz. Tekh. Polyprovdn. 7, 1589, (1973) [Sov. Phys. Semicond. 7, 1058 (1973)].
17. V. K. S. Shante and S. Kirkpatrick, Adv. Phys. 20, 325, (1971).
G. E. Pike and C. H. Seager, Phys. Rev. B 10, 1421 (1974).
18. C. Mark, Proc. Camb. Phil. Soc. 50, 581 (1954).
19. We list here the results for p_c for circles with references.
 $p_c = 0.325$ (ref. 17); $p_c = 0.32 \pm 0.02$ (ref. 18); $p_c = 0.33 \pm 0.02$, D. H. Fremlin, J. Phys. (Paris) 37, 813 (1976); $p_c = 0.324 \pm 0.002$, E. T. Gawlinski and H. E. Stanley, J. Phys. A 14, L129, (1981); $p_c = 0.322 \pm 0.005$, T. Vicsek and J. Kertesz, J. Phys. A, 14, L31, (1981).
20. I. Balberg, C. H. Anderson, S. Alexander, and N. Wagner, Phys. Rev. B 30, 3933 (1984).
21. L. Onsager, Ann. N. Y. Acad. Sci. 51, 627 (1949).
22. R. Zallen, The Physics of Amorphous Solids, (John Wiley & Sons, New York, 1983).
23. A. S. Roach, Theory of Random Clumping, (Spottiswoode and Ballantyne, London, 1968).
24. J. V. Baron, J. Chem. Phys. 56, 4730(1972).
25. J. B. Keller, J. Math. Phys. 5, 548 (1964).
26. K. S. Mendelson, J. Appl. Phys. 46, 917 (1974).
27. W. T. Elam, A. R. Kerstein and J. J. Rehr, Phys. Rev. Lett., 52, 1516 (1984).

28. J. Sofo, J. Lorenzana and E. N. Martinaez in reprint (1987).

Part II

Elastic Percolation and Tricritical Point of
Stretched Spring Model on Honeycomb Lattice

I Introduction

Percolation of elastic networks has been an interesting subject for the past decade. de Gennes¹ was the first to introduce the isotropic force model for the elastic modulus of a gel. The model is defined on a lattice and described by elastic energy

$$V = \frac{1}{2} \sum_{\langle ij \rangle} B (u_i - u_j)^2 g_{ij} \quad (1)$$

where B is the spring constant and u_i is the small displacement of site i . $g_{ij} = 1$ when a spring between site i and site j is present with probability p and $g_{ij} = 0$ if a spring is missing with probability $1-p$. de Gennes pointed out that the elastic percolation problem of this model is identical to the conductivity percolation problem which has been studied in great detail.^{2,3} This is reflected by the fact¹ that the two problems can be mapped into each other and therefore (i) the percolation thresholds of the elastic and conductivity percolation problems are the same; (ii) the critical exponents describing the vanishing bulk moduli and conductivity near the percolation threshold are identical.

Feng and Sen⁴ proposed the central force model described by elastic energy

$$V = \frac{1}{2} \sum_{\langle ij \rangle} \alpha \{ (\vec{u}_i - \vec{u}_j) \cdot \hat{r}_{ij} \}^2 g_{ij} \quad (2)$$

where α is the spring constant and \hat{r}_{ij} is the unit vector from site i to site j . Feng and Sen further pointed out that the elastic percolation described by potential (2) is different from that of (1). Again this is reflected by the fact that the percolation thresholds and critical exponents are different for (1) and (2). In fact they belong to different class of the problems^{4,5}. More specifically, in two dimensions the percolation thresholds, according to Thorpe's constraint counting method⁶, are

$$p_c = \frac{2}{z} \quad \text{for isotropic force model} \quad (3)$$

$$p_{\text{cen}} = \frac{4}{z} \quad \text{for central force model.} \quad (4)$$

Here z is the number of nearest neighbors of a lattice. The two models are special cases of the more general Born model⁷

$$V = \frac{1}{2} \sum_{\langle ij \rangle} \{ \alpha [(\vec{u}_i - \vec{u}_j) \cdot \hat{r}_{ij}]^2 g_{ij} + \beta (\vec{u}_i - \vec{u}_j)^2 g_{ij} \} \quad (5)$$

Feng and Sen also studied the elastic percolation of Born model⁴ and concluded that even with a small nonzero β the elastic percolation crosses over from the central force model to the isotropic force model. For example, the percolation threshold p_{cen} changes to p_c of the isotropic force model (see Fig. 2.1).

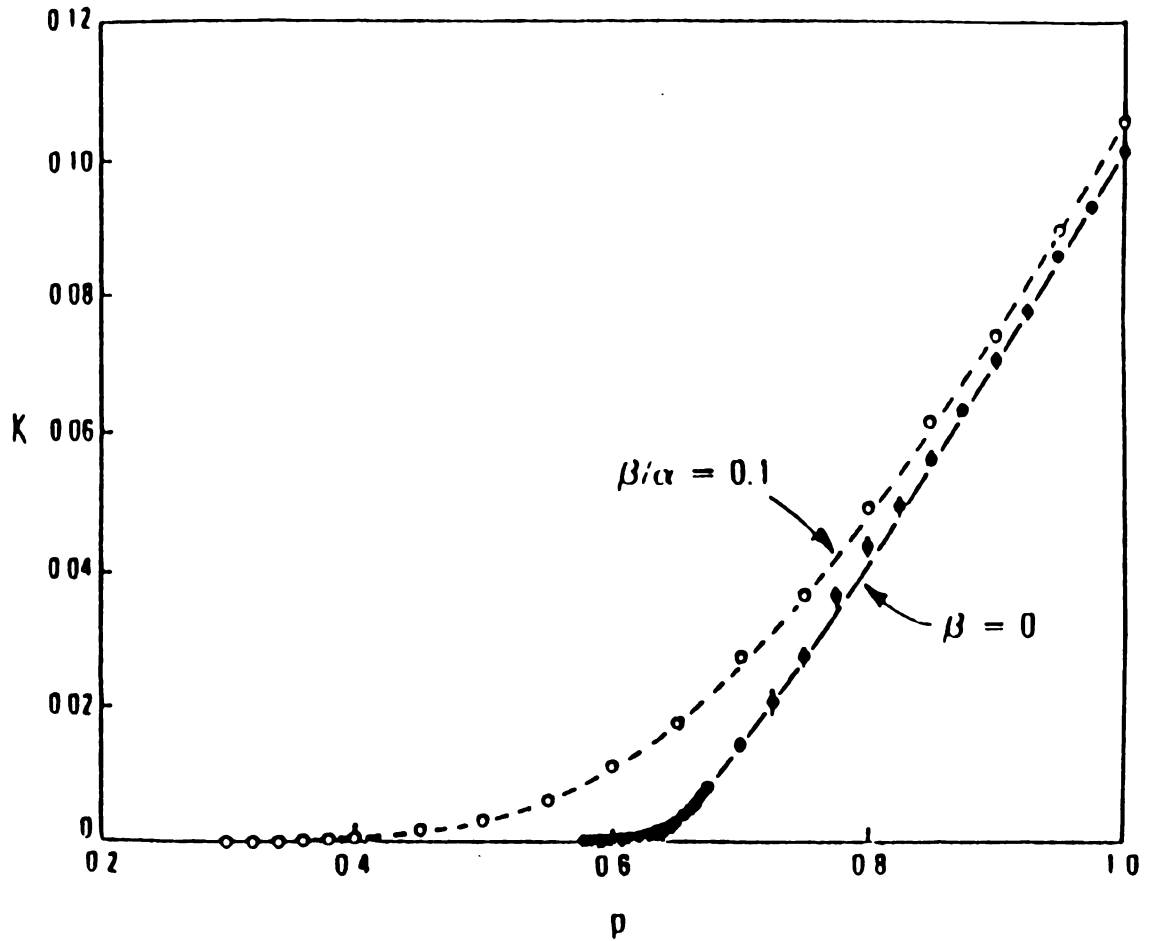


Fig. 2.1 Bulk moduli vs. ρ for central force model ($\beta = 0$, solid line) and Born model ($\beta/\alpha = 0.1$, dash line) for 2D triangular lattice. A strong crossover is shown in latter case. Fig. is from ref. 4.

Recently Tang and Thorpe introduced the stretched spring model⁸ with elastic energy

$$V = \frac{1}{2} \sum_{\langle ij \rangle} K_{ij} (l_{ij} - L_0)^2 \quad (6)$$

where K_{ij} is the spring constant between site i and site j . K_{ij} 's have values of $K_{ij} = 1$ with probability p and $K_{ij} = 0$ with probability $1-p$. L_0 is the spring's natural length and l_{ij} is the distance between site i and site j . Using the relation

$$l_{ij} = |\hat{R}_i - \hat{R}_j + \vec{u}_i - \vec{u}_j|, \quad (7)$$

where \hat{R}_i and \hat{R}_j are the equilibrium positions of site i and site j , potential (6) can be written as

$$\begin{aligned} V = & \frac{1}{2} \sum_{\langle ij \rangle} K_{ij} (L_{ij} - L_0)^2 + \sum_{\langle ij \rangle} K_{ij} (L_{ij} - L_0) (\vec{u}_{ij} \cdot \hat{r}_{ij}) \\ & + \frac{1}{2} \sum_{\langle ij \rangle} K_{ij} \{ (1 - L_0/L_{ij}) \vec{u}_{ij}^2 + L_0/L_{ij} (\vec{u}_{ij} \cdot \hat{r}_{ij})^2 \} + O(\vec{u}_{ij}^3). \quad (8) \end{aligned}$$

In (8) $L_{ij} = |\hat{R}_i - \hat{R}_j|$ and $\vec{u}_{ij} = \vec{u}_i - \vec{u}_j$. The higher order terms are neglected. Comparing (8) with (1) and (2) one can see that the isotropic force model and the central force model are also special cases of the stretched spring model at $L_0/L_{ij} = 0$ and $L_0/L_{ij} = 1$. Therefore by changing L_0/L_{ij} continuously, the stretched spring model can serve as

a bridging model between the isotropic force model and the central force model. One will also notice that the central force model and stretched spring model described by (2) and (6) are rotationally invariant while the isotropic force model described by (1) is not. Most computer simulations have been done on triangular lattice in the stretched region where $0 \leq L_0/L_{ij} \leq 1$ while simulations in the compressed region are still in progress. The major conclusion of Tang and Thorpe is that the stretched spring force model can serve as a bridging model between the isotropic force and central force model and the percolation threshold p_c changes with L_0/L .

In this paper we study the elastic percolation of the stretched spring model on honeycomb lattice. The motivation of this study is as follows:

(i) In honeycomb lattice the number of nearest neighbors (z) is three so the constraint counting method or effective medium theory^{6,9} will give $p_{cen} = \frac{4}{3}$, which is meaningless, for the central force model. However, what $p_{cen} = \frac{4}{3}$ tells us is that in the central force model the honeycomb lattice is unstable against dilution. In other words, if a spring is removed and the network is compressed then it will collapse or have zero elastic bulk modulus. In triangular lattice this is not the case. Therefore by studying the honeycomb lattice we expect to see some new phenomena associated with the instability.

(ii) From eq. (8) we notice that there are two quadratic elastic energy terms of u_{ij} which correspond to the isotropic force and the central force components in the stretched spring model. So as $L_0/L \rightarrow 1$

a small isotropic force can help to stabilize the network. In the limit, when the strength of isotropic force goes to zero, we should be able to obtain the correct prediction of the percolation threshold.

(iii) A new effective medium theory must be developed to accommodate the phenomena associated with the instability mentioned before.

The layout of this paper is as following. In section II we first discuss the elasticity of stretched spring model for the perfect lattice and then use an one defect effective medium theory to estimate the percolation threshold as a function of L_0/L_{ij} . In section III we present computer simulation results on the honeycomb lattice and the explanations of the anomalous behavior of the elastic moduli associated with the instability of central force model on the honeycomb lattice. In section IV we use Landau's phase transition theory to establish a tricritical point observed in the computer simulations. We also develop a new effective medium theory which addresses the behavior of the elastic constants and predicts the location of the tricritical point.

II Elasticity of Pure Honeycomb Lattice And Estimate of the Percolation Thresholds

We define the stretched spring model on a perfect honeycomb lattice with elastic energy (6) defined in section I.

$$V = \frac{1}{2} \sum_{\langle ij \rangle} K_{ij} (l_{ij} - L_0)^2 \quad (6)$$

Here every bond of the lattice is represented by a Hook spring of strength K_{ij} and natural length L_0 . l_{ij} is simply the distance between site i and site j . As stated in section I, the elastic energy can be written as (8) for a small external strain. In the rest of discussion we restrict ourselves in the stretched spring region where $0 \leq L_0/L \leq 1$.

The physical meaning of each of the terms in expansion (8) are discussed in ref. 8. Here we just mention them again for reader's convenience. The first term

$$V_0 = \frac{1}{2} \sum_{\langle ij \rangle} K_{ij} (L_{ij} - L_0)^2 \quad (8a)$$

is the static elastic energy term because L_{ij} is the equilibrium distance of lattice sites i and j and no \vec{u}_{ij} is involved. The second term in (8) is

$$V_2 = \sum_{\langle ij \rangle} K_{ij} (L_{ij} - L_0) (\vec{u}_{ij} \cdot \hat{r}_{ij}) \quad (8b)$$

which is the elastic energy due to the tension of the springs because it is linear in displacements. The third term

$$V_3 = \frac{1}{2} \sum_{\langle ij \rangle} K_{ij} \left\{ (1 - L_0/L_{ij}) \vec{u}_{ij}^2 + L_0/L_{ij} (\vec{u}_{ij} \cdot \hat{r}_{ij})^2 \right\} \quad (8c)$$

is the quadratic elastic energy term of displacements \vec{u}_{ij} . This term determines the elastic moduli of the system. By comparing (8c) with Born model (5) one can see that

$$\alpha = K_{ij} (1 - L_0/L_{ij}) \quad (9a)$$

and
$$\beta = K_{ij} (L_0/L_{ij}) \quad (9b)$$

while
$$\alpha + \beta = K_{ij} . \quad (9c)$$

Notice that $L_0/L_{ij} = 1$ case corresponds to the central force model while $L_0/L_{ij} = 0$ case to the isotropic force model. For an arbitrary L_0/L_{ij} , in general, there is a lot of stress in the system due to the stretched and compressed springs. One may also notice that the full elastic potential (6) is rotationally invariant because it only involves the distances between springs.

(1) Elasticity of Pure Honeycomb Lattice.

Now we first discuss the elastic moduli of model (8) without any dilution (i.e. perfect lattice case). In this case $L_{ij} = L$, the lattice spacing, and $K_{ij} = K$. It can be found in the literature^{7,10} that the strain energy can always be written as

$$V = \sum_{\alpha\beta} S_{\alpha\beta} \epsilon_{\alpha\beta} + \frac{1}{2} \sum_{\alpha\beta\gamma\tau} C_{\alpha\beta\gamma\tau} \epsilon_{\alpha\beta} \epsilon_{\gamma\tau} \quad (10)$$

where $S_{\alpha\beta}$ are the elements of the stress tensor and $C_{\alpha\beta\gamma\tau}$ are the second order elastic constants which are directly associated with the elastic moduli. The quantity $\epsilon_{\alpha\beta}$ is called the strain and defined by

$$\epsilon_{\alpha\beta} = \frac{\partial u_{\alpha}}{\partial x_{\beta}} \quad \alpha, \beta = x, y$$

where u_{α} and x_{β} are the components of $\vec{u} = (u\hat{x} + v\hat{y})$ and \vec{r} . In two dimensions

$$\begin{aligned} \epsilon_{xx} &= \frac{\partial u}{\partial x} & \epsilon_{yx} &= \frac{\partial u}{\partial y} \\ \epsilon_{xy} &= \frac{\partial v}{\partial x} & \epsilon_{yy} &= \frac{\partial v}{\partial y} \end{aligned} .$$

Therefore an uniform displacement for a Bravais lattice in two dimensions can be written as

$$u = x\epsilon_{xx} + y\epsilon_{yx} \quad (11a)$$

$$v = x\epsilon_{xy} + y\epsilon_{yy} . \quad (11b)$$

Now let us put a small force on the frame which holds the springs in place of the honeycomb lattice. The lattice will respond to this small force by rearranging the lattice sites so that the elastic energy (8) is at a minimum. The response of a Bravais lattice such as the

square lattice or triangular lattice is a small uniform displacement expressed in (11a) and (11b). The honeycomb lattice is not a Bravais lattice but can be regarded as a lattice composed of two interpenetrating triangular lattices which are Bravais lattices. Thus the response on the honeycomb lattice will be two identical small uniform displacements such as (11a) and (11b) on the two sublattices and an uniform relative shift of the two sublattices^{11,12}. In other words the displacements between any two sites of lattice A and lattice B [see Fig.2.2] can always be written as

$$u = x\varepsilon_{xx} + y\varepsilon_{yx} + u' \quad (12a)$$

$$v = x\varepsilon_{xy} + y\varepsilon_{yy} + v' \quad (12b)$$

where x and y are the x and y components of the distance between two sites. Quantities u' and v' are the relative shifts of the two sublattices in x and y directions and can be determined by minimizing the elastic energy (8).

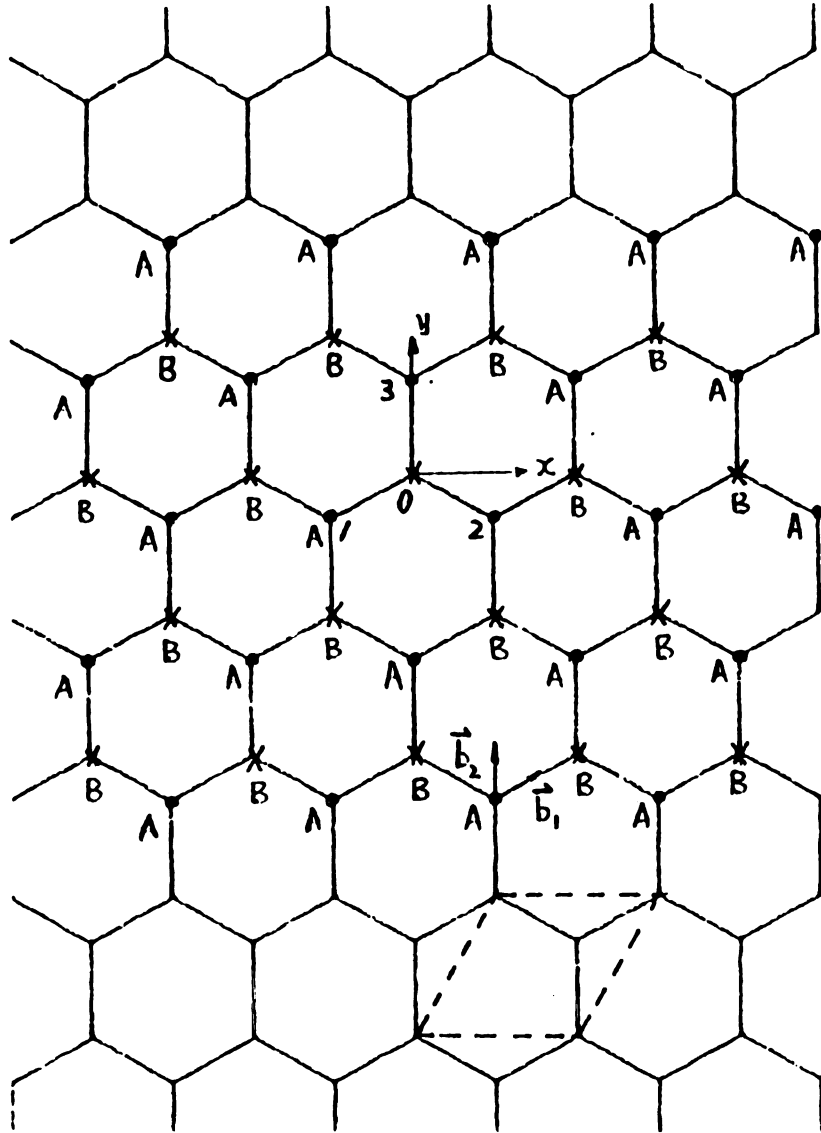


Fig. 2.2 Honeycomb lattice is decomposed into two triangular sublattices A and B. Directions of \vec{b}_1 and \vec{b}_2 are shown.

Equation (10) can be rewritten as

$$\begin{aligned}
 V = V_0 + S_{xx}\epsilon_{xx} + S_{yy}\epsilon_{yy} + S_{xy}\epsilon_{xy} + S_{yx}\epsilon_{yx} + \frac{C_{xxxx}}{2}(\epsilon_{xx}^2 + \epsilon_{yy}^2) \\
 + C_{xxyy}\epsilon_{xx}\epsilon_{yy} + \frac{C_{xyxy}}{2}(\epsilon_{xy}^2 + \epsilon_{yx}^2) + C_{xyyx}\epsilon_{xy}\epsilon_{yx} . \quad (13)
 \end{aligned}$$

In (13) we have also considered the symmetries of the honeycomb lattice to reduce the number of independent elastic constants¹³. By minimizing the elastic energy with respect to u' and v' one can find that [see Appendix I]

$$C_{xxxx} = C_{11} = \frac{a^2 + 5aB + 4B^2}{2\sqrt{3}(2B + a)} = \frac{4 - 3\eta}{2 - \eta} \frac{K}{2\sqrt{3}} \quad (14a)$$

$$C_{xxyy} = C_{12} = \frac{a^2 + aB}{2\sqrt{3}(2B + a)} = \frac{\eta}{2 - \eta} \frac{K}{2\sqrt{3}} \quad (14b)$$

$$C_{xyxy} = \tilde{C}_{44} = \frac{4B^2 + 3aB}{2\sqrt{3}(2B + a)} = \frac{\eta(1 - \eta)}{2 - \eta} \frac{K}{2\sqrt{3}} \quad (14c)$$

$$C_{xyyx} = C_{44} = \frac{aB}{2\sqrt{3}(2B + a)} = \frac{(1 - \eta)(4 - \eta)}{2 - \eta} \frac{K}{2\sqrt{3}} \quad (14d)$$

$$S_{xx} = S_{yy} = T = \frac{B}{\sqrt{3}} = (1 - \eta) \frac{K}{\sqrt{3}} \quad (14e)$$

and

$$S_{xy} = S_{yx} = 0.$$

In the second column we have used the conventional notation $C_{xxxx} = C_{11}$, $C_{xxyy} = C_{12}$, $C_{xyxy} = \tilde{C}_{44}$ and $C_{xyyx} = C_{44}$. In the fourth column we have used $\alpha = K\eta$, $\beta = K(1 - \eta)$ and $\eta = L_0/L$.

We first see that (14d) is zero when $\eta = L_0/L = 1$. This is the case where the instability, as mentioned in the introduction, rises. It means that even a perfect honeycomb lattice can not resist a shear distortion in the central force limit. We will see later that this instability gives an extra zero frequency mode beside the acoustic modes in the dynamic matrix and leads to the wrong prediction for the percolation threshold $p_{\text{cen}} = \frac{4}{3}$. We can also see that

$$C_{11} - C_{12} = C_{44} + \tilde{C}_{44} . \quad (15)$$

Equation (15) just reflects the fact that honeycomb system, due to the geometric symmetry, is isotropic in any direction.⁸ The bulk modulus is defined by

$$B = \frac{1}{2}(C_{11} + C_{12}) . \quad (16a)$$

Using (14a) and (14b) we obtain

$$B = \frac{K}{2\sqrt{3}} . \quad (16b)$$

Equation (16b) just states that bulk modulus is a constant independent of η . The bulk modulus is, however, unstable against dilution in the

central force model limit, that is, the bulk modulus will be zero if one spring is removed when $\eta = L_0/L = 1$. It can also be seen that

$$\frac{1}{2}(C_{44} - \tilde{C}_{44}) = T. \quad (17)$$

Equation (17) reflects the fact that the strain energy is rotationally invariant.⁸

(2) Estimate of the Elastic Percolation Thresholds of Honeycomb Lattice

We now discuss the theoretical estimate of elastic percolation thresholds of model (8). The method was first developed by Feng, Thorpe and Garboczi⁹ to calculate the percolation threshold for the central force model. Tang and Thorpe⁸ generalized it to the stretched spring model. In ref. 9 authors obtained the percolation threshold for the central force model (2)

$$p_{\text{cen}} = \frac{2d}{z}. \quad (18)$$

For two dimensional honeycomb lattice $p_{\text{cen}} = \frac{4}{3}$. Obviously this is unphysical because p must always equal or less than one. This unphysical threshold $p_{\text{cen}} = \frac{4}{3}$ is associated with the instability of the central force model on honeycomb lattice. This is clearly seen by the vanishing shear modulus $C_{44} = 0$ in previous discussion. The consequence of this vanishing shear modulus will be discussed. In ref. 8 the estimate of the percolation threshold is obtained by removing a single spring and calculating the energy change ΔE afterward. A straight line is then

used to extrapolate ΔE to a point in the p axis where the energy is zero (see Fig. 2.3). Of course the elastic energy generally does not decrease linearly against dilution but with some curvature. Therefore the approach is just an estimate of the percolation threshold. We call this estimate, denoted by $p_{(E)}$, the extrapolated intercept or the initial slope of the elastic energy and $p_{(E)}$ is different from the actual percolation threshold. However, in some cases, for example in the isotropic force model and the central force model, this theory gives very accurate predictions. One may also wish to calculate the similar extrapolated intercepts (or initial slopes) from tension (T) and elastic modulus (B) curves (see Fig. 2.3) denoted by $p_{(T)}$ and $p_{(B)}$ respectively. The extrapolated intercept is often used as a guide to roughly locate the percolation thresholds and it is very helpful in computer simulations.

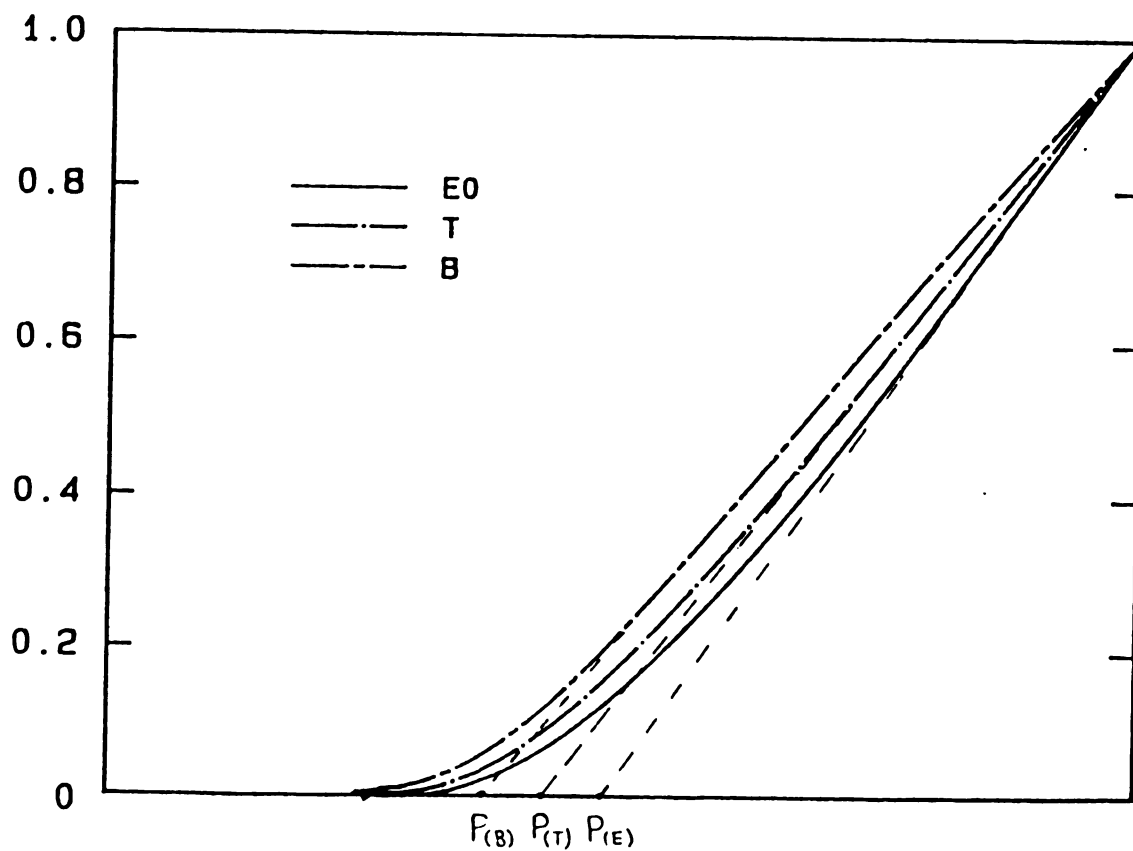


Fig. 2.3 The extrapolated intercepts for elastic energy (E_0), tension (T) and bulk modulus (B). It is clear that these intercepts overestimate the actual percolation threshold.

A derivation of $p_{(E)}$ using the same method in ref. 8 for elastic energy (8) is given below. $P_{(T)}$ and $p_{(B)}$ can also be obtained in the similar manner after differentiating the elastic energy with respect to L . Notice that in the $L_0/L = 1$ limit (8) corresponds to the central force model. During the course of derivation we will point out the crucial step which may lead to the wrong prediction. The previous derivation was on a Bravais lattice and it is now generalized to the honeycomb lattice which is composed of two interpenetrating Bravais sublattices. $p_{(E)}$ of the stretched spring model (8) can be written as [see Appendix II]

$$P_{(E)} = \frac{K}{2Nz} \sum_{\delta} \sum_{\vec{k}} \text{Tr} \left\{ -\hat{\delta}\hat{\delta}(A + D) + \hat{\delta}\hat{\delta}C e^{i\vec{k}\cdot\vec{R}_{\delta}} + \hat{\delta}\hat{\delta}B e^{i\vec{k}\cdot\vec{R}_{\delta}} \right\} \quad (19)$$

where sum over δ extends over nearest neighbors and sum over \vec{k} is restricted to the first Brillouin zone. In (19) the \vec{R}_{δ} 's are the position vectors of nearest neighbors once a site is chosen and $\hat{\delta}$'s are the corresponding unit vectors in \vec{R}_{δ} 's directions. Matrices A , B , C and D are defined by

$$\begin{aligned} A &= D_{AB}^{-1} (-D_{AB}^{-1}D_{AA} + D_{BB}^{-1}D_{BA})^{-1} \\ B &= D_{BB}^{-1} (-D_{AB}^{-1}D_{AA} + D_{BB}^{-1}D_{BA})^{-1} \\ C &= D_{AA}^{-1} (-D_{AA}^{-1}D_{AB} + D_{BA}^{-1}D_{BB})^{-1} \end{aligned} \quad (20)$$

$$D = D_{BA}^{-1} (-D_{AA}^{-1} D_{AB} + D_{BA}^{-1} D_{BB})^{-1}$$

where 2 X 2 Matrices D_{AA} , D_{AB} , D_{BA} and D_{BB} are the following.

$$D_{AA} = \begin{vmatrix} 3(\alpha + 2B)/2 & 0 \\ 0 & 3(\alpha + 2B)/2 \end{vmatrix} \quad D_{AB} = \begin{vmatrix} -a_1 & -a_2 \\ -a_2 & -a_3 \end{vmatrix}$$

$$D_{BA} = - \begin{vmatrix} a_1^* & a_2^* \\ a_2 & a_3 \end{vmatrix} \quad D_{BB} = \begin{vmatrix} 3(\alpha + 2B)/2 & 0 \\ 0 & 3(\alpha + 2B)/2 \end{vmatrix}$$

$$\text{and } a_1 = B e^{ik_1 \sqrt{3}a} + (B + \frac{3}{4} \alpha) e^{ik_2 \sqrt{3}a} + (B + \frac{3}{4} \alpha) e^{ik_1 \sqrt{3}a + ik_2 \sqrt{3}a}$$

$$a_2 = \alpha \frac{\sqrt{3}}{4} e^{ik_2 \sqrt{3}a} (1 - e^{ik_1 \sqrt{3}a})$$

$$a_3 = (\alpha + B) e^{ik_1 \sqrt{3}a} + (B + \frac{\alpha}{4}) e^{ik_2 \sqrt{3}a} + (B + \frac{\alpha}{4}) e^{ik_1 \sqrt{3}a + ik_2 \sqrt{3}a}.$$

In above expressions $\alpha = K(L_0/L)$, $B = K(1 - L_0/L)$ and a_i^* is the complex conjugate of a_i . k_1 and k_2 are the k components along the \vec{b}_1 and \vec{b}_2 directions.[see Fig. 2.2]

In the central force limit ($L_0/L = 1$), $p(E) = p_{\text{cen}}$ should be given by (19) as a special case. By simply substituting $B = 0$, however, one will find that matrices A , B , C and D do not exist because matrices $(-D_{AB}^{-1} D_{AA} + D_{BB}^{-1} D_{BA})$ and $(-D_{AA}^{-1} D_{AB} + D_{BA}^{-1} D_{BB})$ can not be inverted. One may

recall that in the central force limit the shear modulus is zero. It is this vanishing shear modulus which introduces a zero frequency in the dynamic matrices so that the determinants of the two matrices are zero. This is a crucial step. If one ignores the fact that $(-D_{AB}^{-1}D_{AA} + D_{BB}^{-1}D_{BA})$ and $(-D_{AA}^{-1}D_{AB} + D_{BA}^{-1}D_{BB})$ are no longer invertible and symbolically works out the algebra, one may indeed find $p_{\text{cen}} = \frac{4}{3}$. So now we understand that the unphysical prediction is associated with the instability of the central force model on the honeycomb lattice. To obtain the correct $p_{(E)}$ in the central force limit one should allow a small β , which helps to stabilize the network, and take the limit $\beta \rightarrow 0$. Following this procedure one will obtain the correct extrapolated intercept $p_{(E)} = p_{\text{cen}} = 1$ in the central force limit. Obviously it is hopeless to write down an explicit function of L_0/L for (18) because it is so complicated. However, the values of $p_{(E)}$ can be calculated by using a computer. In Fig. 2.4(a) $p_{(E)}$ is plotted against L_0/L . Clearly $p_{(E)}$ goes to one when $L_0/L = 1$. The extrapolated intercepts $p_{(T)}$ and $p_{(B)}$ are also plotted in Fig. 2.4(a) for honeycomb lattice. The same quantities for triangular lattice are plotted in Fig. 2.4(b). By comparing two figures we find (i) on the triangular lattice and the honeycomb lattice both $p_{(E)}$ and $p_{(T)}$ approach $\frac{2}{3}$ and 1 respectively as $L_0/L \rightarrow 1$. However, the slopes for approaching $L_0/L \rightarrow 1$ are different. (ii) while $p_{(B)}$ approaches two thirds as $L_0/L \rightarrow 1$ on the triangular lattice that of the honeycomb lattice stays almost constant. This means the initial slopes for bulk modulus on honeycomb lattice change very little as L_0/L changes from zero to one. This is a unique feature of the honeycomb lattice

which will explain the sudden discontinuities in B in the next section. In Fig. 2.4(a) we also plot the corresponding quantities (in symbols) from one defect computer simulations. There are some small discrepancies between the theoretical curves and the simulation data points. They are expected and will be explained in the following paragraph. We can also develop a more sophisticated effective medium theory which is capable of dealing with more defects and we will discuss it in section IV.

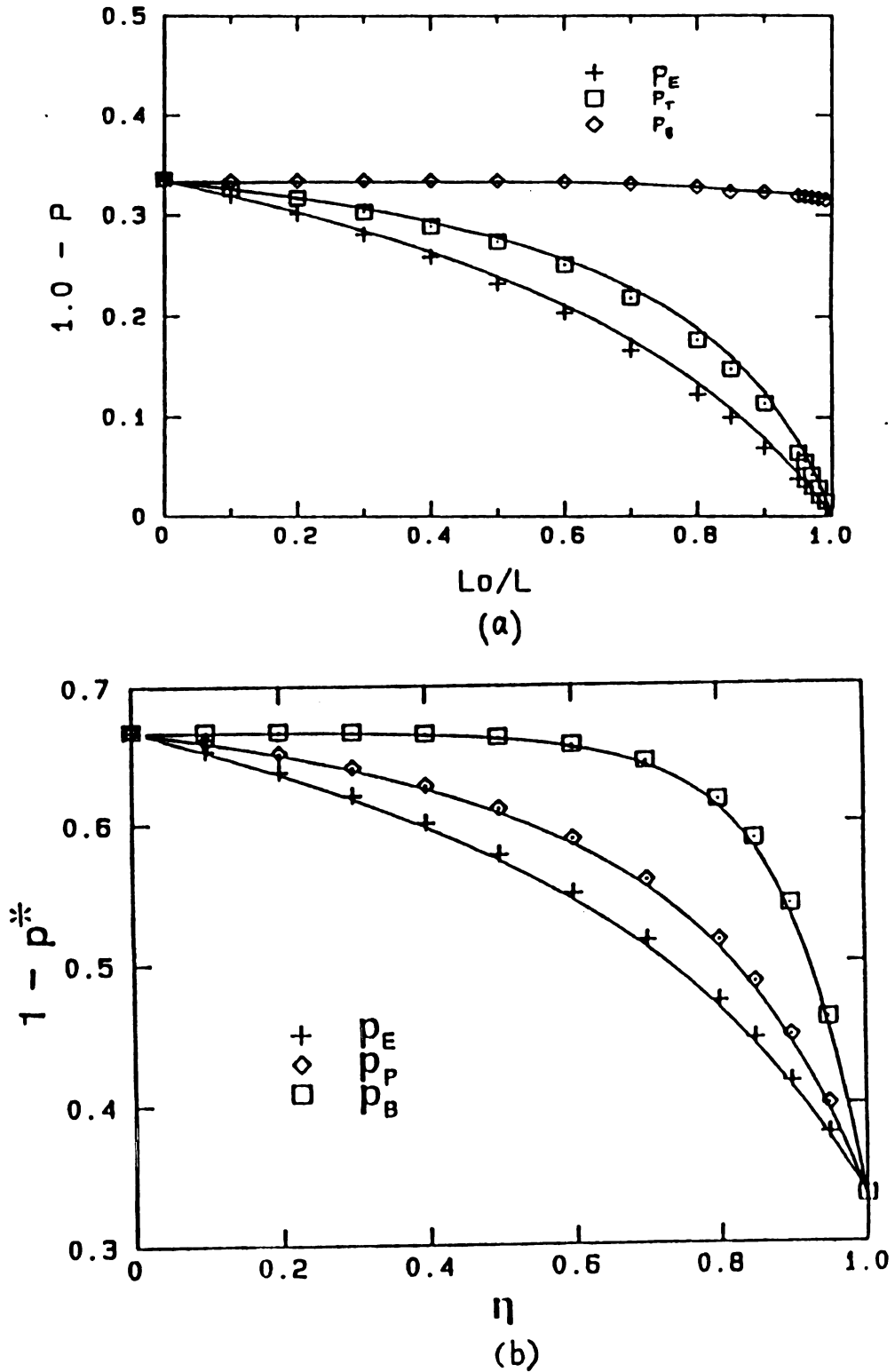


Fig. 2.4 (a) the quantities p_E , p_T and p_B vs. L_0/L (solid lines). The corresponding quantities from one defect computer simulations are also plotted; (b) the same quantities for the triangular lattice from ref.9.

(3) Parabolicity of Effective Elastic Potential

We have discussed above how to obtain the estimate of the percolation thresholds (extrapolated intercepts) using a one defect effective medium theory. We can also ask what the effective spring constant each spring will have when one spring is removed from the system. Suppose a spring between site i and site j is removed. According to ref. 9 the effective spring constant will be

$$K_{\text{eff}} = \frac{1 - a^*}{a^*} K \quad (21)$$

where $K = \alpha + \beta$ is the original spring constant of the Hooke springs and $a^* = p(E)$ can be calculated from (19). Notice that K_{eff} is defined in the neighborhood where the distance between site i and site j is L (the lattice spacing). We can also consider the case where one spring is removed and the network is allowed to relax so that the distance between site i and site j is $L_{\text{eq}} \neq L$. Tang and Thorpe⁸ found

$$L_{\text{eq}} = \frac{L - L_0 a^*}{1 - a^*} \quad (22)$$

In obtaining L_{eq} in (22), however, the authors used the effective spring constant $K_{\text{eff}} = \frac{1 - a^*}{a^*} K$ for small deformation near L_{eq} which is not justified. Fig. 2.5 is a schematic drawing of elastic potential when one spring is removed. The whole curve may not be a parabolic, however,

for small Δl close to L_{eq} it is indeed parabolic.[see Fig. 2.6] The point indicated by L is the point where a spring is removed and the distance between site i and site j is L . Since the whole curve is not parabolic the effective spring constants deduced from points close to L_{eq} and L may not be the same. We use K_{eff}^b to denote the effective spring constant near L_{eq} . In Fig. 2.6 we show some of the computer simulation results for the elastic potential for different L_0/L . We can see that for small Δl the potentials are indeed parabolic. The values of K_{eff}^b are calculated from the potential curves near $\Delta l = 0$. In Fig. 2.7 we plot K_{eff} and K_{eff}^b vs. L_0/L . The solid line is for K_{eff} and the squares are for K_{eff}^b . It can be seen that K_{eff}^b in general is less than K_{eff} . The difference in K_{eff}^b and K_{eff} explains the discrepancies in Fig. 2.4(a) because one uses K_{eff} to calculate the solid line while computer simulation are done in the neighborhood where the effective constant is K_{eff}^b .

We can now conclude that for small Δl close to L_{eq} the elastic potentials are parabolic but with K_{eff}^b different from K_{eff} . No theory is available to calculate K_{eff}^b . The second derivative of elastic potential at L gives $K_{eff} = \frac{1 - a^*}{a^*} K$ which can be obtained from the one defect effective medium theory.

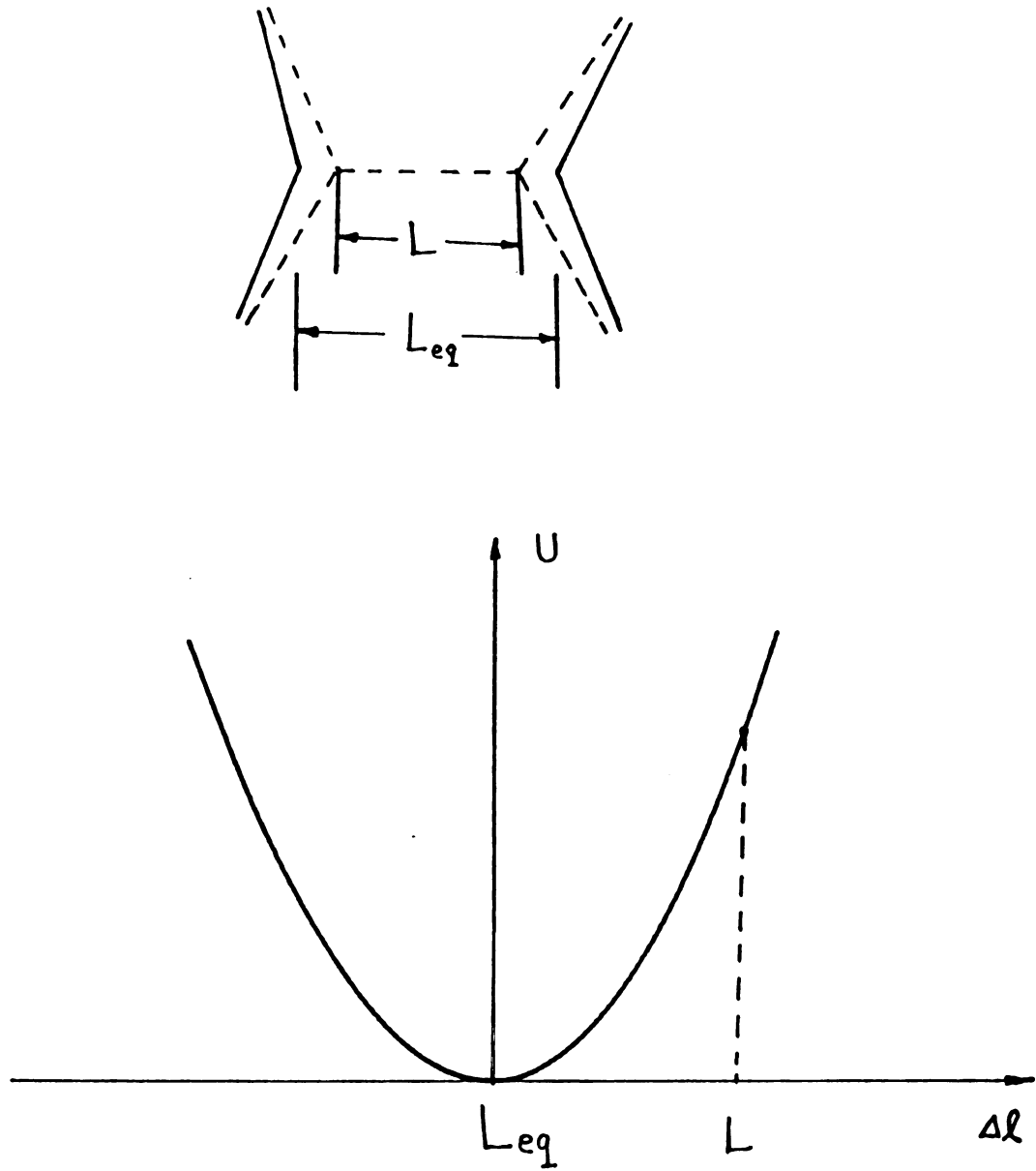


Fig. 2.5 Schematic drawing of the equilibrium positions when a spring is removed and the corresponding elastic potential.

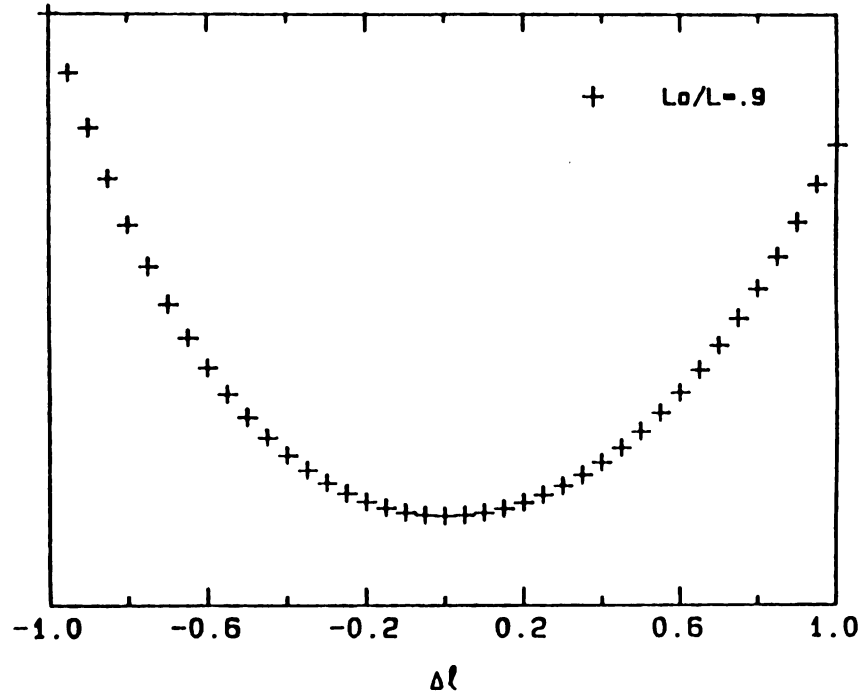
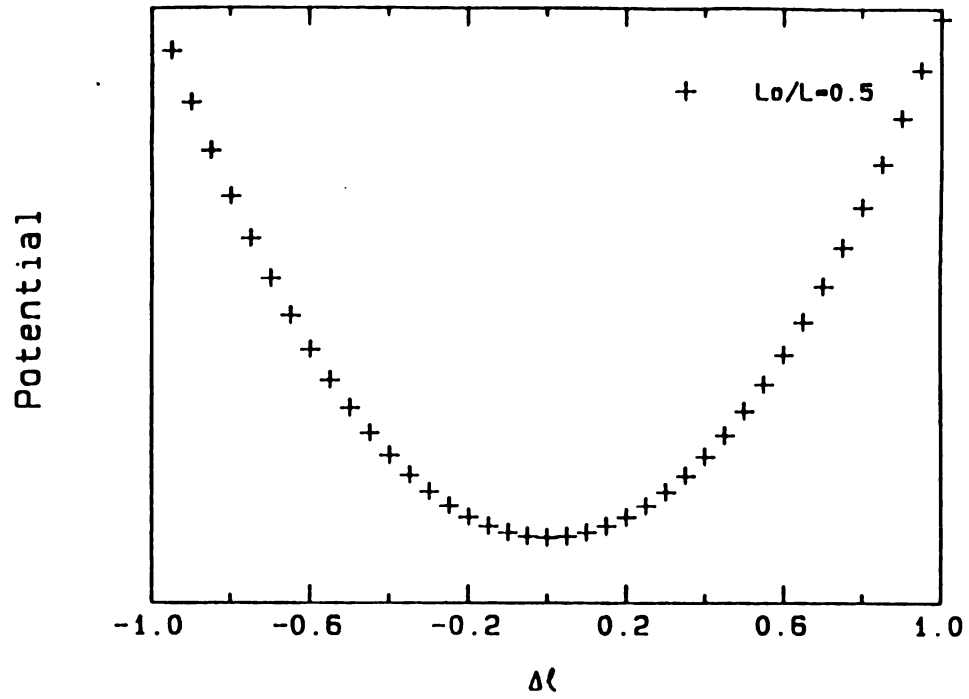


Fig. 2.6 Computer simulation results of the elastic potentials for $L_0/L = 0.5, 0.9$. For small Δl they are parabola.

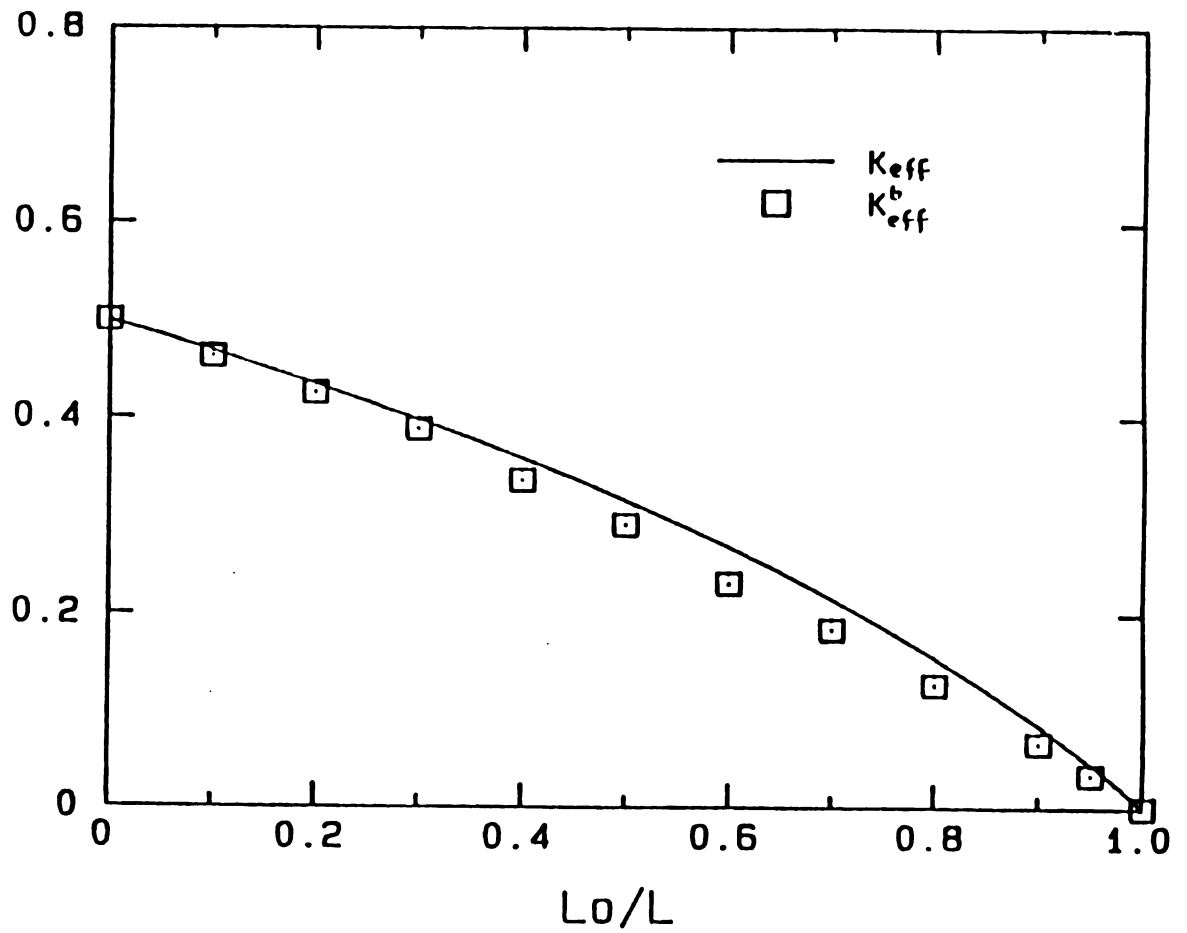


Fig. 2.7 K_{eff} and K_{eff}^b vs. L_0/L . K_{eff} is from (21) and K_{eff}^b is deduced from the computer simulation results of the potential wells.

III Computer Simulations And Effective Medium Theory Approach

Now we discuss the computer simulation results. Simulations are done in the stretched spring region where $0 \leq L_0/L \leq 1$ for the model with elastic energy (6) on the honeycomb lattice. The numerical techniques to relax the network and obtain the static energy(E_0), internal tension (T) and various elastic constants are as follows. Interested readers will find more details from ref. 8.

- (i) For a given L_0 , the honeycomb network is diluted by randomly removed springs with probability $1-p$.
- (ii) The resulting network is then relaxed using the same methods and criteria as in ref. 8.
- (iii) After the relaxation is completed the static energy (E_0) and tension (T) are calculated.
- (iv) Various elastic constants are consequently obtained by applying certain designated small strains in two opposite directions in order to eliminate the linear terms in the elastic energy.

In our computer simulations we calculate the following major quantities: static elastic energy (E_0), internal tension (T) (called pressure in ref.8), bulk modulus (B) and the quantity $b = \frac{1}{2} (C_{11} - C_{12})$. For some samples we also calculate some additional quantities such as $\mu_s = \frac{1}{2} (C_{44} + \tilde{C}_{44})$ and $\mu_r = \frac{1}{2} (C_{44} - \tilde{C}_{44})$ to check the relations (15) and (17). In Fig. 2.8 quantities E_0 , T and B are plotted against probability p for $L_0/L = 0, 0.4, 0.7, 0.8, 0.86$ and 0.9 . The solid lines are the least square fit curves through the data points of the corresponding quantities.

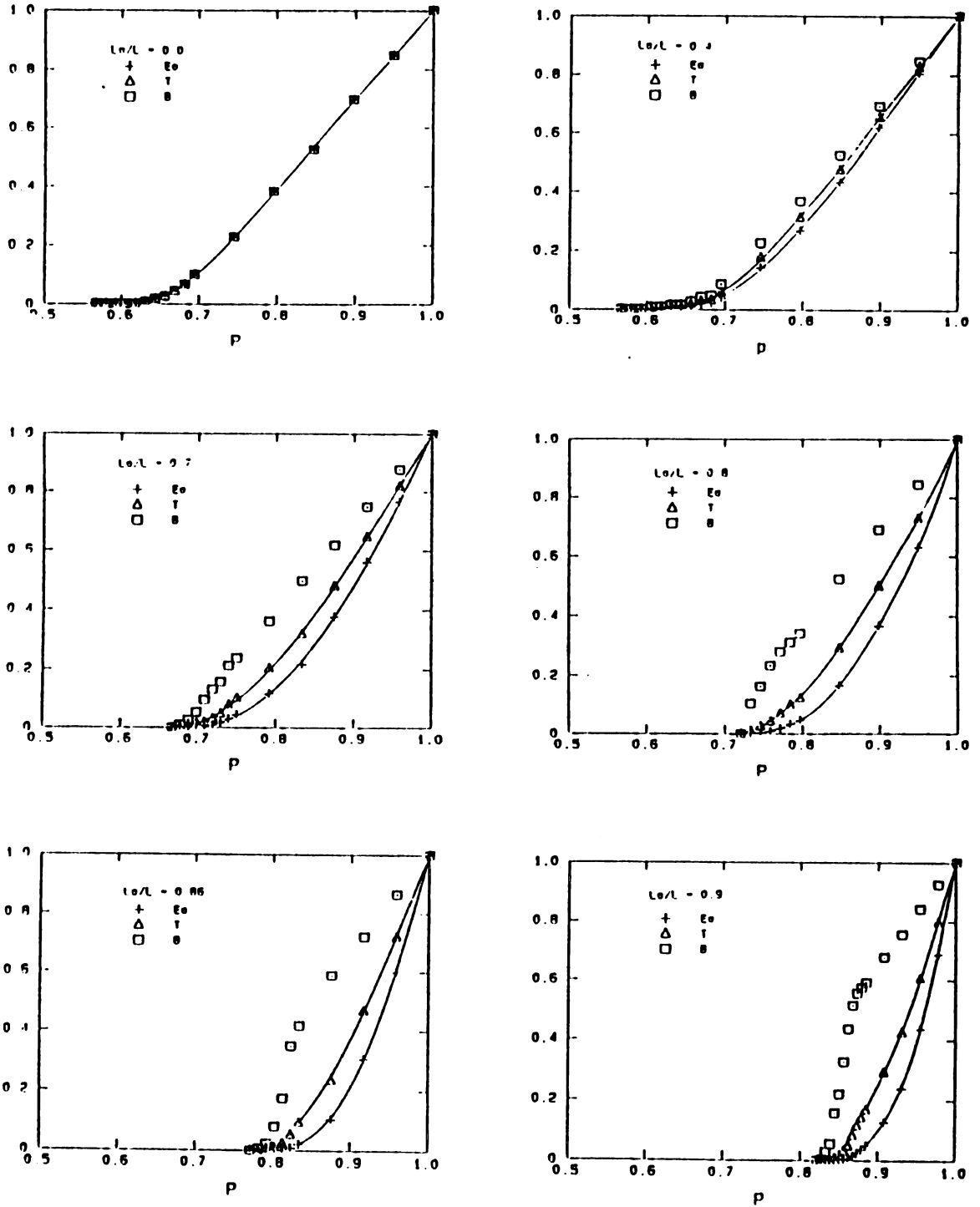


Fig. 2.8 Static energy E_0 , tension T and bulk modulus B are plotted vs. p for $L_0/L = 0, 0.4, 0.7, 0.8, 0.86, 0.9$. Discontinuities in B is clearly observed. The solid lines are the least square fits to the corresponding data points.

We observe the following features in the graphs

(i) Quantities such as E_0 and T decrease almost linearly for small p and vanish at the percolation thresholds for all L_0/L . This is similar to what Tang and Thorpe have observed on triangular lattice⁸.

(ii) The bulk modulus B also decreases almost linearly for small p and vanishes at the percolation thresholds for $L_0/L < 0.8$. For $L_0/L \geq 0.8$ there are sudden drops in bulk modulus B at the percolation thresholds and the magnitudes of the discontinuities increase as L_0/L increases. We start to see the discontinuity about $L_0/L \approx 0.8$. There is some rounding in the discontinuities near the percolation thresholds due to finite size effects and averaging over many different configurations. This is because each different configurations has a distinct discontinuity at a slightly different percolation threshold and the average just smears out the distinct discontinuity. In the limiting case when $L_0/L = 1$ we can think of the magnitude of the discontinuity as one. [see discussion below]

In Fig. 2.9 we present two sets of typical results that can serve to check the two equivalence relations (15) and (17). Fig. 2.9(a) is for $L_0/L = 0.6$ and Fig. 2.9(b) is for $L_0/L = 0.9$. One can see that these two relations are still true in the diluted lattice network where springs are randomly removed. Also the discontinuity in bulk modulus B does not have any effect in the two equivalence relations.

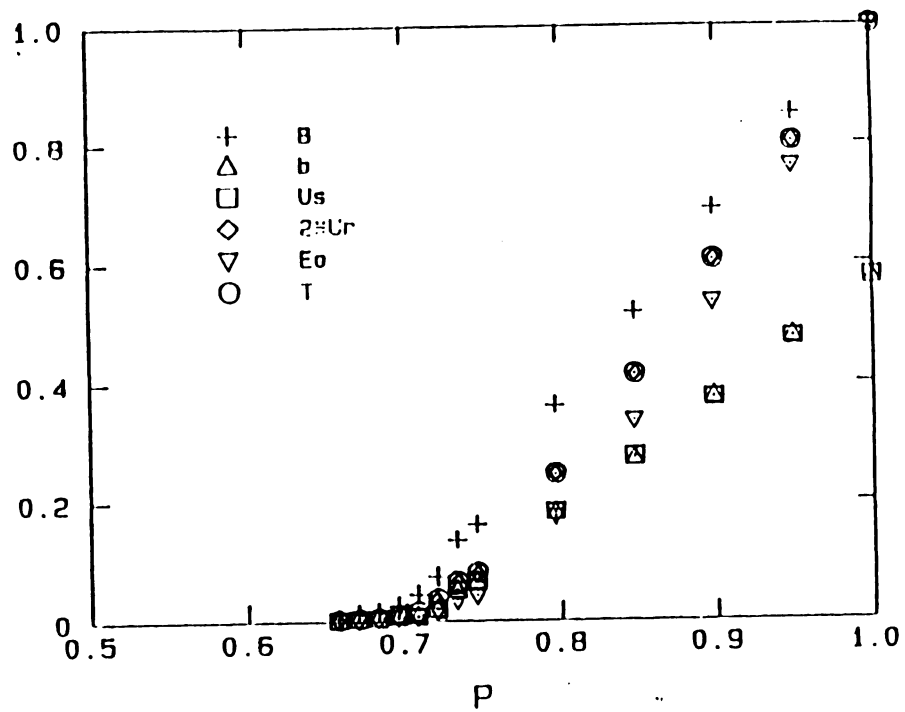
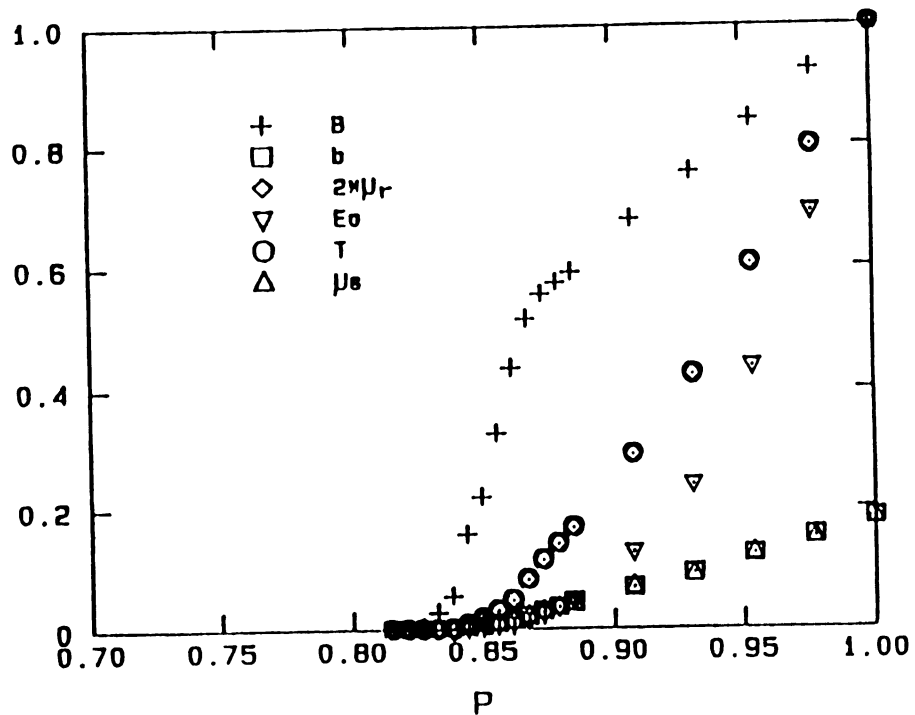
$L_0/L = 0.6$  $L_0/L = 0.9$ 

Fig. 2.9 Equivalence relations $T = 2\mu_r$ (15) and $b = \mu_s$ (17) are checked for $L_0/L = 0.6$ and 0.9 .

It is also interesting to see which quantities have discontinuities at percolation thresholds and which do not. From Fig. 2.9(b) and Fig. 2.10 it is clear that quantities such as E_0 , T , μ_s , μ_r and b are continuous while B , C_{11} and C_{12} are discontinuous at the percolation thresholds. We will discuss the discontinuity in detail below. From Fig. 2.8 one can determine the percolation thresholds for different L_0/L . In Fig. 2.11 the percolation thresholds from the computer simulations are plotted against L_0/L . One may notice that p_c for $L_0/L = 0$ is not $1 - \frac{2}{3} = \frac{1}{3}$. This is because our system is not large enough. By studying different system sizes and using an extrapolating method one may obtain more accurate percolation thresholds. Our purpose here is to show that p_c changes with L_0/L . Fig. 2.11. is called the phase diagram because it indicates two phases. The region above the curve is the region corresponds to the concentration above percolation thresholds and therefore is called rigid phase while the region below the curve is the floppy region and there is a rigid-floppy phase transition cross the boundary. ^{6,14}

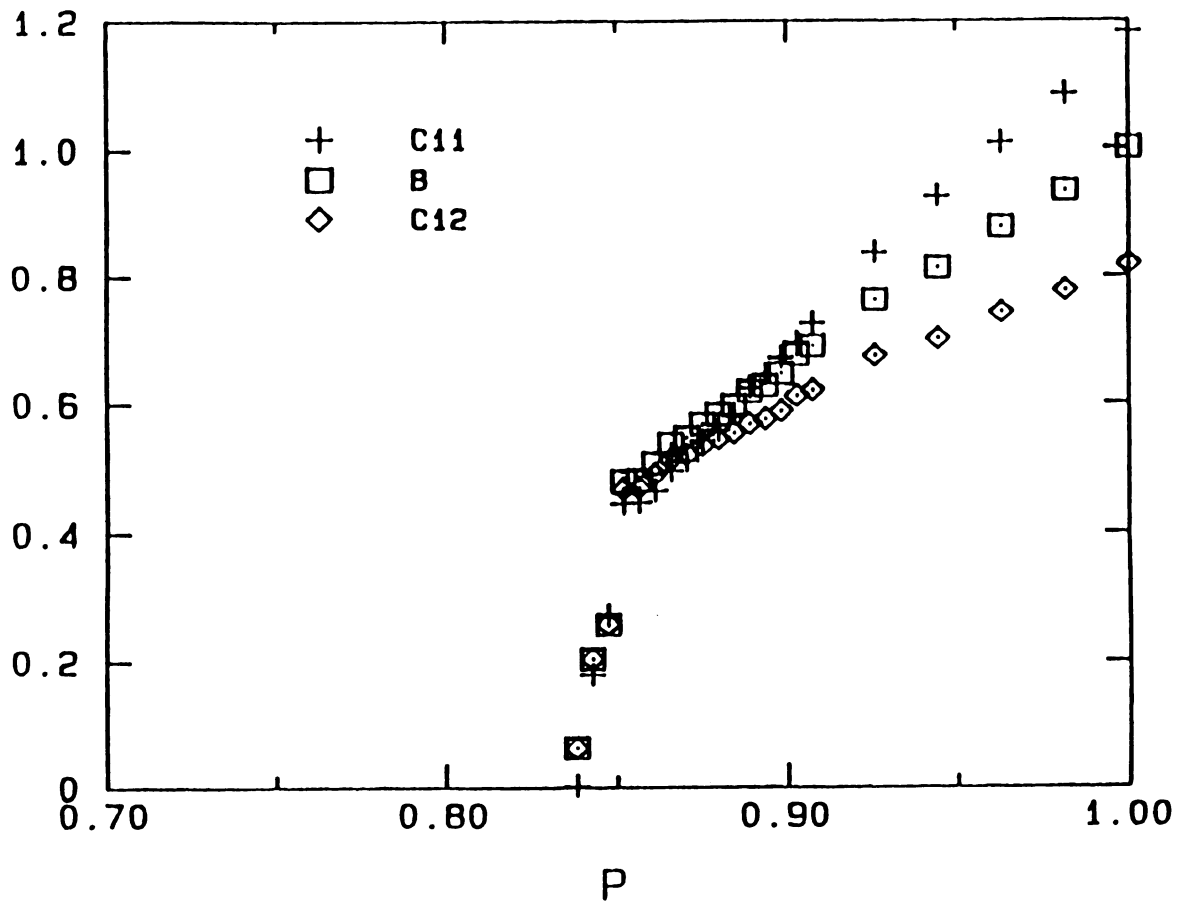


Fig. 2.10 The quantities with sudden discontinuity at percolation threshold such as C_{11} , C_{12} and B are plotted vs. p for $L_0/L = 0.9$.

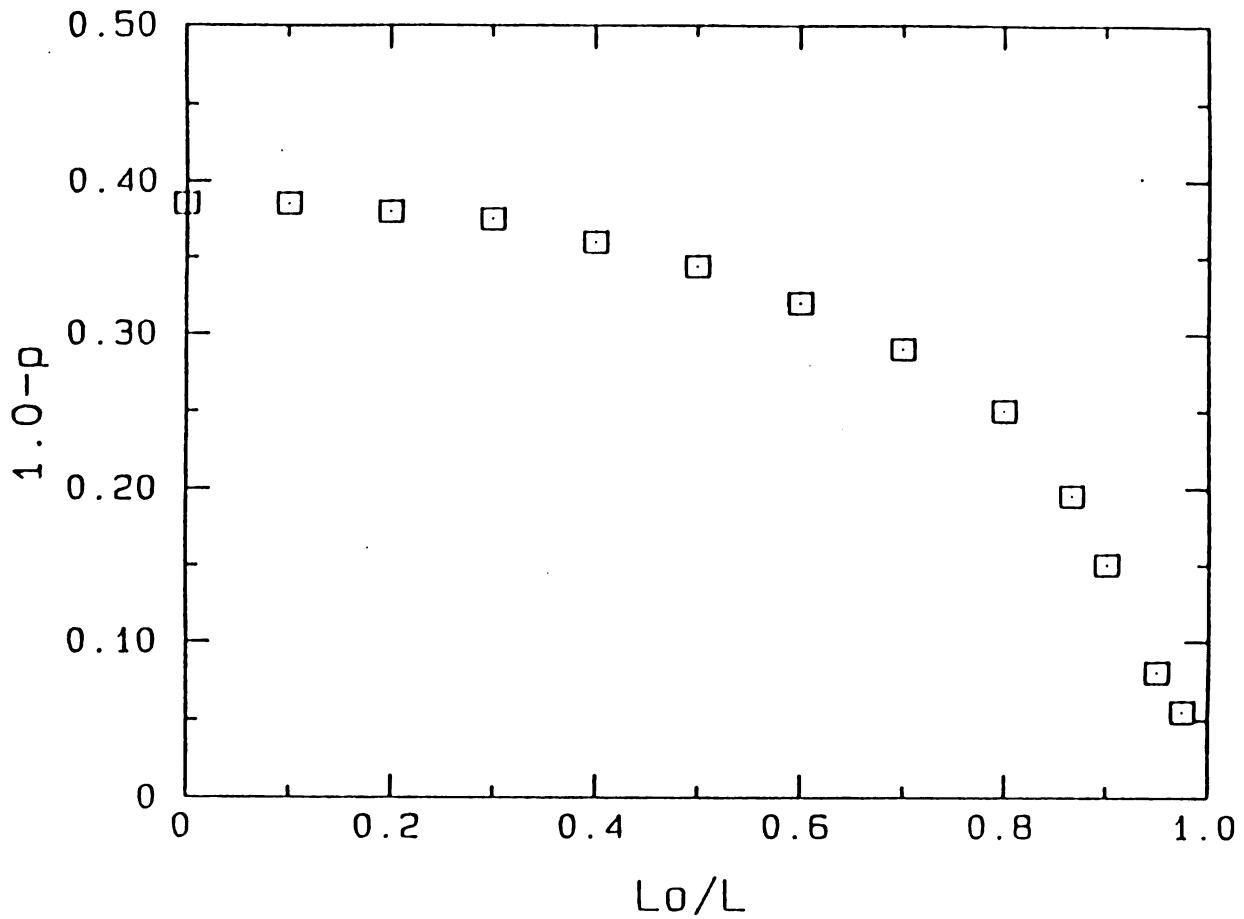
Percolation Threshold vs L_0/L 

Fig. 2.11 The actual percolation thresholds for the stretched spring model from computer simulations are plotted against L_0/L .

(2) Physical Reasons For Discontinuity

We have seen above that simulation results indicate that for $L_0/L \geq 0.8$ quantities such as C_{11} , C_{12} and B have discontinuities at the percolation thresholds. Since the three quantities are related by $B = \frac{1}{2}(C_{11} + C_{12})$ and the deformations associated with C_{11} and B are more readily visualized we consider C_{11} and B here. We only need to discuss the case for B since the arguments applies equally well to C_{11} .

Now let us consider model (6) on a honeycomb lattice with $L_0/L = 1$ which is the central force limit. The perfect lattice has bulk modulus $B = \frac{1}{2\sqrt{3}} K$. Once the system is diluted, for example one spring is removed, then the bulk modulus is zero. The arguments are the following. Suppose the spring between site i and site j is removed. Since each spring is at their natural length then the positions of all sites will not change at all when the spring is removed. If one tries to measure the bulk modulus by applying small strains at the boundaries one will find that sites i and site j can simply pop in with their natural lengths and by doing so to allow other springs to retain their natural lengths.[see Fig. 2.12] This deformation will cost no energy and therefore the bulk modulus is zero. This is verified in computer simulations. In the triangular lattice at the central force limit this argument is not true because site i and site j are connected each by five springs and they can not simply pop in with their natural lengths and by doing so to allow other springs to retain their natural lengths.

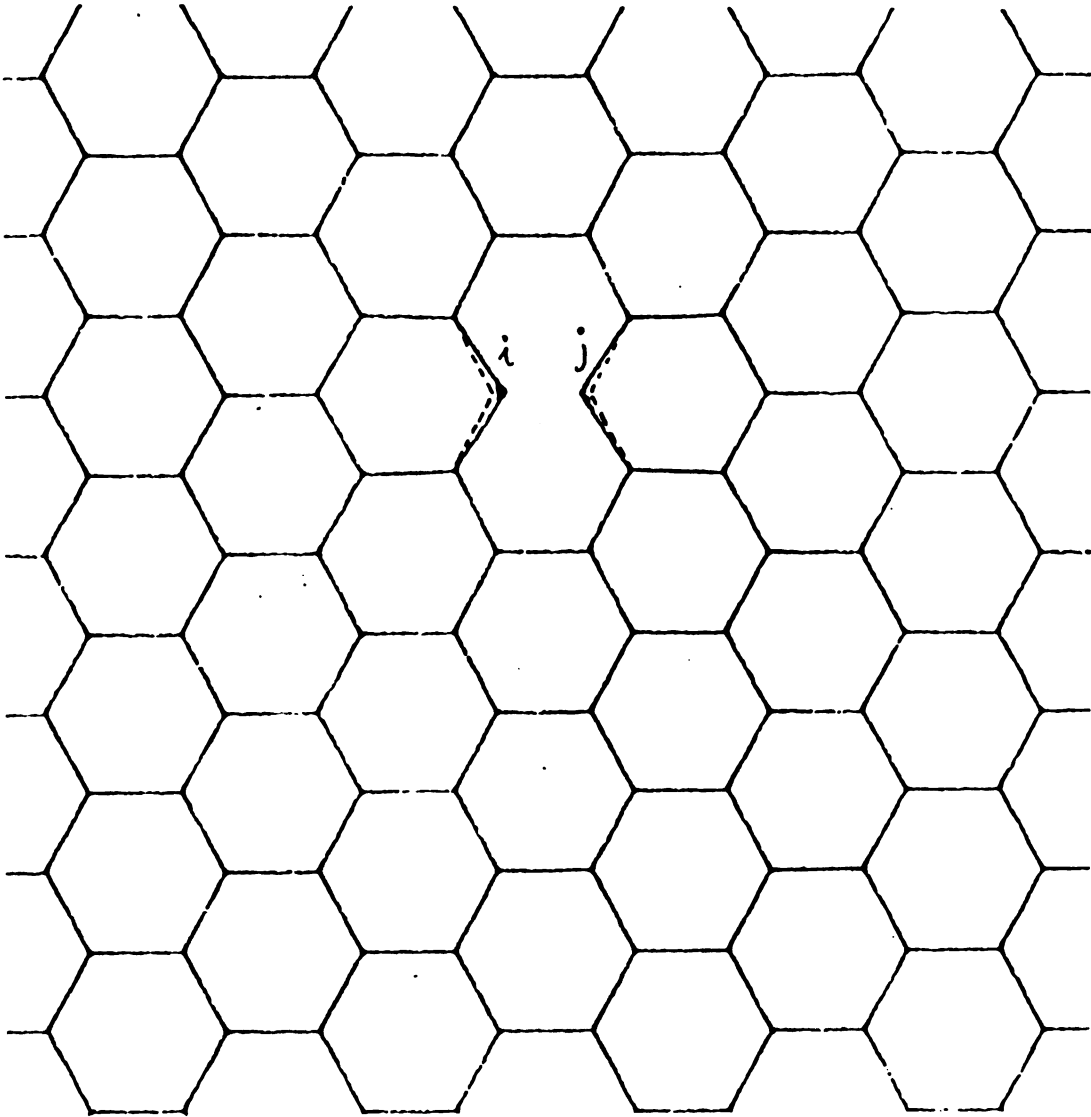


Fig. 2.12 Site i and site j pop in with their natural length and by doing so to allow other springs to retain their natural length which results in the zero bulk modulus.

Notice that when $L_0/L \neq 1$, above argument is also not true on the honeycomb lattice because every spring is stretched and removing just one spring is not enough to relax the remaining springs (which are of order of N) without any change in energy. This is also verified by computer simulations. Now we can conclude that in the central force limit (i. e. $L_0/L = 1$) the honeycomb lattice will have zero bulk modulus if a single spring is removed in the central force limit. One may also recall that shear modulus vanishes even without removing any springs. We will use these instability arguments in the following discussions.

Now we proceed to discuss the physical reasons for the discontinuities in bulk modulus at the percolation thresholds from the effective medium theory point of view. As we mentioned earlier a more sophisticated effective medium theory which is capable of dealing with more defects can be developed. The procedures of constructing such a theory are as follows. When many spring are removed, we can imagine an effective medium surrounds the remaining and missing springs. We can calculate the energy fluctuation of the remaining and missing spring surrounded by the effective medium. The fluctuation in tension between the effective medium and the remaining and missing springs can also be calculated. In this effective medium lattice all springs will have effective strength K_{eff} and effective natural length L_{eff}^0 . Obviously the effective spring constant will be weaker. By requiring that the fluctuation of elastic energy and tension be zero, a set of self-consistent recursive relations can be derived. The detail of this effective medium theory will be in section IV. In this section we emphasize here that in

the process of constructing a multi-defect effective medium theory, one will always obtain an effective medium network with an effective spring constant K_{eff} and an effective spring natural length L_{eff}^0 . So for a given L_0/L when the quantity $L_{\text{eff}}^0/L \rightarrow 1$, as we argued above in the central force limit, the bulk modulus will be zero even if only one effective spring is removed. Since the bulk moduli above the percolation thresholds, for $L_0/L \geq 0.8$, have finite magnitudes which is roughly controlled by the initial slopes in Fig. 2.4 (a), then the bulk moduli at the percolation thresholds require sudden discontinuities to go to zero. Therefore a more sophisticated effective medium theory should be able to explain the sudden discontinuities and predict the percolation thresholds when $L_{\text{eff}}^0/L = 1$.

The quantity L_{eff}^0/L discussed so far is purely from an effective medium theory point of view. To see how it is related to real physical quantities which can be measured, at least in a computer simulation sense, one may do the following analysis. From (8a) and (14e), the static energy and internal tension for the perfect honeycomb lattice are

$$E_0 = \frac{2}{\sqrt{3}} (1 - L_0/L)^2 K \quad (23a)$$

$$T = \frac{1}{\sqrt{3}} (1 - L_0/L) K . \quad (23b)$$

If one uses the physical pictures given by the effective medium theory then one can write down the static energy and internal tension similar

to (23a) and (23b) when springs are removed. By replacing K and L_0/L with K_{eff} and L_{eff}^0/L , we have

$$E_{0(p)} = \frac{2}{\sqrt{3}} (1 - L_{\text{eff}}^0/L)^2 K_{\text{eff}} \quad (24a)$$

$$T_{(p)} = \frac{1}{\sqrt{3}} (1 - L_{\text{eff}}^0/L) K_{\text{eff}} \quad (24b)$$

where p is the probability that a spring is present. Of course $E_{0(p)}$ and $T_{(p)}$ are also functions of L_0/L , but for a given L_0/L they are functions of p . Obviously quantities L_{eff}^0/L and K_{eff} are also functions of p for a given L_0/L . For convenience we denote L_{eff}^0/L by η_{eff} . What we are trying to do here is to extract K_{eff} and η_{eff} from computer simulation results of $E_{0(p)}$ and $T_{(p)}$ and to see whether they are still meaningful and useful when comparing with other simulation results. From (24a) and (24b) we have

$$K_{\text{eff}} = 2T_{(p)}^2/E_{0(p)} \quad (25a)$$

$$\eta_{\text{eff}} = 1.0 - E_{0(p)}/2T_{(p)} \quad (25b)$$

Now we make least square fits, which are plotted in solid lines in Fig. 2.8, to discrete data points of $E_{0(p)}$ and $T_{(p)}$ to obtain values of K_{eff} and η_{eff} against p . In Fig. 2.13 η_{eff} is plotted against p for $L_0/L = 0, 0.2, 0.4, 0.6, 0.7, 0.8, 0.86, 0.9$ and 0.95 . We notice that maximum

value of η_{eff} is one for $L_0/L \geq 0.8$. As we explained before, the bulk modulus drops to zero when η_{eff} hits one.

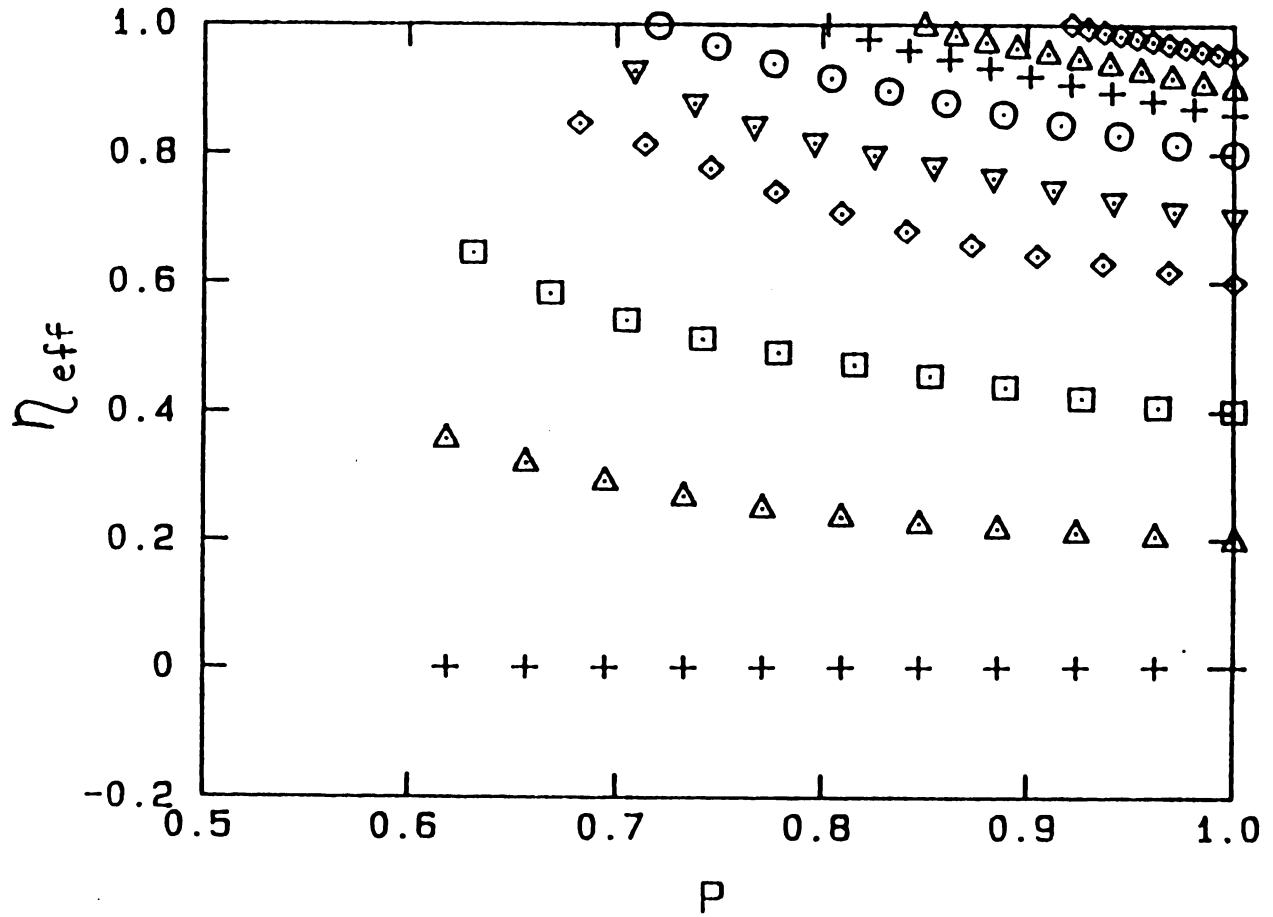


Fig. 2.13 $\eta_{eff} = L_{eff}^0 / L_{eff}$ deduced from the computer simulation results of $E_0(p)$ and $T(p)$ using (25b). The data sets from bottom to top are for $L_0/L = 0, 0.2, 0.4, 0.6, 0.7, 0.8, 0.86, 0.9$ and 0.95 respectively.

One may also recall the equations (14a)-(14d) and (16b) for elasticity of pure honeycomb lattice. By replacing K and η with K_{eff} and η_{eff} one may write down immediately the similar equations for systems with some springs removed. They are as follows

$$C_{11} = \frac{4 - 3\eta_{\text{eff}}}{2 - \eta_{\text{eff}}} \frac{K_{\text{eff}}}{2\sqrt{3}} \quad (26a)$$

$$C_{12} = \frac{\eta_{\text{eff}}}{2 - \eta_{\text{eff}}} \frac{K_{\text{eff}}}{2\sqrt{3}} \quad (26b)$$

$$C_{44} = \frac{(1 - \eta_{\text{eff}})(4 - \eta_{\text{eff}})}{2 - \eta_{\text{eff}}} \frac{K_{\text{eff}}}{2\sqrt{3}} \quad (26c)$$

$$b = \frac{1}{2}(C_{11} - C_{12}) = \frac{2(1 - \eta_{\text{eff}})}{2 - \eta_{\text{eff}}} \frac{K_{\text{eff}}}{2\sqrt{3}} \quad (26d)$$

$$B = \frac{K_{\text{eff}}}{2\sqrt{3}} . \quad (26e)$$

Equation (26e) indicates that B is proportional to K_{eff} . Now we use K_{eff} and η_{eff} extracted from $E_0(p)$ and $T(p)$ and calculate $C_{11}(p)$, $C_{44}(p)$, $B(p)$ and $b(p)$ using (26a-e). The results are plotted vs. p in solid lines in Fig. 2.14 for $L_0/L = 0, 0.4, 0.7, 0.8, 0.86$ and 0.9 . Also plotted in Fig. 2.14 are the corresponding quantities from computer simulations (in symbols).

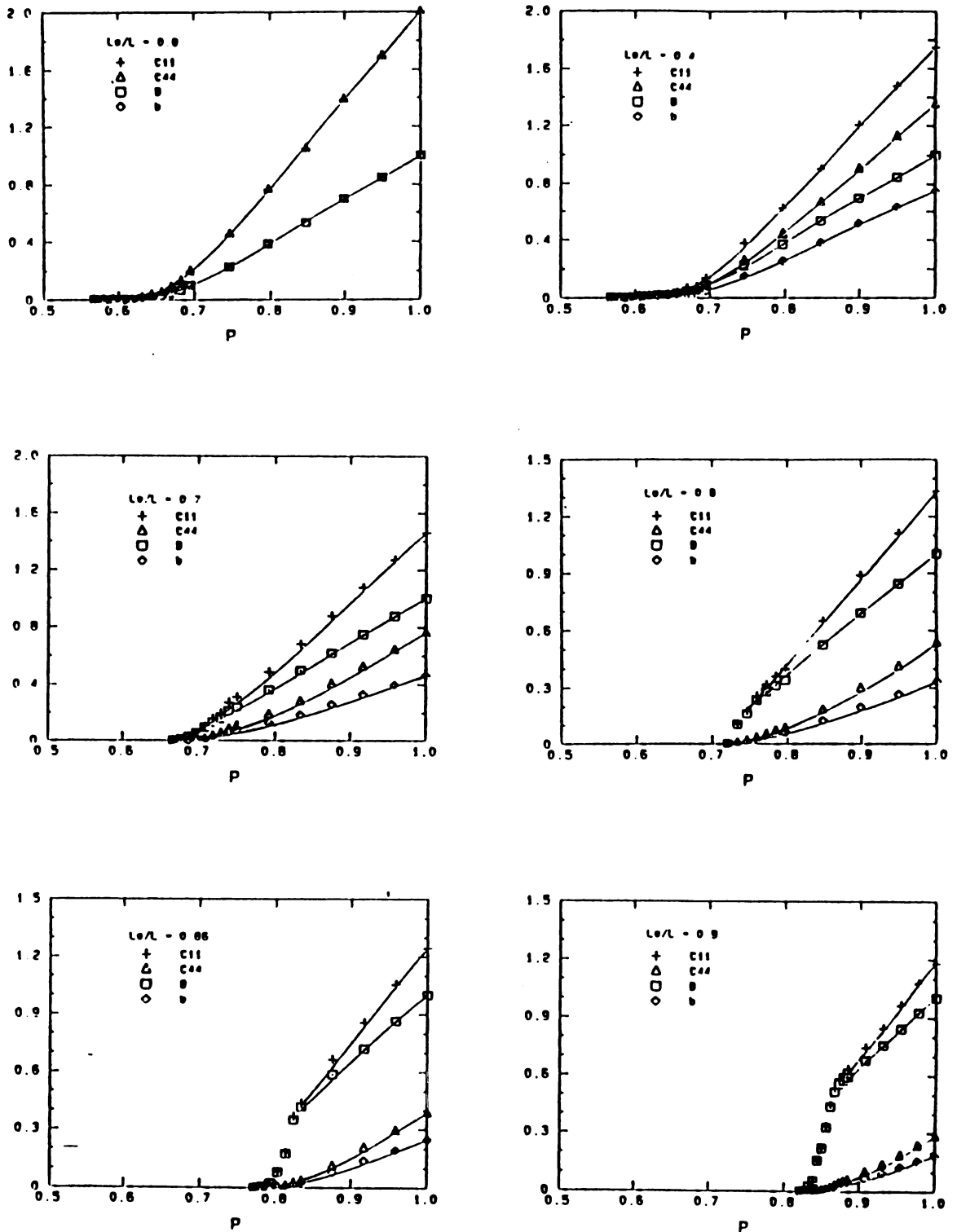


Fig. 2.14 $C_{11}(p)$, $C_{44}(p)$, $B(p)$ and $b(p)$ are plotted vs. p . The symbols are direct computer simulation results and the corresponding solid lines are calculated curves from (26a)-(26e) using only K_{eff} and η_{eff} .

In Fig. 2.14 all quantities are normalized to $\frac{1}{2\sqrt{3}}$. From Fig. 2.14 we observe the following features:

- (i) The agreements between simulation results of C_{11} , C_{44} , b and B and the calculated corresponding quantities using only K_{eff} and η_{eff} from $E_0(p)$ and $T(p)$ are very good.
- (ii) K_{eff} 's decrease to zero with p for $L_0/L < 0.8$ while those stay finite at the percolation thresholds for $L_0/L \geq 0.8$.

Therefore by combining the observations of Fig. 2.13 and 2.14 we can conclude that

- (i) K_{eff} and η_{eff} are very meaningful and useful quantities to study in the stretched spring model.
- (ii) As more and more springs are removed, the static energy E_0 and tension T approach zero with vanishing K_{eff} for $L_0/L < 0.8$ and the bulk moduli decrease to zero continuously.
- (iii) E_0 and T approach zero with vanishing $1.0 - \eta_{\text{eff}}$ for $L_0/L \geq 0.8$ while K_{eff} 's stay finite and the bulk moduli have discontinuities.
- (iv) The two different regions can be distinguished by whether K_{eff} decreases to zero continuously or stays at a finite value at the percolation thresholds.

One more interesting quantity to study is the ratio of C_{44} to C_{11} . From (26a) and (26c) we find

$$\frac{C_{44}}{C_{11}} = \frac{(1 - \eta_{\text{eff}})(4 - \eta_{\text{eff}})}{4 - 3\eta_{\text{eff}}} \quad (27)$$

In Fig. 2.15 we plot C_{44}/C_{11} , from computer simulation results, vs. p . The corresponding solid lines in Fig 2.15 are calculated values of (27) using only K_{eff} and η_{eff} extracted from $E_0(p)$ and $T(p)$. Again they agree very well. The last point of each curve indicates the ratio of C_{44}/C_{11} at percolation threshold. We call this critical ratio of C_{11}/C_{44} . We can see that critical value of C_{44}/C_{11} changes from one for $L_0/L = 0$ to zero for $L_0/L = 1$. In Fig. 2.16(b) critical values of C_{44}/C_{11} are plotted vs. L_0/L . We can see that it is quite close to a straight line. The point where $C_{44}/C_{11} = 0$ corresponds to that where discontinuities in B begin to show up. Fig. 2.16(a) is the same as Fig. 2.11. We can locate the point on the phase diagram where quantity C_{44}/C_{11} is zero by comparing the two graphs. In phase transition language, it turns out (see next section) that there are two types of phase transitions across the boundary. In the region $L_0/L < 0.8$, where C_{44}/C_{11} are finite, the rigid to floppy phase transitions are of second order, as studied before^{8,14}, while those for $L_0/L \geq 0.8$ are first order. Therefore there is a tricritical point about $L_0/L \sim 0.8$ in the phase diagram Fig. 2.15(a) to separate the two different types of the phase transitions. Using Landau type phase transition theory we can also study the smoothness of phase boundary at the tricritical point.

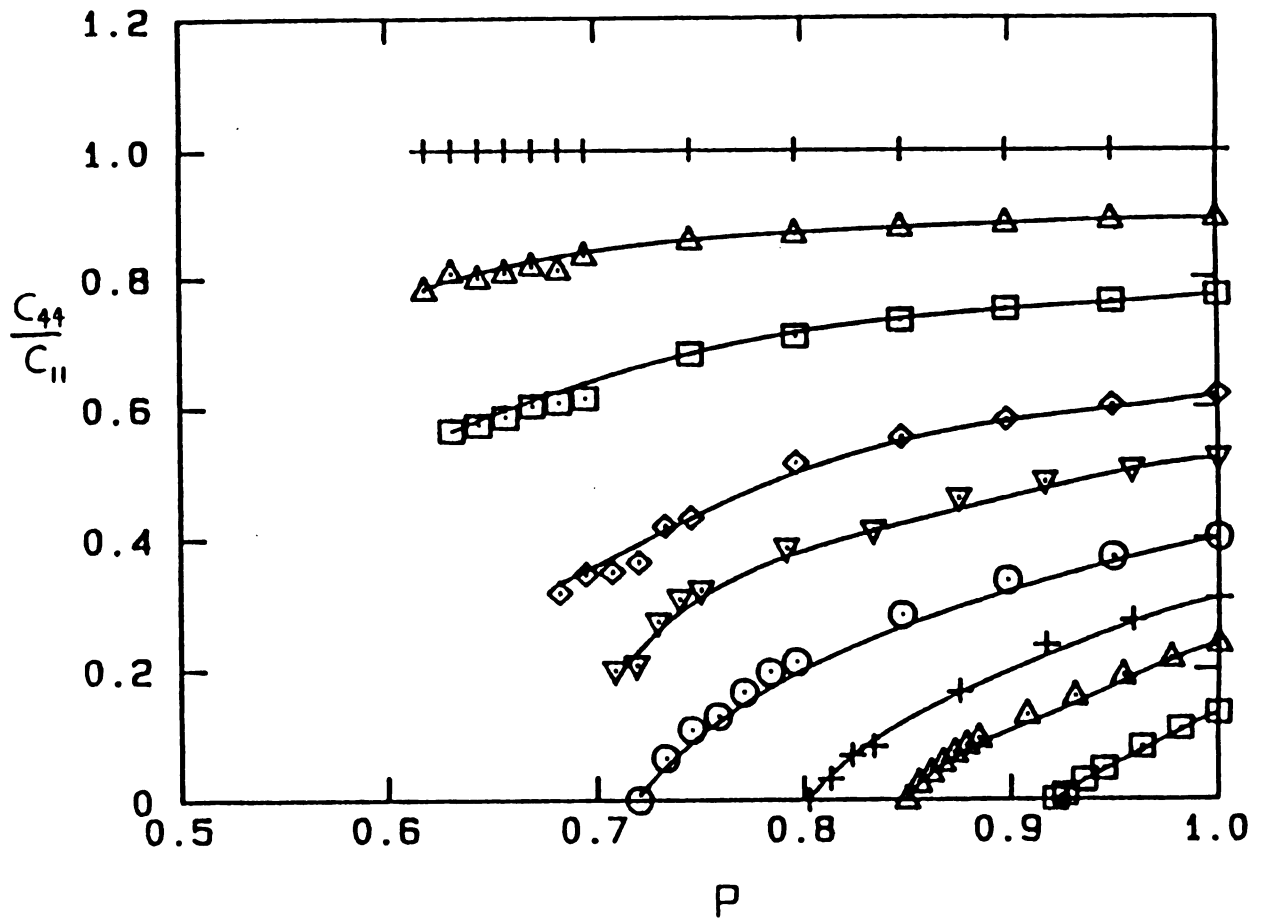


Fig. 2.15 C_{44}/C_{11} are plotted vs. p . The symbols are from direct computer simulation results of C_{11} and C_{44} and the corresponding solid lines are the calculated curves using (27). The data set from bottom to top are for $L_0/L = 0, 0.2, 0.4, 0.6, 0.7, 0.8, 0.86, 0.9$ and 0.95 .

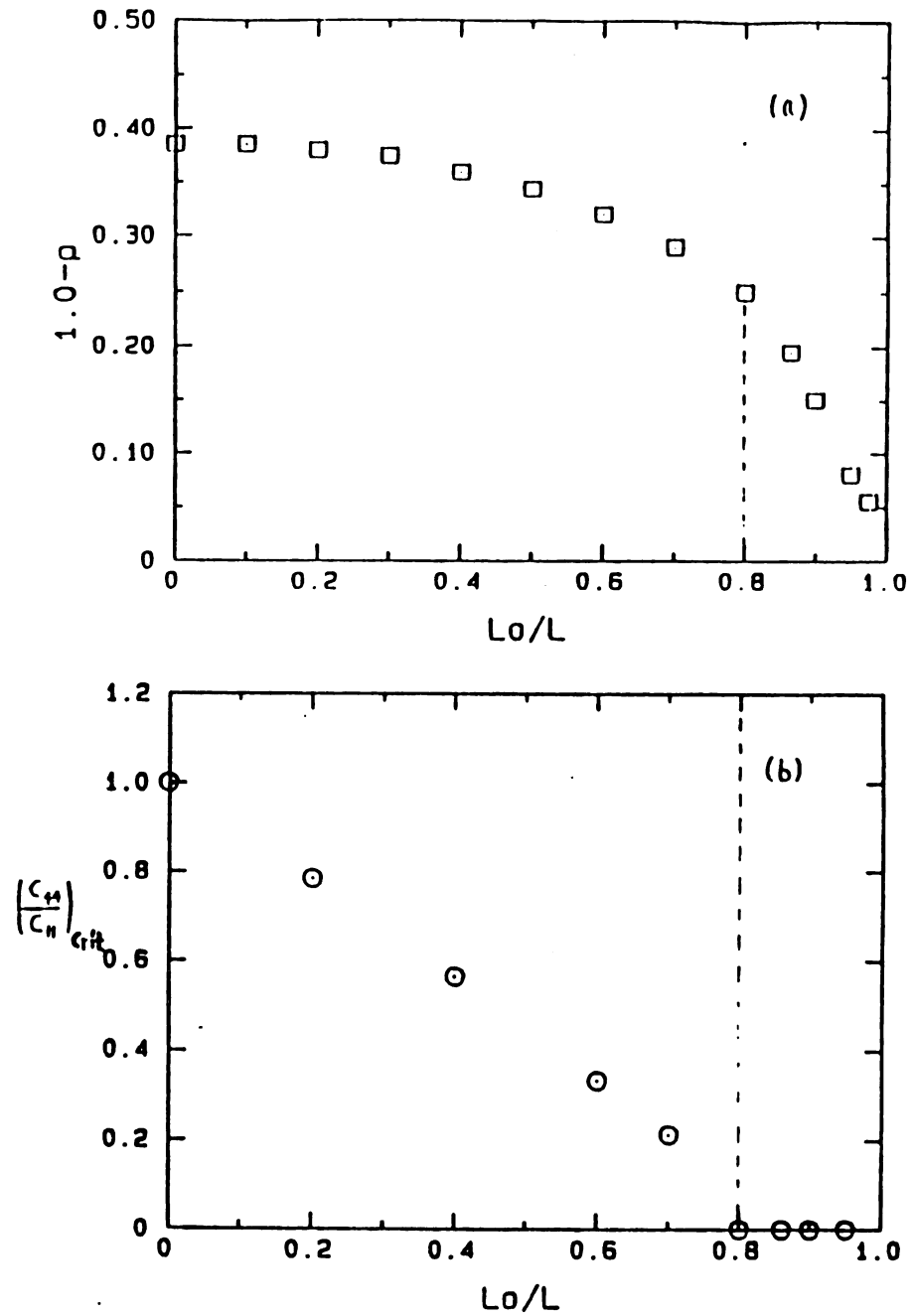


Fig. 2.16 (a) is the same as Fig. 2.10. In (b) the critical ratio C_{44}/C_{11} is plotted vs. L_0/L . A tricritical point about $L_0/L \approx 0.8$ is located.

IV Tricritical Point and Effective Medium Theory

We have seen in the previous section that the phase diagram Fig. 2.11 can be divided into two regions in which bulk modulus (or K_{eff}) behaves differently. For $L_0/L \leq 0.8$, the bulk modulus (or K_{eff}) decreases with decreasing p and vanishes at the percolation threshold. The phase transition in this region is of the conventional second order rigid \rightarrow floppy phase transition^{6,14}. For $L_0/L > 0.8$, on the other hand, the bulk modulus (or K_{eff}) drops discontinuously at the percolation threshold and the transition in this region is of a first order phase transition. In order to understand this we first study the Landau type phase transition theory and draw an parallel analogy between the phase transition theory and what we have observed in the computer simulations.

(1) Landau Phase Transition Theory and the Tricritical Point

In a conventional Landau type phase transition theory,^{15,16} the free energy can be written as

$$F = \frac{1}{2}a M^2 + \frac{1}{4}b M^4 + \frac{1}{6}c M^6 - H M \quad (28)$$

where M is the order parameter which indicates the phase transition, H is the external field, a , b , and c are the phenomenological constants independent of M . In (28) the coefficients of M^3 and M^5 terms are zero due to the symmetry of the system. In the magnetic model, for example,

M is the magnetization and H is the external magnetic field. When considering a second order phase transition, $b > 0$ and c can be neglected. Thus the free energy has the following form

$$F = \frac{1}{2}a M^2 + \frac{1}{4}b M^4 - H M \quad (29)$$

and
$$\frac{\partial F}{\partial M} = a M + b M^3 - H \quad (30)$$

$$\frac{\partial^2 F}{\partial M^2} = a + 3b M^2 \quad (31)$$

The sufficient condition for the maximum and minimum of the free energy (30) is

$$\frac{\partial F}{\partial M} = a M + b M^3 - H = 0$$

Depending on whether $\frac{\partial^2 F}{\partial M^2}$ is greater than zero or less than zero the free energy will be at minimum or maximum. For the convenience of the discussion we set $a = a_0(T - T_c)$ where T can be regarded as the temperature. The different cases are discussed below. We use \bar{M} to denote the order parameter at the minimum or maximum.

(i) When $H = 0$, $T > T_c$ (i.e. $a > 0$) and $b > 0$, it is easy to see that $\bar{M} = 0$ is the only minimum. Therefore in this phase the order parameter is zero.

(ii) When $H = 0$, $T < T_c$ and $b > 0$, it can be shown that $M = \pm M_{\pm} = \left[\frac{a_0(T_c - T)}{b} \right]^{1/2}$ are the minima of the system. Thus in this phase as $T \rightarrow T_c$ (a critical point) the order parameter M decreases continuously to zero.

Combining (i) and (ii) we see that the order parameter decreases to zero and is continuous at the critical point $T = T_c$. Therefore the transition is of the second order. In the case when b is equal or less than zero, we must consider the M^6 term. So the free energy is

$$F = \frac{1}{2}a M^2 + \frac{1}{4}b M^4 + \frac{1}{6}c M^6 - H M \quad (32)$$

and
$$\frac{\partial F}{\partial M} = a M + b M^3 + c M^5 - H \quad (33)$$

$$\frac{\partial^2 F}{\partial M^2} = a + 3b M^2 + 5c M^4 \quad (34)$$

For convenience c is set to be positive. When $H = 0$, using $\frac{\partial F}{\partial M} = 0$, we expect the free energy reaches minimum or maximum at $\bar{M} = 0$, $\pm M_{\pm}$ and $\pm M_{\pm}$ where

$$M_{\pm}^2 = \frac{1}{2c} [-b \pm (b^2 - 4a_0(T - T_c)c)^{1/2}] \quad (35)$$

Now we discuss the following cases when $H = 0$.

(i) If $a < 0$, it can be shown that $\bar{M} = \pm M_{\pm}$ correspond to two minima while $\bar{M} = 0$ to a maximum.

(ii) If $a_0(T-T_c) > 0$, and $b > 0$ then $\bar{M} = 0$ is the only minimum and therefore in this phase the order parameter is zero.

(iii) If $a_0(T-T_c) > 0$ and $b < 0$ then the minima of the free energy occur at $\bar{M} = 0, \pm M_+$. It can be shown that $F_{(\pm M_+)} \geq 0$. So $\bar{M} = \pm M_+$ may not be the lowest minima. This is true in the phase where $\bar{M} = 0$ is the lowest minimum. Since $F_{(0)} = 0$, the location of the other two minima is determined by requiring $F_{(\pm M_+)} = 0$. Thus we have three co-minima in this phase. Using $F_{(\pm M_+)} = 0$ and $\frac{\partial F}{\partial M} \Big|_{M=\pm M_+} = 0$ we obtain

$$M_+^2 = - \frac{4a_0(T-T_c)}{b} \quad (36)$$

From (iii) we can conclude that in one phase $\bar{M} = 0$ and in the other phase $\bar{M} = M_+ = \left[- \frac{4a_0(T_1-T_c)}{b} \right]^{1/2}$. In general $T_1 \neq T_c$, therefore the order parameter changes discontinuously at the critical point T_1 . The jump or the discontinuity in M is $\Delta M = \left[- \frac{4a_0(T_1-T_c)}{b} \right]^{1/2}$ where T_1 is the first order phase transition point. The phase boundary for the first order transition is determined by equating (35) and (36)

$$\text{i.e.} \quad \frac{1}{2c} [-b \pm (b^2 - 4a_0(T_1 - T_c)c)^{1/2}] = - \frac{4a_0(T_1 - T_c)}{b} \quad (37)$$

From (37) we obtain

$$b = -4[ca_0(T_1 - T_c)/3]^{1/2}$$

or

$$T_1 = T_c + \frac{3b^2}{16a_0c} \quad (38)$$

In Fig. 2.17 we plotted the phase boundary T vs. b . For $b < 0$ the phase transition is of the first order while for $b > 0$ the transition is of the second order. The two regions meet at $b = 0$ where the discontinuity ΔM vanishes. This point is called the tricritical point. We also notice that the first derivative, with respect to b , of the phase boundary at the tricritical point is continuous.

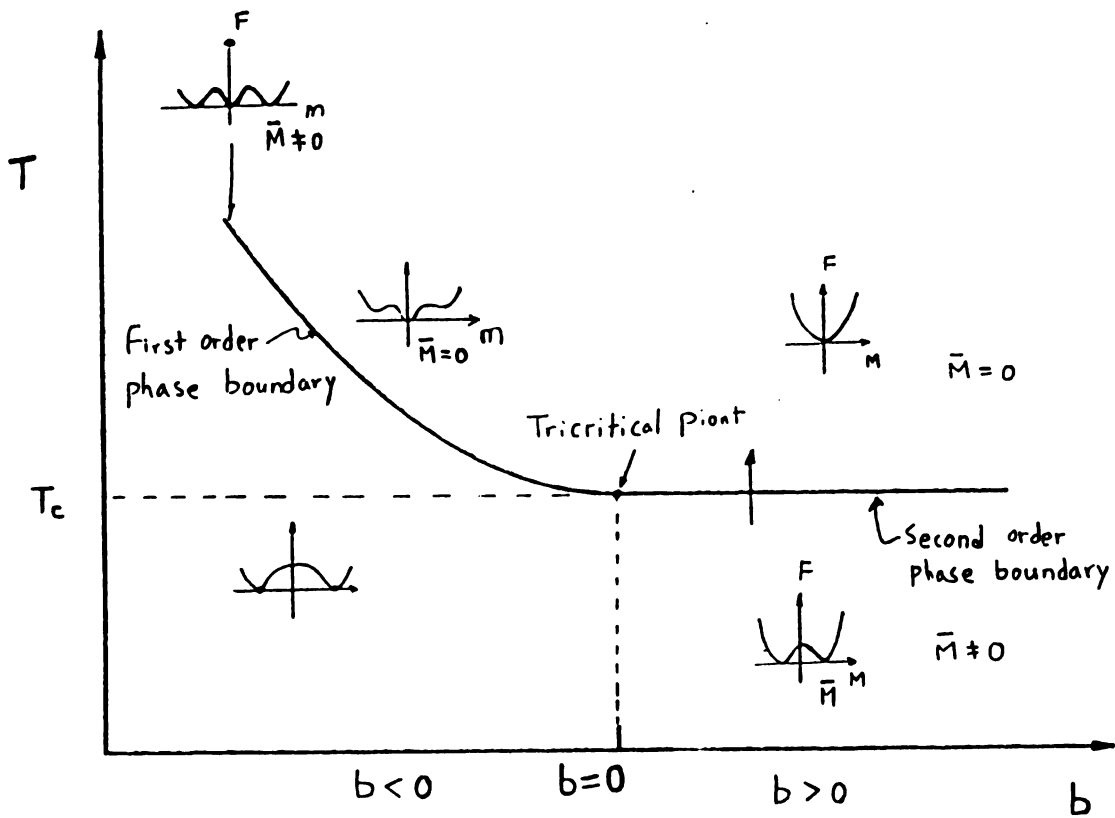


Fig. 2.17 The phase boundary is plotted vs. b . For $b < 0$ the transition is first order while $b > 0$ the transition is second order. $b = 0$ is the tricritical point.

With above phase transition picture in mind, we are ready to draw an analogy between the conventional Landau theory and the observation in the simulations. An analogy between the phase transition theory and the geometric percolation theory was suggested almost two decades ago¹⁷. Of course this was restricted to the second order phase transition. The quantity p , the probability that a spring is present, corresponds to the temperature T in the phase transition theory. Thus the percolation threshold corresponds to the critical transition temperature. The quantity similar to the order parameter in percolation theory is the probability, denote by $P(p)$, that a site chosen at random belongs to the infinite cluster. $P(p)$ is a much more difficult quantity to study in the elastic percolation problem than in the geometric percolation problem⁵. The bulk modulus, on the other hand, is a much easier quantity to study and has the same behavior as $P(p)$, so we choose the bulk modulus as the order parameter. The analogy is quite obvious now. For $L_0/L \leq 0.8$, the bulk modulus decreases continuously to zero and is continuous from rigid phase to floppy phase. Therefore the transition is a second order phase transition. For $L_0/L > 0.8$ the bulk modulus drops to zero discontinuously from the rigid phase to floppy phase and the transition is a first order one. There is a tricritical point around $L_0/L \sim 0.8$ to separate the phase diagram into two regions. Here L_0/L is similar to b in the phase transition theory. Our computer simulation results indicate that there is a tricritical point near $L_0/L \sim 0.8$, and a more accurate determination of the tricritical point needs more computer simulations. This tricritical point can be determined from the

phase transition theory once the phenomenological constants a , b and c are known, but unfortunately this is not the case here. Thus we have to determine the tricritical point from an new effective medium theory described below.

(2) Effective Medium Theory

We start discussing the effective medium theory by first considering the case where only one spring is removed. As shown in Fig. 2.5, when a spring is removed the distance between the sites, where the spring is removed, will change from L to L_{eq} . Let us assume that the resulting spring network will have an effective elastic constant K_e if the distance is restored back to its original length before any spring is removed [also see discussions in appendix II]. Therefore after one spring is removed the elastic energy is decreased by

$$\Delta E = -\frac{1}{2}K(L - L_0)^2 - \frac{1}{2}K_e(L - L_{eq})^2 \quad (39)$$

where K and L_0 are the spring constant and natural length of the removed spring. The first term is due to the missing spring and the second term is due to the relaxation afterward. By minimizing ΔE with respect to L we have

$$\frac{\partial \Delta E}{\partial L} = K(L - L_0) + K_e(L - L_{eq}) = 0 \quad (40)$$

From (40) we obtain

$$L_{eq} = L + \frac{K}{K_e} (L - L_0) \quad (41)$$

Using $K_e = K \frac{1 - a^*}{a}$ where a^* is equal to $P_{(E)}$ as in (19), (41) becomes

$$L_{eq} = \frac{L - L_0 a^*}{1 - a^*} \quad (42)$$

We have discussed in section II that $K_e = K \frac{1 - a^*}{a}$ is just an approximation, but it is a rather good approximation. Substituting (42) back to (39) and using $K_e = K \frac{1 - a^*}{a}$, the energy change ΔE can be written as

$$\Delta E = -\frac{1}{2} K (L - L_0)^2 / (1 - a^*) \quad (43)$$

Eq. (43) indicates that removing one spring decreases more elastic energy than $\frac{1}{2}K(L - L_0)^2$. This is because the network is under tension ($L \neq L_0$) and the relaxation to L_{eq} releases an additional amount of elastic energy.

Now let us add a spring of spring constant K' and natural length L'_0 in the place of the missing spring. The elastic energy will increase by

$$\Delta E = +\frac{1}{2}K'(L' - L'_0)^2 + \frac{1}{2}K_e(L' - L_{eq})^2 \quad (44)$$

Again the first term is simply due to the added spring and the second term is due to the relaxation of the distance from L_{eq} to L' afterward. By minimizing ΔE with respect to L' we have

$$\frac{\partial \Delta E}{\partial L'} = K(L' - L'_0) + K_e(L' - L_{eq}) = 0 \quad (45)$$

So

$$L' = \frac{K_e L_{eq} + K' L'_0}{K' + K_e} \quad (46)$$

where K_e and L_{eq} are the same as defined before. Substituting (46) back to (44) and using (42), the energy change can be written as

$$\Delta E = \frac{1}{2} \frac{K' K_e}{K' + K_e} \left(\frac{L - L_0}{1 - a^*} - L'_0 + L_0 \right)^2$$

The net energy change after replacing a single spring of K and L_0 with K' and L'_0 is then

$$\begin{aligned} \Delta E &= \frac{1}{2} \frac{K' K_e}{K' + K_e} \left(\frac{L - L_0}{1 - a^*} - L'_0 + L_0 \right)^2 - \frac{K}{2} \frac{(L - L_0)^2}{1 - a^*} \\ &= \frac{K}{2(1 - a^*)} \left[\frac{K'}{K'a^* + K(1 - a^*)} (L - L_0 a^* - L'_0 + L'_0 a^*)^2 - (L - L_0)^2 \right] \quad (47) \end{aligned}$$

If $K' = 0$, Eq. (47) is reduced to (43). If $K' = K$ and $L'_0 = L_0$ then $\Delta E = 0$ as expected. So (47) is checked.

We now construct an effective medium theory using (47). For a given L_0/L at p , from the effective medium point of view, we can imagine an effective medium elastic network of N effective springs with spring constant K^α and natural length L_0^α . Here the superscript α denotes the quantities of the effective medium network. Of course K^α and L_0^α are functions of p for a given L_0/L . Let us replace n effective springs with n springs of strength K_i and natural length L_{0i} . Therefore the total energy of the resulting effective network, using (47) and replacing * with α , is

$$E = E_0 + \Delta E = \frac{NK^\alpha}{2} (L - L_0^\alpha)^2 + \frac{1}{2} \sum_i \frac{K_i K_e}{K_i + K_e} \left[\frac{L - L_0^\alpha}{1 - a^\alpha} - L_{0i} + L_0^\alpha \right]^2 - \frac{1}{2} \sum_i \frac{K^\alpha (L - L_0^\alpha)^2}{1 - a^\alpha} \quad (48)$$

where $K_e = K^\alpha \frac{1 - a^\alpha}{a^\alpha}$ and $a^\alpha = a^\alpha(L_0^\alpha/L)$. The first term, denoted by E_0 , in (48) is the static elastic energy of a perfect effective medium network similar to (24a). The second and third term, denoted by ΔE , are the energy fluctuations due to replacing n effective springs with springs of K_i and L_{0i} . In (48) we neglect the interactions between the replaced springs. The tension is defined by $T = - \frac{\partial E}{\partial V}$. In 2D, $T = - \frac{1}{2L} \frac{\partial E}{\partial L}$. Using (48) we obtain

$$\begin{aligned}
T \sim - \frac{\partial E}{\partial L} = T_0 + \Delta T = & -NK^\alpha(L - L_0^\alpha) - \sum_i \frac{K_i K_e}{K_i + K_e} \left[\frac{L - L_0^\alpha}{1 - a^\alpha} - L_{0i} + L_0^\alpha \right] \frac{1}{1 - a^\alpha} \\
& + \sum_i \frac{K^\alpha(L - L_0^\alpha)}{1 - a^\alpha} + b^\alpha \frac{L_0^\alpha}{L^2} \left\{ \sum_i \frac{K_i K_e}{K_i + K_e} \left[\frac{L - L_0^\alpha}{1 - a^\alpha} - L_{0i} + L_0^\alpha \right] \frac{L - L_0^\alpha}{(1 - a^\alpha)^2} \right. \\
& \left. - \frac{1}{2} \sum_i \left(\frac{K_i}{K_i + K_e} \right)^2 \frac{K^\alpha}{a^{2\alpha}} \left[\frac{L - L_0^\alpha}{1 - a^\alpha} - L_{0i} + L_0^\alpha \right]^2 - \frac{1}{2} \sum_i \frac{K^\alpha(L - L_0^\alpha)^2}{(1 - a^\alpha)^2} \right\} \quad (49)
\end{aligned}$$

where $b^\alpha = \frac{\partial a^\alpha}{\partial \eta^\alpha}$ and $\eta^\alpha = L_0^\alpha / L$. In obtaining (49) one should realize that K_e and a^α are also the functions of L . The first term in (49) is the static tension, denoted by T_0 , similar to (24b) and the second term and third term are the fluctuations of tension, denoted by ΔT , in the diluted effective medium network. By requiring

$$\langle \Delta E \rangle = 0 \quad (50a)$$

$$\langle \Delta T \rangle = 0 \quad (50b)$$

we obtain two equations describing the effective medium network. In (50), $\langle \rangle$ implies the anseble average. The two equations are

$$\frac{1}{N} \sum_i \frac{K_i K_e}{K_i + K_e} \left[\frac{L - L_0^\alpha}{1 - a^\alpha} - L_{0i} + L_0^\alpha \right]^2 = \frac{1}{N} \sum_i \frac{K^\alpha(L - L_0^\alpha)^2}{1 - a^\alpha} \quad (51a)$$

$$\begin{aligned}
& \frac{1}{N} \sum_i \frac{K_i K_e}{K_i + K_e} \left[\frac{L - L_0^\alpha}{1 - a^\alpha} - L_{0i} + L_0^\alpha \right] \frac{1}{1 - a^\alpha} - \frac{1}{N} \sum_i \frac{K^\alpha (L - L_0^\alpha)}{1 - a^\alpha} = \\
& b^\alpha \frac{L_0^\alpha}{L^2} \left\{ \frac{1}{N} \sum_i \frac{K_i K_e}{K_i + K_e} \left[\frac{L - L_0^\alpha}{1 - a^\alpha} - L_{0i} + L_0^\alpha \right] \frac{L - L_0^\alpha}{(1 - a^\alpha)^2} \right. \\
& \left. - \frac{1}{2N} \sum_i \left(\frac{K_i}{K_i + K_e} \right)^2 \frac{K^\alpha}{a^{2\alpha}} \left[\frac{L - L_0^\alpha}{1 - a^\alpha} - L_{0i} + L_0^\alpha \right]^2 - \frac{1}{2N} \sum_i \frac{K^\alpha (L - L_0^\alpha)^2}{(1 - a^\alpha)^2} \right\} \quad (51b)
\end{aligned}$$

In our case $K_1 = K$ and $L_{01} = L_0$ with probability p , and $K_2 = 0$ with probability $1-p$. So (51a) and (51b) become

$$p \frac{K K_e}{K + K_e} \left[\frac{L - L_0^\alpha}{1 - a^\alpha} - L_0 + L_0^\alpha \right]^2 = \frac{K^\alpha (L - L_0)^\alpha}{1 - a^\alpha} \quad (52a)$$

$$\begin{aligned}
& p \frac{K K_e}{K + K_e} \left[\frac{L - L_0^\alpha}{1 - a^\alpha} - L_0 + L_0^\alpha \right] \frac{1}{1 - a^\alpha} - \frac{K^\alpha (L - L_0)^\alpha}{1 - a^\alpha} = \\
& b^\alpha \frac{L_0^\alpha}{L^2} \left\{ p \frac{K K_e}{K + K_e} \left[\frac{L - L_0^\alpha}{1 - a^\alpha} - L_0 + L_0^\alpha \right] \frac{L - L_0^\alpha}{(1 - a^\alpha)^2} \right. \\
& \left. - \frac{p}{2} \left(\frac{K}{K + K_e} \right)^2 \frac{K^\alpha}{a^{2\alpha}} \left[\frac{L - L_0^\alpha}{1 - a^\alpha} - L_0 + L_0^\alpha \right]^2 - \frac{1}{2} \frac{K^\alpha (L - L_0)^\alpha}{(1 - a^\alpha)^2} \right\} \quad (52b)
\end{aligned}$$

Eq (52b) can still be simplified by using (52a) to eliminate the second term in the left hand side of (52b). By using $K_e = K^\alpha \frac{1 - a^\alpha}{a^\alpha}$ and

defining $Q^\alpha = K^\alpha/K$, $\eta^\alpha = L_0^\alpha/L$ and $\eta = L_0/L$ (52a) and (52b) can be written as

$$\frac{p}{a^\alpha + Q^\alpha(1-a^\alpha)} (1 - \eta^\alpha a^\alpha - \eta - \eta^\alpha a^\alpha)^2 = (1 - \eta^\alpha)^2 \quad (53a)$$

$$\frac{1 - b^\alpha \eta^\alpha (1 - \eta^\alpha) / (1 - a^\alpha)}{[1 - \eta^\alpha + (\eta^\alpha - \eta)(1 - a^\alpha)]} = \frac{1}{1 - \eta^\alpha} + \frac{b^\alpha \eta^\alpha (1 - Q^\alpha)}{2[a^\alpha + Q^\alpha(1 - a^\alpha)]} \quad (53b)$$

Here superscript α is used to indicate the effective medium network. K^α and η^α are the quantities characterising the effective medium network and should be compared with K_{eff} and η_{eff} from section III. Eq. (53a) and (53b) are the self-consistent recursive equations. For a given L_0/L , Eq. (53a) and (53b) must be solved self-consistently and iteratively starting from $p=1$, $a^\alpha = a^*$ and $b^\alpha = b^* = \frac{\partial a^*}{\partial (L_0/L)}$. We obtain K^α and η^α as functions of p and these values should be compared with the values deduced, using (25a) and (25b), from the computer simulations. The percolation threshold p_c can also be calculated as a function of η using (53a) and (53b). We use η_t to denote the value of η at the tricritical point. For $\eta < \eta_t$, $Q^\alpha = K^\alpha/K = 0$ at the percolation threshold thus (53a) and (53b) are solved iteratively for a given $\eta < \eta_t$ until $Q^\alpha = 0$. For $\eta > \eta_t$, $\eta^\alpha = L_0^\alpha/L = 1$ at the percolation threshold, again (53a) and (53b) are solved iteratively for a given $\eta > \eta_t$ until $\eta^\alpha = 1$. In the neighborhood sufficiently close to the tricritical point, (50a) and (50b) can be further simplified. After some lengthy algebra we obtain

$$\frac{p}{a^\alpha + Q^\alpha(1-a^\alpha)} [1 + b^\alpha(1 - \eta)]^2 = 1 \quad (54a)$$

$$\frac{(1 - \eta)(b^\alpha - c^\alpha/2)}{[1 + b^\alpha(1 - \eta)]} = \frac{b^\alpha(1 - Q^\alpha)}{2[a^\alpha + Q^\alpha(1 - a^\alpha)]} \quad (54b)$$

where $c^\alpha = \frac{\partial^2 a^\alpha}{\partial(\eta^\alpha)^2}$. At the tricritical point $Q^\alpha = 0$, $\eta^\alpha = 1$, $a_{(1)}^\alpha = 1$, $b_{(1)}^\alpha = 0.958$, and $c_{(1)}^\alpha = 4.16$. Thus from (54b) we obtain

$$1 - \eta_t = \frac{b^\alpha}{2b^\alpha + c - b^{\alpha 2}} = 0.186$$

or $\eta_t = 0.814$

Using $Q^\alpha = 0$, $\eta_t = 0.814$, $a_{(1)}^\alpha = 1$, $b_{(1)}^\alpha = 0.958$ and (54a) we obtain

$$p_t = 0.720$$

or $1 - p_t = 0.280$

Thus the effective medium theory gives the location of the tricritical point at $p_c = 0.28$ and $\eta_t = 0.81$. In Fig. 2.18 we plot the phase boundary obtained from the effective medium theory and from computer simulation results (squares). The tricritical point is also marked in the figure. The value of η_t is very close to our estimates $L_0/L \sim 0.8$ from the computer simulation result. We notice that p_c , determined from

the computer simulations, at $L_0/L = 0$, is 0.38 instead of $1 - 2\sin(\frac{\pi}{18}) = 0.316$ which is the exact result³. This is due to the finite size effect. As the system size becomes larger and larger one should be able to extract the exact value by using a scaling rule³. It is more important here to know how p_c changes with L_0/L . The most interesting feature in Fig. 2.18 is that the first derivative of p_c , with respect to L_0/L , is not continuous at the tricritical point. In Landau phase transition theories, as we have discussed, the first derivative at the tricritical point is continuous. The discrepancy may be due to the negligence of the interactions between the springs in the effective medium theory. An effective medium theory capable of dealing with the interactions is very complicated and technically impossible to apply.

After obtaining K^α and η^α as functions of p , we can use equations (26) to calculate various quantities such as $E_{0(p)}$, $T_{(p)}$, and $B_{(p)}$. Notice that Eq. (48) and (49) are the same as (24a) and (24b) when $\langle \Delta E \rangle = 0$ and $\langle \Delta T \rangle = 0$, which determine the effective medium network. In Fig. 2.19 we plot η^α against p for $L_0/L = 0, 0.2, 0.4, 0.6, 0.7, 0.8, 0.86, 0.9, 0.95$. The corresponding results from the computer simulations using (25b) are also plotted (symbols). The overall agreement is satisfactory. The agreement are very good for small $1-p$, as we can expect, and above the tricritical point. In Fig. 2.20 we compare the quantities $E_{(p)}$, $T_{(p)}$, and $B_{(p)}$ obtained from the effective medium theory and the computer simulations. We can see that the agreement, in general, is also quite good although the effective medium theory overestimates the percolation threshold in some cases. Therefore we conclude

general, is also quite good although the effective medium theory overestimates the percolation threshold in some cases. Therefore we conclude that the new effective medium theory works quite well for the honeycomb spring network under tension although it has some shortcomings. It predicts a tricritical point and the different behavior of K^a and η^a in the first and second phase transition regions. These are the most successful features of the effective medium theory.

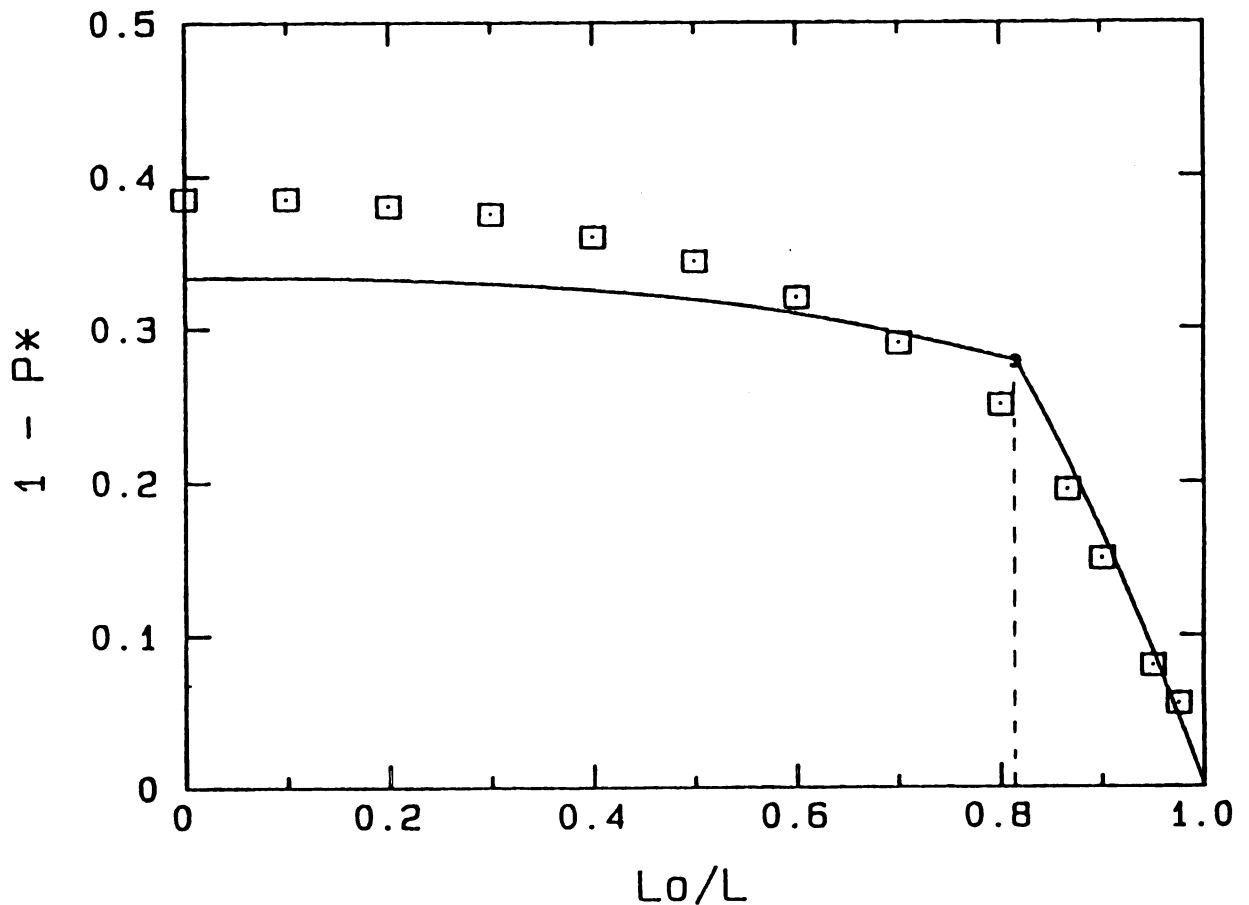


Fig. 2.18 The phase boundary from the effective medium theory (solid line) and computer simulations (squares) are plotted against η . The tricritical point is marked.

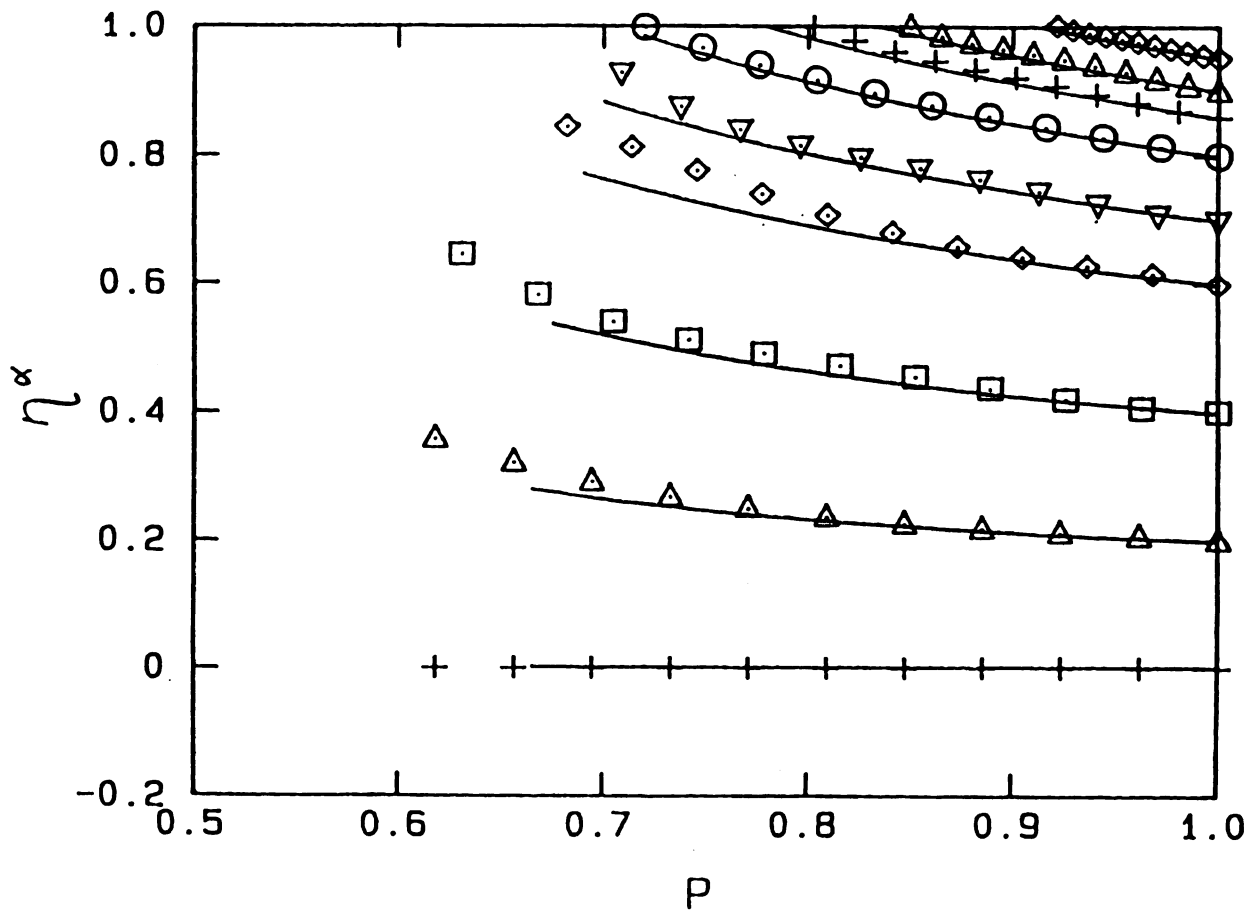


Fig. 2.19 The quantity η^α is plotted vs. p for $L_0/L = 0.0, 0.2, 0.4, 0.6, 0.7, 0.8, 0.86, 0.9$ and 0.95 (solid lines). The corresponding quantities from the computer simulations are also plotted (symbols).

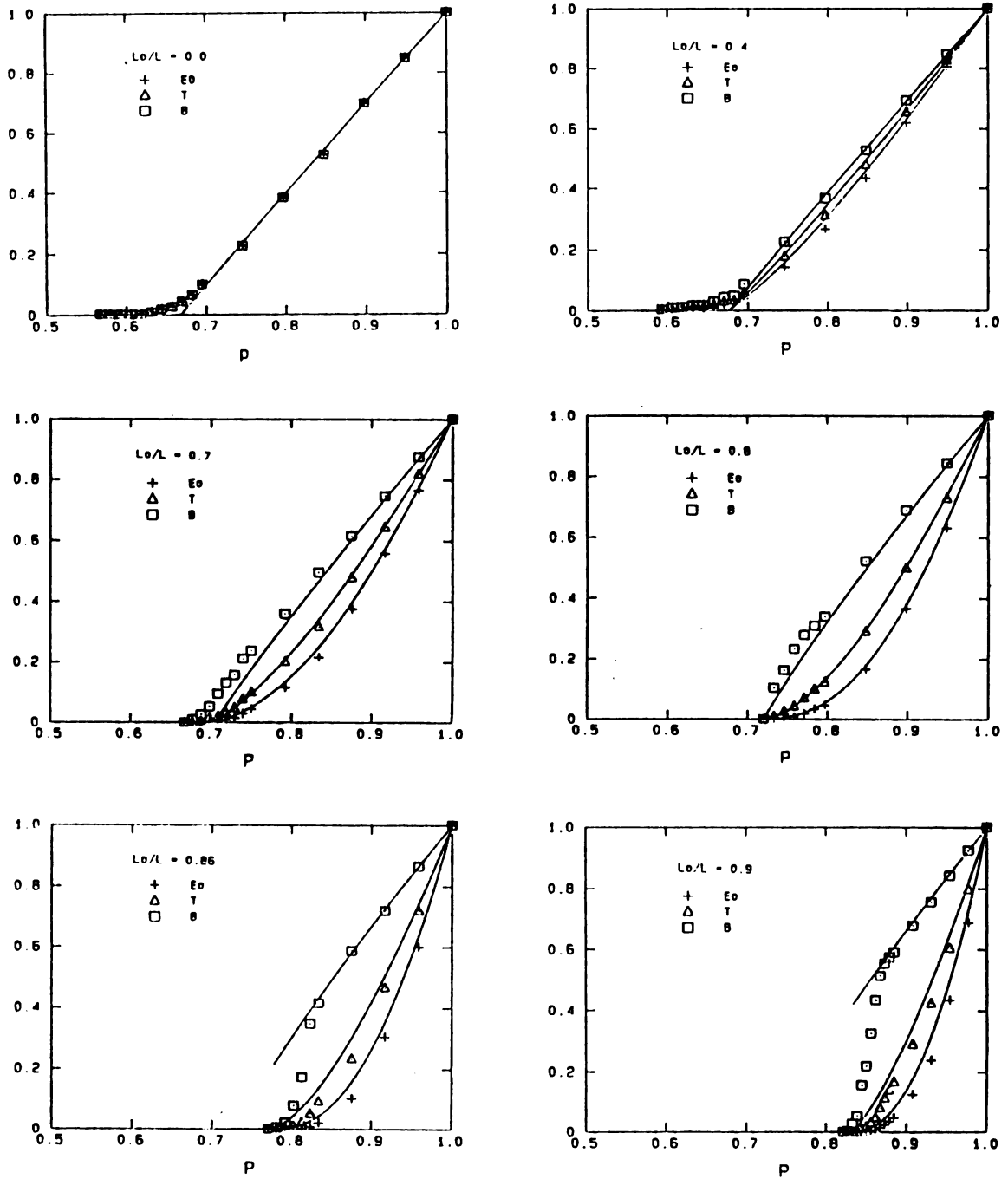


Fig. 2.20 The quantities E_0 , T and B calculated from the effective medium theory (solid lines) are compared with the corresponding quantities from computer simulations (symbols) for $L_0/L = 0.0, 0.4, 0.7, 0.8, 0.86$ and 0.9 .

V Conclusions

We have studied the elastic percolation problems of the stretched spring model on the honeycomb lattice and found two types of rigid \rightarrow floppy transitions. In the region where $L_0/L \leq 0.81$, the rigid \rightarrow floppy transition is the conventional second order phase transition studied before⁸ while in the region where $L_0/L > 0.81$ the transition is a first order phase transition. The difference between the two types of transition is that the bulk modulus is continuous in the second order phase transition and discontinuous in the first order phase transition. Landau phase transition theory can be applied to explain the two types of phase transitions and the tricritical point observed in the computer simulations. A new self-consistent effective medium theory has been developed to calculate various elastic constants, phase boundary and the tricritical point. The agreement between the effective medium theory and the computer simulation results is quite good. We have also found that the the elastic percolation threshold of the stretched spring model is 1 rather than $\frac{4}{3}$ in the central force limit on the honeycomb lattice.

VI REFERENCES

1. P. G. de Gennes, J. Phys. (Paris) 37, L-1,(1976).
2. S. Kirkpatrick in Ill-Condensed Matter-Les Houche 1978, Ed. By R. Balian, R. Maynard and G. Thoulus, (North-Holland, Amsterdam, 1979).
3. D. Stauffer, Introduction to Percolation Theory (Taylor and Francis, London, 1985).
4. S. Feng and P. N. Sen, Phys. Rev. Lett. 52, 216 (1984).
5. A. R. Day, R. R. Tremblay and A. -M. S. Tremblay, Phys. Rev. Lett. 56, 2501 (1986).
6. M. F. Thorpe, J. Non-Crys. Sol. 57, 355 (1983).
7. M. Born and K. Huang, Dynamical Theory of Crystal Lattice (Oxford, Univ. Press, New York, 1954).
8. W. Tang and M. F. Thorpe, Phys. Rev. B 37, 5539 (1988); W. Tang, Ph. D. Thesis, Michigan State Univ (unpublished).
9. S. Feng, M. F. Thorpe and E. Garboczi, Phys. Rev. B 31, 276 (1985).
10. T. H. K. Barron and M. L. Klein, Proc. Phys. Soc. 85, 523 (1965).
11. C. Kittel, Introduction to Solid State Physics (J. Wiley & Sons, Inc. New York, 4th Edition, 1971).
12. P. N. Keating, Phys. Rev. 145, 637 (1966).
13. A. E. H. Love, A Treatise on the Mathematical Theory of Elasticity, (Dover, New York 1944).
14. H. He and M. F. Thorpe, Phys. Rev. Lett. 54, 2107 (1985).

15. L. D. Landau, Phys. Z. Sowjetunion 11, 26 (1937); V. L. Ginzburg and L. D. Landau, Zh. Eksp. Teor. Fiz. 20, 1064 (1950); R. B. Griffiths, Phys. Rev. Lett. 24, 715 (1970).
16. Kerson Huang, Statistical Mechanics (John Wiley & Sons, New York, 2nd Edition, 1987).
17. R. Zallen, The Physics of Amorphous Solids, (John Wiley & Sons, New York, 1983).

Part III

The Vibrational Spectra of Random

Superconducting - Normal Networks

I. Introduction

It is well known that the vibrational excitation density of states for homogeneous systems obeys the Debye law

$$g(\omega)d\omega \sim \omega^{d-1}d\omega \quad (1a)$$

in the low frequency or long wavelength limit. Here ω is the vibrational frequency, $g(\omega)$ is the density of states and d is the dimensionality of the problem. Naturally one can ask such question as what happens to (1a) when disorder or inhomogeneity is introduced. Obviously Eq (1a) will break down for inhomogeneous systems. However, for certain disordered systems, Eq (1a) simply takes the following form¹

$$g(\omega)d\omega \sim \omega^{\tilde{d}-1}d\omega \quad (1b)$$

where \tilde{d} is called the spectral dimensionality which is different than d . A fractal network is a suitable inhomogeneous system for studying quantity \tilde{d} . There have been extensive studies on dilute random percolation networks, which are fractals, in the past five years¹⁻⁸. If we think of the vibrational model as an array of springs, then the vibrational equations of motion are very similar to those of diffusion and a tight-binding Hamiltonian [see (2a) below]. Because of the similarities among the diffusion equation, equations of spring vibrations and the equations of motion for a system described by a tight binding Hamiltonian (or an

elastic Hamiltonian) it is clear that there are two approaches to evaluating \tilde{d} .

One approach is to examine the low frequency dynamical response of the system described by the Hamiltonian

$$H = \sum_{\langle ij \rangle} V_{ij} (a_i^\dagger a_i - a_i^\dagger a_j) \quad (2a)$$

where the V_{ij} are randomly distributed on the nearest neighbor bonds according to the probability distribution

$$P(V_{ij}) = p\delta(V - V_{ij}) + (1 - p)\delta(V_{ij}) \quad (2b)$$

and we restrict the sum to sites on the infinite cluster. The a_i, a_i^\dagger are either Bose or Fermi operators (the results are the same when only one particle excitations are considered) and the diagonal term is present in (2a) to preserve translational invariance. This dilute tight binding Hamiltonian describes the physics of several different random systems; dilute magnetic systems, random resistor networks and random scalar elastic networks. By scalar elasticity we mean for example displacements perpendicular to the elastic network. Symbol E has the unit of energy and when $\hbar=1$ we call it frequency for convenience. The low frequency density of states at p_c is predicted to behave as

$$g(E) \sim E^{\frac{1}{2}(\tilde{d} - 2)} \quad (3)$$

where \tilde{d} is the spectral dimensionality that can be expressed as¹⁻²

$$\tilde{d} = \frac{2\bar{d}}{2 + \frac{t-\beta}{\nu}} \quad (4)$$

and t is the conductivity exponent. The quantities β and ν are the geometric exponents⁸ which govern the probability of being on the infinite cluster, and the correlation length, respectively. The fractal dimensionality $\bar{d} = d - \beta/\nu$. Direct numerical evaluation of the density of states in two dimensions³ on dilute spin systems has confirmed equation (4) and that \tilde{d} is close to $4/3$ which Alexander and Orbach¹ have conjectured to be the value of \tilde{d} in all dimensions except 1D.

An alternative approach is to study the anomalous diffusion of a random walker on the infinite percolation cluster. Scaling arguments^{1,2},⁴ suggest that the mean square displacement $\langle r^2 \rangle$ scales with time as

$$\langle r^2 \rangle \sim t^k \quad (5)$$

and $k = \frac{2}{2 + \frac{t-\beta}{\nu}}$ where t , β and ν were defined previously. By relating the probability of return to the origin with the density of states,¹ one obtains $\tilde{d} = \bar{d}k$ in agreement with Eq. (4).

Numerical simulations of random walks on dilute systems are a good indirect way of obtaining the spectral dimensionality \tilde{d} using Eq. (5)

and the relation $\tilde{d} = k\bar{d}$. Values of \tilde{d} obtained in this way⁵ agree with direct simulations³ of the low frequency density of states at p_c .

The randomly dilute problem discussed above can be considered as a random system of strong bonds V_s and weak bonds V_w in the limit $V_s \rightarrow V$, $V_w \rightarrow 0$. The other limit, $V_s \rightarrow \infty$, $V_w \rightarrow V$, is also of considerable interest and is the subject of this article. It would describe a random superconducting network or the elastic properties of a system with rigid grains weakly coupled by soft springs. In the general problem, the density of states is divided into bands: a high frequency band associated with internal modes of the clusters of strong bonds and a low frequency band associated with vibrations of the soft regions. In the limit $V_w \rightarrow 0$, $V_s \rightarrow 1$, the low frequency band becomes a delta function at the origin and the spectral dimension describes the low frequency edge of the high frequency band. In the limit $V_w \rightarrow 1$, $V_s \rightarrow \infty$, the high frequency band is driven off to infinity and the delta function broadens. There will be a different spectral dimension associated with this low frequency edge.

In diffusion language, the superconducting limit is the problem of termite diffusion⁹ which has been the subject of considerable work¹⁰⁻¹² and some controversy. In principle, it should provide information about the density of states and the spectral dimension \tilde{d} for the problem but in practice this is not the case because the random walk is completely dominated by the distances moved on the superconducting clusters. As has been pointed out by Hong et al.,¹¹ there is no region where $\langle r^2 \rangle \sim t^k$ because even at time zero, $\langle r^2 \rangle \sim \xi^{2-B/\nu}$, the average radius

of the superconducting clusters. The low frequency excitations we are interested in are associated with the small, time dependent contribution to $\langle r^2 \rangle$ superimposed on the divergent $\xi^{2-B/\nu}$. Clearly this is impossible to obtain numerically and we therefore believe that direct simulations of the low frequency response is the best way to evaluate the spectral dimension.

From ones physical intuition and experiences one will also expect that (a) the contributions to the lower frequency part of the vibration density of states are associated with the collective vibrational modes of clusters and because such collective modes involve large masses therefore result in lower frequencies; (b) those of high frequency part are due to the internal vibrational modes of clusters or local vibrational modes which are associated with small masses and therefore with higher frequencies. While the lower frequency part can be explained using scaling hypothesis, the major features in high frequency part can be explained by just consider the local vibrational modes. The layout of this paper is as follows. In section II we describe the procedures of obtaining Density Of States (DOS) for Hamiltonian (1) by using Equation Of Motion technique (EOM) and present the computer simulation results for spectral dimensionality \tilde{d} . In section III we present the scaling cross-over hypothesis to describe the cross-over from phonon region to anomalous region for systems above two dimensions and in section IV one dimensional case is treated separately because of uncommon features in one dimension.

II. Density of States

In this article we obtain the density of states and hence the spectral dimension \tilde{d} for the superconducting case. The system is described by the Hamiltonian (2a) but with the interaction strength distribution

$$P(V_{ij}) = p \delta(V_{\infty} - V_{ij}) + (1 - p) \delta(V - V_{ij}) \quad (6)$$

where $V_{\infty} = \infty$ in the superconducting limit. The wavefunction of the system at time t can be written as

$$|\Psi(t)\rangle = \sum_k c_k(t) a_k^+ |0\rangle \quad (7a)$$

where $|0\rangle$ is the vacuum state, a_k^+ the creation operator at site k and $c_k(t)$ the amplitude of excitation at site k at time t . By substituting $|\Psi(t)\rangle$ into Schrodinger equation

$$i\hbar \frac{\partial |\Psi(t)\rangle}{\partial t} = H |\Psi(t)\rangle \quad (7b)$$

with Hamiltonian H of (1) then (7b) becomes

$$i\hbar \sum_k a_k^+ |0\rangle \partial c_k(t) / \partial t = \sum_{ijk} v_{ij} (a_i^+ a_i - a_i^+ a_j) a_k^+ |0\rangle c_k(t) \quad (7c)$$

We are interested in how amplitudes $c_k(t)$ evolve with time t . By using either commutation or anticommutation rule

$$[a_i^+ , a_j]_{\mp} = \delta_{ij} \quad (7d)$$

the equations of motion for $c_k(t)$ in (7c) are now

$$i\hbar \frac{\partial c_k}{\partial t} = \sum_{\ell} v_{k\ell} (c_k - c_{\ell}) \quad (7)$$

Here the c_k 's are the amplitudes of the wavefunction on the k site.

Two sites k and ℓ connected by a bond $v_{k\ell} = \infty$ have the same amplitude so that $c_k = c_{\ell}$ can be considered as a single site of mass 2. This process is repeated for all superconducting bonds so each superconducting cluster has one degree of freedom and a mass M equal to the number of sites in the cluster. We consider a site connected to no superconducting bonds to be a cluster of size 1. The equations of motion for the clusters so defined are

$$i\hbar M_k \frac{\partial c_k}{\partial t} = \sum_{\ell} v_{k\ell} n_{k\ell} (c_k - c_{\ell}) \quad (8)$$

where k, ℓ are now cluster indices and $n_{k\ell}$ is the total number of normal bonds between the k and the ℓ cluster. By defining $\sqrt{M_k} c_k = c_k'$, we have the Hermitian equation of motion

$$i\hbar \frac{\partial c_k'}{\partial t} = \sum_{\ell} v_{k\ell} n_{k\ell} \left(\frac{c_k'}{M_k} - \frac{c_{\ell}'}{\sqrt{M_k M_{\ell}}} \right) \quad (9)$$

which we solve numerically using the equation of motion technique.¹³

If the original system has N sites, there are only Nf clusters^{14,15} so we have reduced the number of degrees of freedom by a factor of f . For small p

$$f = 1 - \frac{zp}{2} + \dots \quad (10)$$

where z is the number of nearest neighbors and p is the probability that a bond is present. The number of clusters in equation (10) actually is the sum of number of monomers, dimers, trimers and etc. normalized to total number of sites. Here monomers, dimers, trimers and etc. have mass of one, two, three and etc. respectively. For square lattice, as shown in Fig. 3.1, the probabilities of having monomers, dimers and trimers are $(1-p)^4$, $2p(1-p)^6$ and $6p^2(1-p)^8$ respectively. In above expressions powers of p represent the presence of bonds and powers of $(1-p)$ represent the absence of bonds. The coefficients in the front indicate number of different configurations one can possibly have with fixed number of bonds. The probabilities of having clusters of less than five bonds can also be written down by just inspection and those for more than five bonds can be obtained by using graph theory¹⁵. Therefore by definition the number of clusters at p on square lattice is

$$f = (1-p)^4 + 2p(1-p)^6 + 6p^2(1-p)^8 + \dots \quad (10a)$$

Extending (10a) to a general lattice with z nearest neighbors we can write down immediately the contributions from monomers, dimers and trimers etc.

$$f = (1-p)^z + \frac{z}{2} p(1-p)^{2z-2} + 2(z-1)p^2(1-p)^{z-2} + \dots \quad (10b)$$

So f is a function of p and z . For given z in order to find $f(p_c)$ we have to add the contributions from higher order clusters which can be found in ref. 15. For small p equation (10) can be easily obtained from (10b).

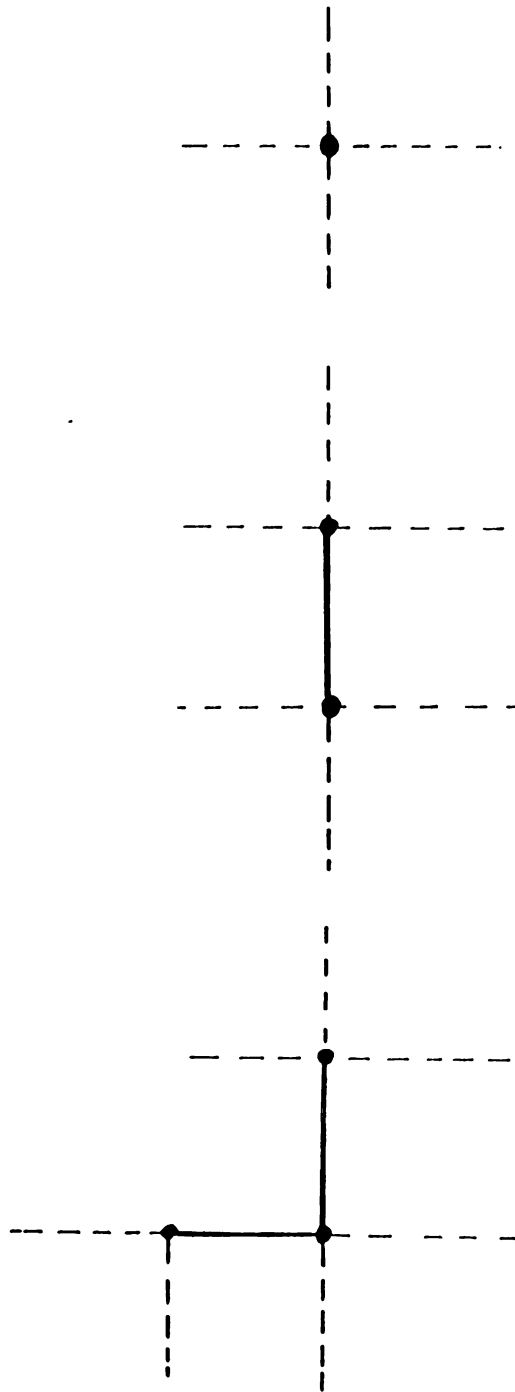


Fig. 3.1 Diagrams of monomer, dimers, trimers. The solid lines represent springs and the dashed lines represent missing springs. There are one configuration for monomer, two for dimers and six for trimers (omitted here).

Note that f decreases to a very small value at p_c . In the square net and simple cubic lattice we find it is 0.098, and 0.27 respectively.¹⁶

Thus setting V_∞ strictly equal to infinity reduces the effective size of the system, especially in 2D, although there is some initial time cost in identifying all the clusters. This advantage cannot be achieved by setting V_∞ large and taking a limiting process. Note also that f is finite at p_c for $d \geq 2$ but it is zero in 1D which affects the scaling arguments for \tilde{d} as we discuss later.

The equations of motion were integrated forward in time from $0 \rightarrow T$ using standard methods.¹³ The first few points were obtained using a fourth order Runge-Kutta algorithm and subsequently a fourth order Adams integration scheme was used.¹⁷ The density of states $g(E)$ is obtained from Fourier transforming the result of the time integration.

$$g(E) = \frac{1}{2\pi} \sum_i M_i \int_{-\infty}^{+\infty} c_i(t) c_i^*(0) e^{iEt} dt \quad (11)$$

This integral is converted to one over positive times only.¹³ Random phases¹³ are put on the clusters so that only the on-site terms required in (11) are retained in the limit of a large system. This is a standard way to obtain densities of states in the equation of motion technique.

In Fig. 3.2 we show the superconducting clusters of one sample at $p = 0.475$ on 40×40 square lattice. On each lattice site there is a single mass. The solid lines represent rigid springs with $V_s \rightarrow \infty$ while missing lines represent the weak springs with $V_w \rightarrow 1$. Dots are the masses

surrounded by weak springs. In Fig. 3.3 , we show results for the square lattice at $p_c = \frac{1}{2}$. The results are from averages over 25 samples of 100×100 networks. Because of the reduction in size due to the f factor only ~ 1000 amplitudes had to be monitored. The insert shows a log-log plot at low frequencies. In Fig. 3.4 , we show similar results for the simple cubic lattice⁸ at $p_c = .2491$. The results are from averages over 25 samples of $21 \times 22 \times 23$ networks. Because of the reduction due to the f factor only ~ 2800 amplitudes had to be monitored. The insert shows a log-log plot at low frequencies. We examined a single sample with about 16 times as many sites in both 2D and 3D and found no significant changes in the slopes in the log-log plots. There are two ways to obtain the spectral dimensionalities. One is simply measuring the slopes of the log-log plots in the inserts. We use a least square fit program to find the slopes. The slope in Fig. 3.3 is 1.05 ± 0.1 which leads to $\tilde{d} = 4.1 \pm 0.2$ from Eq. (3) in 2D. Similar measurements of insert of Fig. 3.4 gives a slope of 1.9 ± 0.15 and hence $\tilde{d} = 5.8 \pm 0.3$ in 3D. Another method is associated with the crossover scaling hypothesis which will be discussed in next section therefore we postpone the discussion of the method.

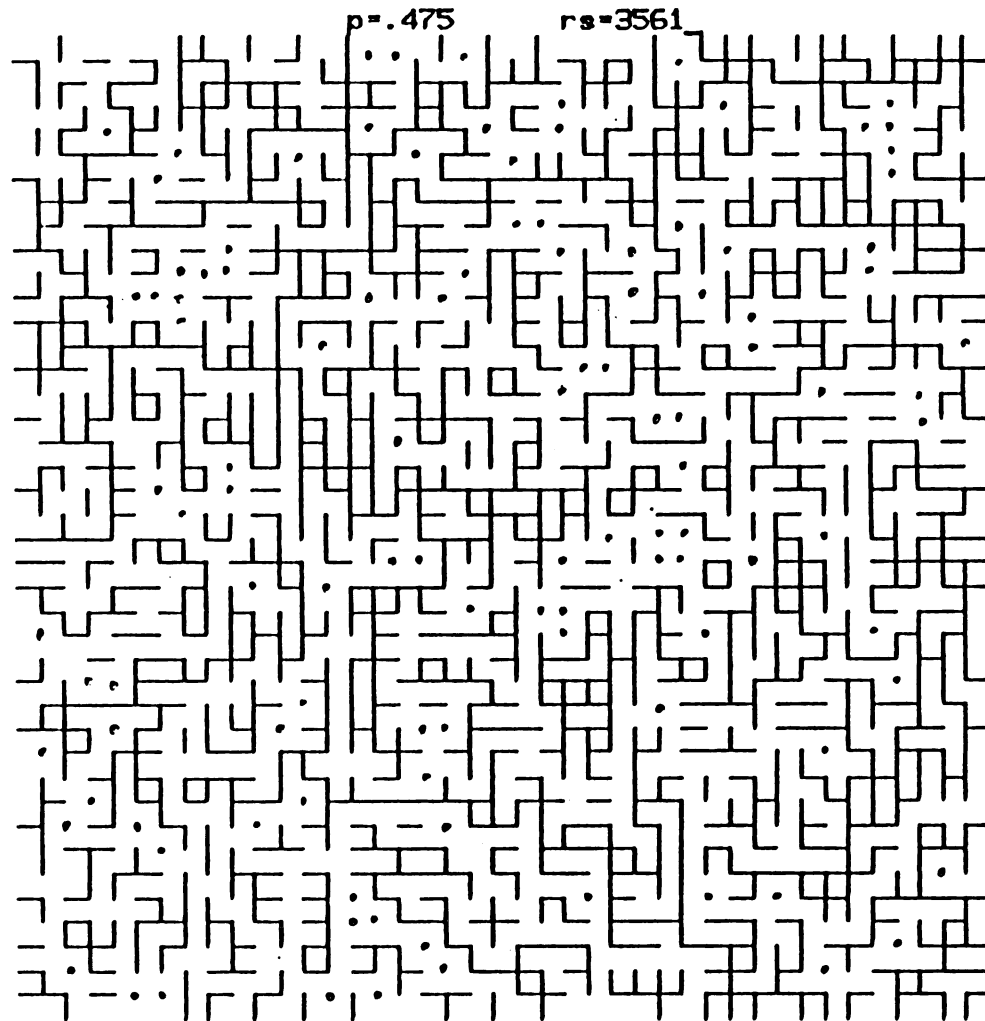


Fig. 3.2 A sample of bond percolation network on square lattice at $p = 0.475$. The solid lines represent rigid springs and the missing lines represent soft springs. The dots are the masses surrounded by soft springs.

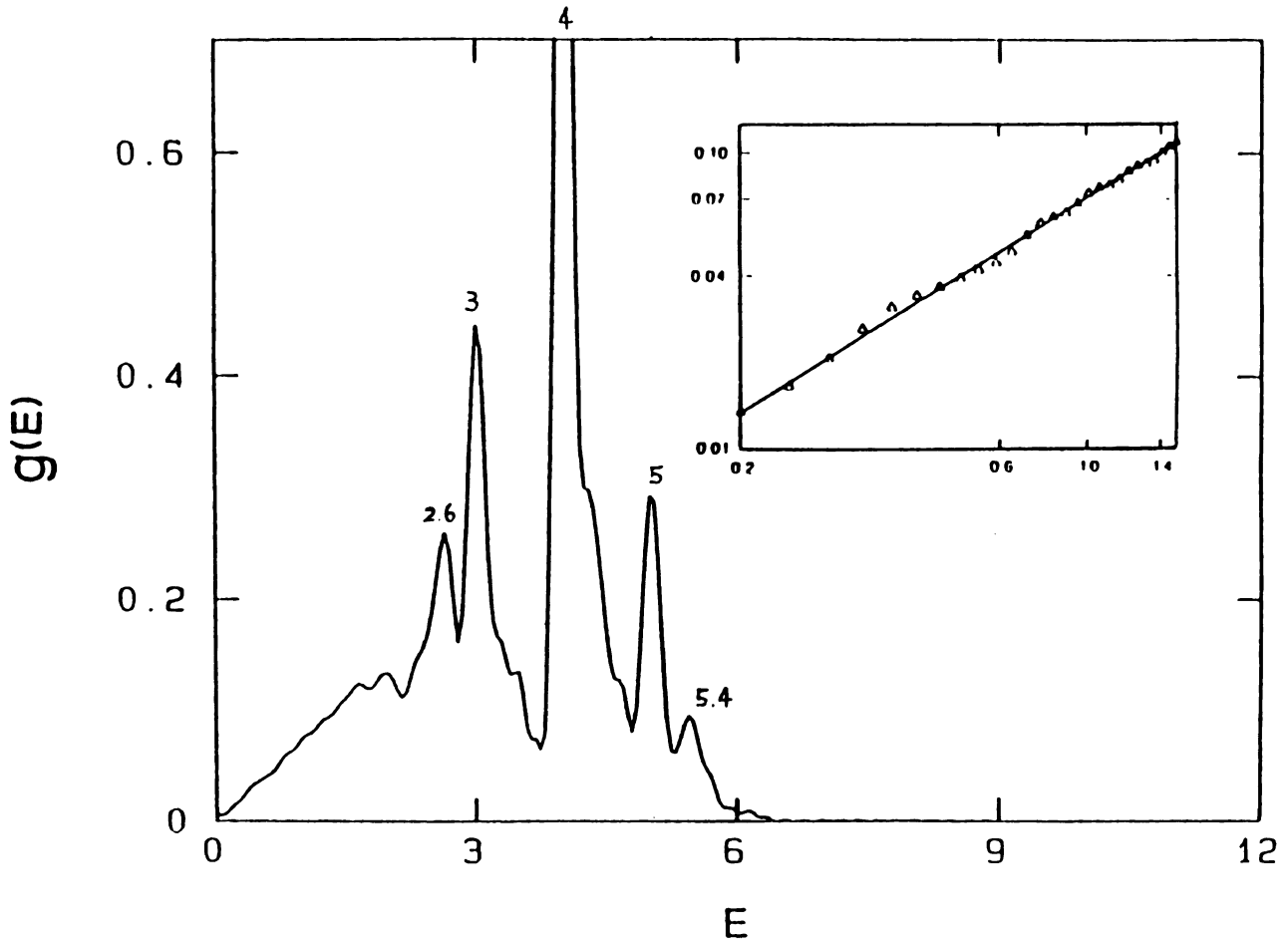


Fig. 3.3 The density of states for a random square lattice of superconducting and normal bonds at $p_c = \frac{1}{2}$. The insert shows the low energy data on a log-log (base 10) plot. The straight line drawn is a least squares fit to the data points shown from which \tilde{d} is obtained via Eqn. 3. The energy is in units with $V = 1$. The energy values of major peaks are also indicated.

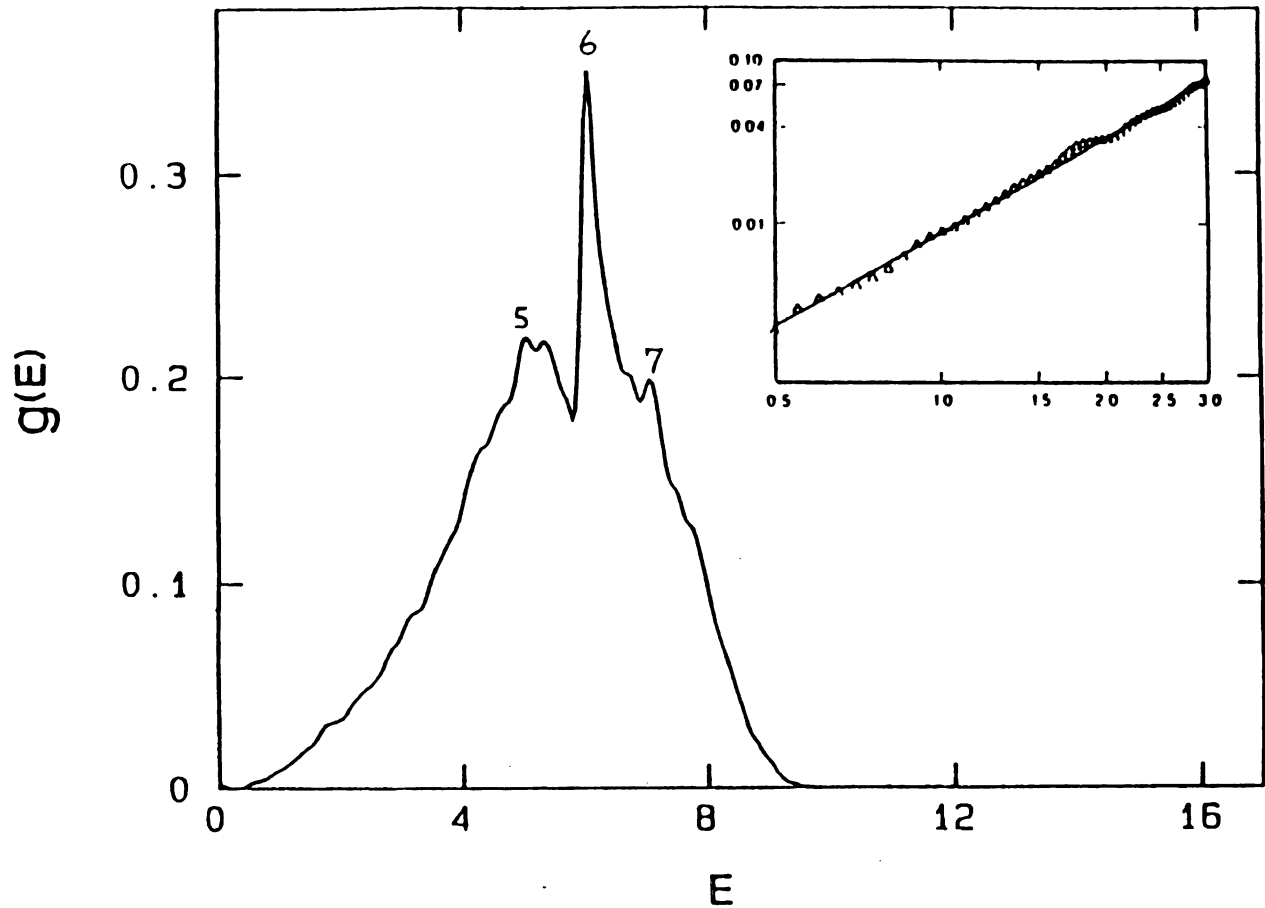


Fig. 3.4 Same as Fig. 3.3 except for a simple cubic lattice at $\rho_c = .249$. The insert shows the low energy data on a log-log (base 10) plot. The energy is in units where $V = 1$. The values of peaks are also indicated.

As we mentioned earlier in the introduction, the higher frequency (or energy) part of spectra are due to local vibrational modes. Therefore the sharp features at higher frequencies in Fig. 3.3 and Fig. 3.4 can be explained by just considering these local vibrational modes. Since all sites are always connected in superconducting case (i.e. $V_s \rightarrow \infty$ and $V_w \rightarrow 1$), at percolation threshold, we can imagine that (1) there is an infinite cluster (largest spanning cluster in computer simulations); (2) there are clusters of different sizes interconnected by weak springs ; (3) there are 'pockets' inside the infinite cluster and large clusters where small masses are surrounded by weak springs and connected back to big clusters. The latter situation is very similar to the case where small islands are surrounded by inland lakes and the lakes are surrounded by continents. Here small masses correspond to small islands, weak springs to inland lakes and big clusters (including the infinite cluster) to continents. The collective vibrations contribute to low frequency part of spectra. Now we consider the vibrational modes of 'pockets'. We assume that big clusters to which the small masses attached are very massive and therefore almost stationary. As shown in Fig. 3.5(a) a single mass is attached to big clusters (represented by the shaded area) with four weak springs of strength V_w which we can always assume to be one. The vibrational frequency is simply $E = 4$ for four neighbors in the 2d square lattice. In Fig. 3.5(b) each site has four springs and there is one spring between the two sites so the secular equation can be written as

$$\begin{vmatrix} 4 - E & -1 \\ -1 & 4 - E \end{vmatrix} = 0 \quad (12a)$$

Equation (12a) gives eigenvalue of $E = 3$ and $E = 5$. In Fig. 3.5(c) two masses, connected by a massless infinite rigid spring, give a frequency of $E = \frac{6}{2} = 3$. Configuration such as one shown in Fig. 3.5(d) gives a secular equation

$$\begin{vmatrix} 4 - E & -1 & 0 \\ -1 & 4 - E & -1 \\ 0 & -1 & 4 - E \end{vmatrix} = 0 \quad (12b)$$

which gives eigenvalues of $E = 4 - \sqrt{2}$, 4 , $4 + \sqrt{2}$. Fig. 3.5(e) gives a frequency of $E = \frac{8}{3} = 2.67$. Of course we can go on to exhaust all possible configurations and obtain the corresponding eigenvalues. However the above local vibrational modes are enough to explain the sharp features in Fig. 3.3 at frequencies $E = 2.6, 3, 4, 5, 5.4$. The relative heights of the peaks are related to the relative abundances of these local vibrational modes which can not be estimated by a simple argument.

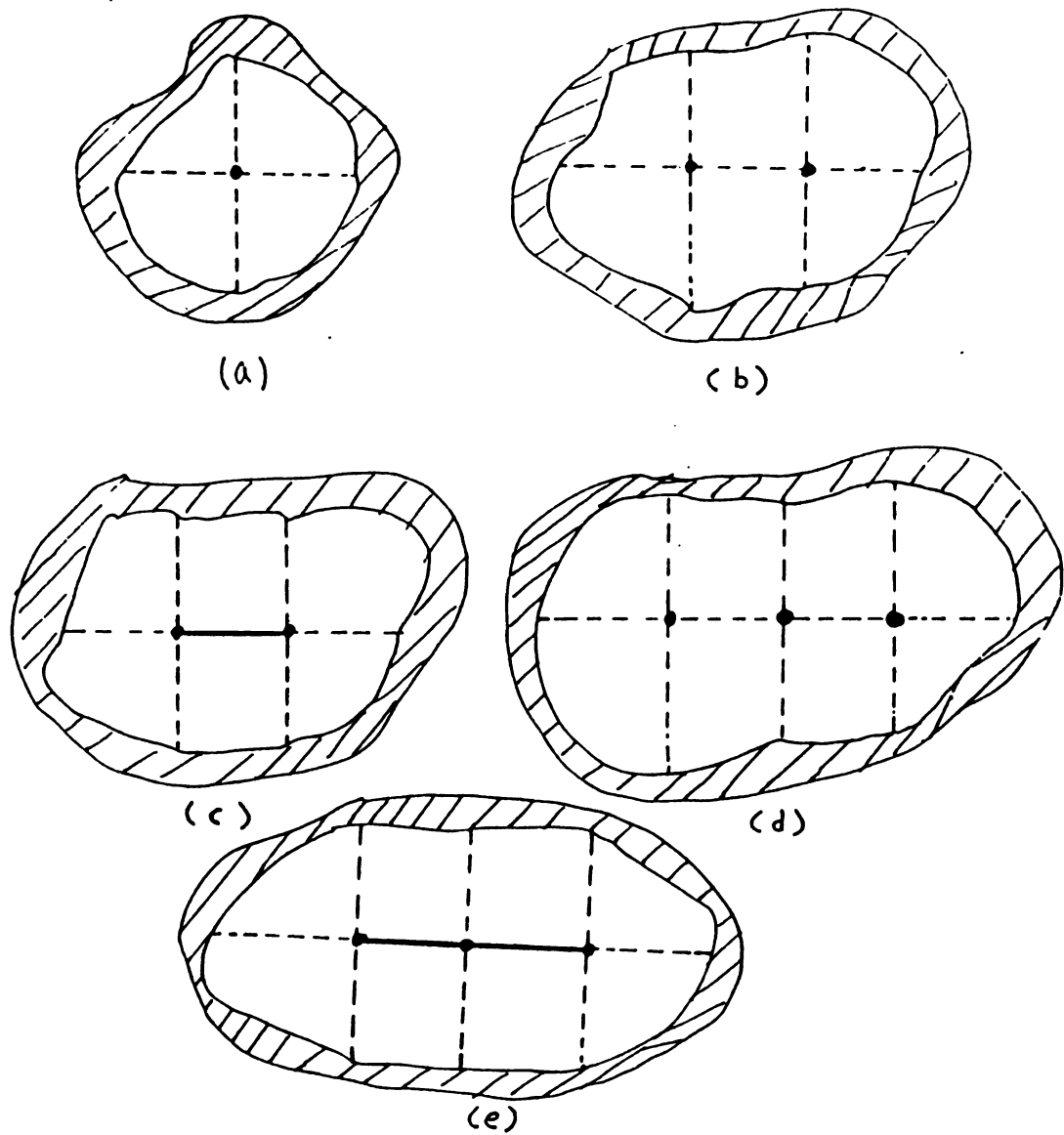


Fig. 3.5 Diagrams showing the vibration modes of 'pockets' in 2D. The solid lines represent rigid springs and the dashed lines represent soft springs. The shaded areas represent infinite masses.

Similarly the major peaks in 3D case (see Fig. 3.4) can be explained in a similar manner. For example, Fig.3.6(a) gives $E = 6$ for six neighbors in 3D simple cubic; Fig. 3.6(b) gives

$$\begin{vmatrix} 6 - E & -1 \\ -1 & 6 - E \end{vmatrix} = 0 \quad (12c)$$

which yields $E = 5$ and $E = 7$; Fig. 3.6(c) gives $E = \frac{10}{2} = 5$; Fig. 3.6(d) gives

$$\begin{vmatrix} 6 - E & -1 & 0 \\ -1 & 6 - E & -1 \\ 0 & -1 & 6 - E \end{vmatrix} = 0 \quad (12d)$$

which results in $E = 6 - \sqrt{2}$, 6 , $6 + \sqrt{2}$; and Fig. 3.8(e) gives $E = \frac{14}{3} = 4.67$. So peaks at frequencies 5, 6, and 7 can be explained. Again the relative heights of the peaks depend on the relative abundances of different modes. We also notice that the relative frequency differences form secular equations in 3D is smaller than those in 2D. Therefore the frequencies in 3D are more close to each other and evenly distributed which results in less spiky spectrum than in the 2D case.

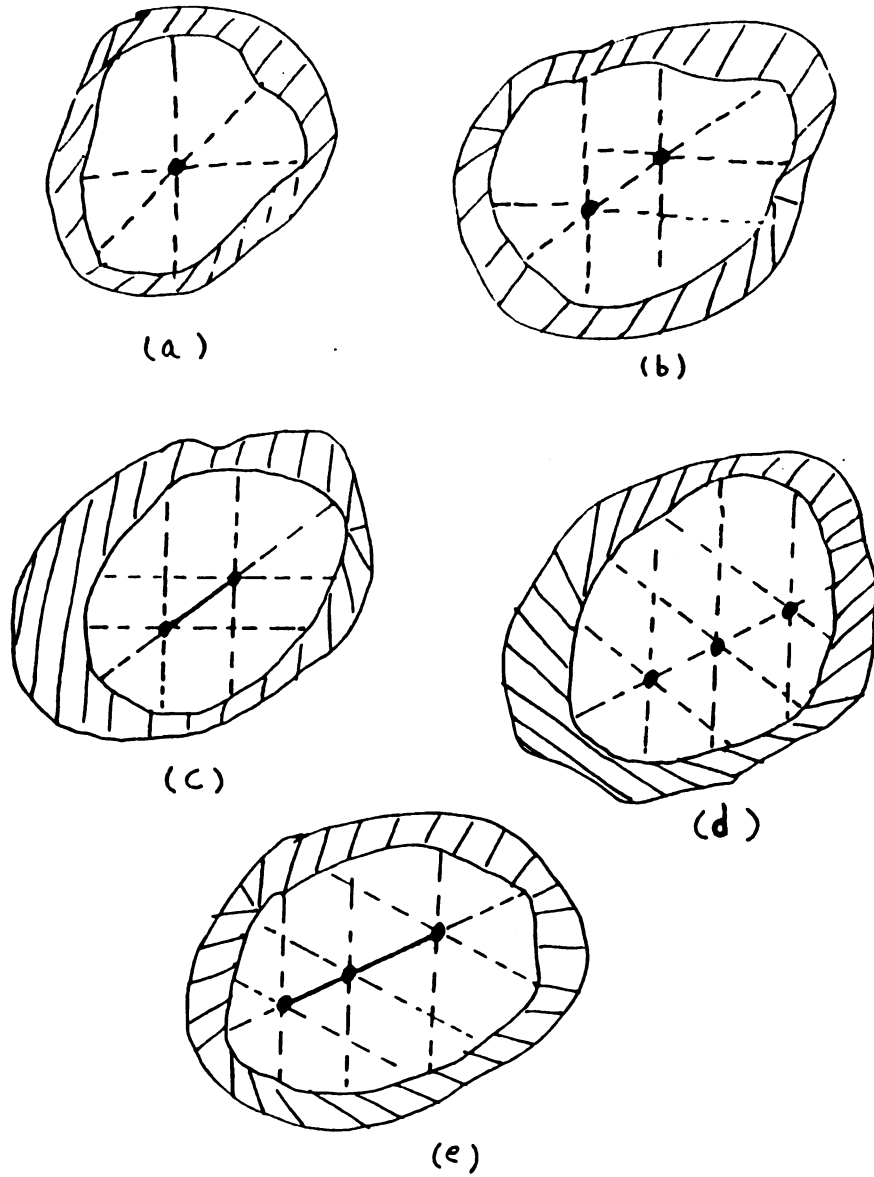


Fig. 3.6 Same as Fig. 3.5 except for 3D simple cubic lattice.

III Scaling Arguments

The scaling argument for \tilde{d} is given below following the ideas developed for the dilute case.^{7,8} It is easiest to use the language of phonons, i.e. vibrations on a network of normal and infinitely rigid springs. The results apply equally well to any system described by the tight binding Hamiltonian (1) with the probability distribution (6). Close to p_c and for systems of size L much greater than the correlation length $\xi \sim (p_c - p)^{-\nu}$ we expect the system to appear homogeneous with an effective elastic modulus $Y \sim (p_c - p)^{-s}$ where s is the superconducting exponent. Because the system is fully connected, all sites contribute to the inertia in the long wavelength limit, the total mass $M \sim L^d$ and thus the mass density ρ is noncritical, i.e. it is independent of ξ . The low frequency excitations are phonons with a sound velocity

$$c^2(\xi) \sim Y/\rho \sim \xi^{s/\nu} \quad . \quad (13)$$

For wavelengths $\lambda \sim \xi$ the fractal structure of the lattice becomes important. The excitations are no longer phonons and we have a fracton-phonon crossover. The crossover frequency is given by

$$\omega_{co} \sim \frac{c(\xi)}{\xi} \sim \xi^{-(2 - s/\nu)/2} \quad . \quad (14)$$

Using a Debye type theory we can write the normalised density of states for the phonons as

$$\rho(\omega) \sim C(\xi)^{-d} \left(\frac{L}{2\pi}\right)^d \omega^{d-1} / Nf \quad (15a)$$

To allow for the fracton-phonon crossover we introduce a scaling function $h(\omega/\omega_{co})$ into (15a) and obtain

$$\rho(\omega) \sim C(\xi)^{-d} \left(\frac{L}{2\pi}\right)^d \omega^{d-1} h(\omega/\omega_{co}) / Nf \quad (15b)$$

For $d \geq 2$, f is noncritical and so the critical behaviour of $\rho(\omega)$ is

$$\rho(\omega) \sim \xi^{-\frac{ds}{2v}} \omega^{d-1} h\left(\frac{\omega}{\omega_{co}}\right) \sim \omega_{co}^{\frac{ds/v}{2-s/v}} \omega^{d-1} h\left(\frac{\omega}{\omega_{co}}\right) \quad (16)$$

where we have used (13) and (14). In the low frequency (phonon) regime $x = \omega/\omega_{co} \ll 1$ and $h(x) \rightarrow \text{constant}$, so that $\rho(\omega) \sim \omega^{d-1}$ as expected. For $\omega > \omega_{co}$, the fracton regime, we rewrite (16) as

$$\rho(\omega) \sim \omega^{\frac{2d}{2-s/v} - 1} \left(\frac{\omega}{\omega_{co}}\right)^{-\frac{ds/v}{2-s/v}} h\left(\frac{\omega}{\omega_{co}}\right) \sim \omega^{\tilde{d}-1} r\left(\frac{\omega}{\omega_{co}}\right) \quad (17)$$

where $r(x) = x^{-\frac{ds/v}{2-s/v}} h(x)$ is expected to tend to a constant for large x because $\rho(\omega)$ should be independent of ξ or equivalently of ω_{co} in this

limit. Equation (17) defines the spectral dimension,

$$\tilde{d} = \frac{2d}{2-s/v} \quad (18)$$

We have discussed scaling relations for vibrational modes. Exactly parallel arguments can be made in all dimensions for tight binding Hamiltonians where $E \sim \omega^2 \sim c^2 k^2$ leading to

$$g(E) \sim E^{\frac{1}{2}(\tilde{d}-2)} . \quad (19)$$

Comparing Eq. (18) with the result for dilute systems Eq. (4), we notice the following differences.

a) The numerator involves d rather than \bar{d} . The excitations in the superconducting case can explore the whole system whereas in the dilute case, Eq. (4) is obtained for excitations on the infinite cluster. If the finite clusters are included in the dilute case⁶ the \bar{d} is also replaced by d in Eq. (4).

b) The conductivity exponent t in Eq. (4) is replaced by the superconducting exponent $-s$ in Eq. (18).

c) The exponent B does not appear in Eq. (18). In the dilute system, the probability of being on the infinite cluster scales as $(p - p_c)^B$. In the low frequency dynamical response of the infinite cluster, this is the inertia term and appears in (4). In the superconducting system, all sites are connected and so contribute to the inertia which is independent of p .

Good estimates of s/v for 2D and 3D are given in Ref. 18. Using $s/v = 0.977 \pm 0.010$ and 0.85 ± 0.04 in 2D and 3D respectively, gives

$\tilde{d} = 3.91 \pm 0.04$ in 2D and $\tilde{d} = 5.2 \pm 0.2$ in 3D. This is in good agreement with our results in 2D and reasonable agreement with our results in 3D where the numerical results are less accurate because the lattices had smaller linear dimensions.

The agreements between the predicted values of \tilde{d} and the computed ones is of course evidences for the existence of the cross-over scaling hypothesis. We now use the scaling property of the system to obtain the best value of \tilde{d} . By using the equivalence of $E \sim \omega^2$, equation (17) can be written as

$$g(E) = E^{\tilde{d}/2 - 1} r(E/E_{co}) \quad (20a)$$

where $r(E/E_{co})$ is the cross-over scaling function and

$$E_{co} \sim \omega_{co}^2 \sim |p - p_c|^{(2-s/\nu)\nu}. \quad (20b)$$

E_{co} is obviously different for different p close to p_c . For different p , $g(E)$ vs. E curves are expected to be different. However, if we rescale the E axis by $1/E_{co}$ then all curves $g(E)$ plotted against E/E_{co} for different p 's must fall into a single universal curve if the scaling hypothesis exists. From equation (20a) we can see that if we divide $g(E)$ by $E^{\tilde{d}/2 - 1}$ we will get the scaling function $r(E/E_{co})$. Since the p 's are away from p_c we expect some phonon excitations in the density of states curves. In the anomalous region, $g(E) \sim E^{\tilde{d}/2 - 1}$, so the scaling

function $r(E/E_{co})$ has to be a constant in that region in order to have the correct $g(E) \sim E^{\tilde{d}/2 - 1}$ behaviour. On the other hand, in the phonon region $g(E) \sim E^{d/2 - 1}$ so $r(E/E_{co})$ has to behave as $(E/E_{co})^{\frac{-ds/v}{2(2-s/v)}}$. Therefore we can write

$$r(E/E_{co}) \sim \begin{cases} \text{constant} & E > E_{co} \\ (E/E_{co})^{\frac{-ds/v}{2(2-s/v)}} & E < E_{co} \end{cases} \quad (20c)$$

For convenience we define

$$y = \tilde{d}/2 - 1 \quad (21a)$$

$$\text{and } x = (2 - s/v)v \quad (21b)$$

so equation (20a) and (20b) become

$$g(E) = r(E/E_{co}) E^y \quad (22a)$$

$$E_{co} = E_0 |\rho - \rho_c|^x \quad (22b)$$

In Fig. 3.7 $g(E)/E^{\tilde{d}/2 - 1} = r(E/E_{co})$ is plotted vs. E/E_{co} using the best values of x and y for $p = 0.475, 0.480, 0.485, 0.490$ and 0.495 where $p_c = 0.5$ is the percolation threshold for the 2D square lattice. It can be

seen that all curves fall into a universal curve extremely well. The procedure of obtaining the best values of x and y is as follows: we first plot $g(E)/E^y$ vs. E/E_{co} by using rough estimates of x and y , so curves scatter a little bit. Then we fine tune x and y so that all the curves fall into a universal curve. The best values of x and y are 1.37 ± 0.03 and 0.95 ± 0.03 respectively. Therefore from (21a) we obtain $\tilde{d} = 3.90 \pm 0.06$. We see that this value of \tilde{d} is closer to the predicted value of 3.91 ± 0.04 . The previous method of obtaining d is simply measuring the slope of log - log plot of low frequency part of spectra at percolation threshold and basically it only uses the information at percolation threshold. Clearly the latter method of extracting \tilde{d} is better because we have more information and we can fine tune the curves to result in the best value of \tilde{d} . However, this method requires much more computer time. In 3D case we can not get as good results as in 2D because the system sizes are not large enough to produce smooth curves for different p 's, but it can be done easily by using a supercomputer.

TABLE 3.1

d	\tilde{d} (This work)	$\tilde{d} = 2d/(2 - s/v)$
2	3.90 ± 0.06	3.91 ± 0.04
3	5.8 ± 0.3	5.21 ± 0.2

Table 3.1 Comparing the spectral dimensionality \tilde{d} obtained directly in this work with the scaling relation (18). Values of s/v are taken from Ref 18.

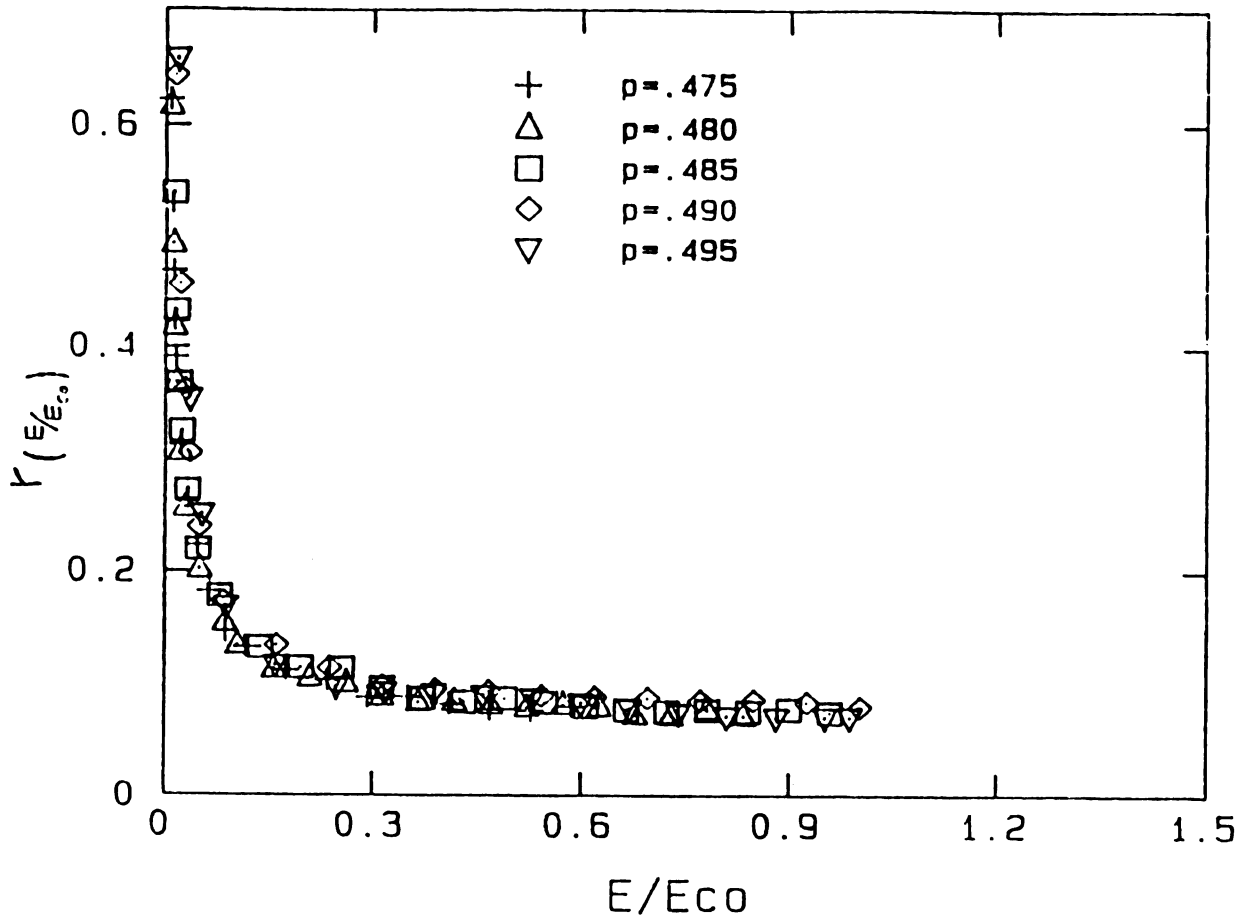


Fig. 3.7 $r(E/E_{co})$ is plotted against E/E_{co} for $p = 0.475, 0.480, 0.485, 0.490$ and 0.495 where $p=0.5$ is the percolation threshold. It shows good scaling behaviour.

IV. One Dimensional Case

The scaling in 1D is rather different because $f = (1 - p) \sim \xi^{-1}$ is critical. We start with the Debye form for the integrated density of states (See Eq. (15)).

$$I(\omega) \sim \frac{1}{Nf} C(\xi)^{-d} \left(\frac{L}{2\pi}\right)^d \omega^d H\left(\frac{\omega}{\omega_{co}}\right) \quad (23a)$$

Setting $d = 1$ and keeping only the critical terms we have

$$\begin{aligned} I(\omega) &\sim \xi^{1 - \frac{s}{2\nu}} \omega H\left(\frac{\omega}{\omega_{co}}\right) \\ &\sim \left(\frac{\omega}{\omega_{co}}\right) H\left(\frac{\omega}{\omega_{co}}\right) \\ &\sim R\left(\frac{\omega}{\omega_{co}}\right) \end{aligned} \quad (23b)$$

where $R(x) = xH(x)$ is expected to tend to a constant for x large. In this limit we have $I(\omega) \sim \omega^{\tilde{d}}$ which leads to $\tilde{d} = 0$ in 1D. This result is expected because in the limit $p = p_c = 1$ we have a perfect superconducting chain which is completely rigid and thus has only one degree of freedom. This can be considered as a zero dimensional object for which $\tilde{d} = d = 0$.

In 1D there are still excitations associated with rigid clusters of length less than ξ . Because the probability of neighboring clusters

having the same mass M is small, we can treat each cluster as an Einstein oscillator of frequency $\omega^2 = \frac{2V}{M}$. The probability of a cluster having mass M is

$$P(M) = (1 - p) p^{M-1} \quad (24a)$$

where we have chosen the mass of a single site to be one, so M is an integer. The density of states

$$\rho(\omega) = P(M) \left| \frac{dM}{d\omega} \right|$$

so

$$\begin{aligned} \rho(\omega) &= (1 - p) p^{M-1} \frac{\omega M^2}{V} \\ &= (1 - p) p^{(2V/\omega^2 - 1)} \frac{4V}{\omega^3}. \end{aligned} \quad (24b)$$

For $(1-p)$ small, we can write $p \simeq e^{-(1-p)}$ and thus

$$\rho(\omega) \simeq \frac{1-p}{p} e^{-2V(1-p)/\omega^2} \frac{4V}{\omega^3}$$

which to leading order in $(1-p)$ gives

$$\rho(\omega) = 4V(1-p)/\omega^3$$

or equivalently in tight binding language

$$g(E) = 2V(1 - p)/E^2 \quad . \quad (24c)$$

The exponential can be replaced by unity as there are other terms $O(1-p)^2$ that we have neglected in deriving Eq. (24c).

This result is special to 1D. In higher dimensions if we tried to consider the superconducting clusters as Einstein oscillators they would have a frequency

$$\omega_i^2 = \frac{n_i V}{M_i} \quad (25)$$

where $n_i = \sum_{l \neq i} n_{li}$ is the number of surface bonds connecting cluster i to other clusters bonds and M_i is the mass of the i cluster. However, for superconducting clusters we find numerically that $\frac{n_i}{M_i} \sim$ constant of order 1, unlike in 1D where $n_i = 2$ always and M_i can take any value. In 1D, the likelihood of having two adjacent clusters with the same mass, and hence the same frequency, is small. Therefore the modes do not hybridize and remain localized with $\tilde{d} = 0$. However for $d \geq 2$, the likelihood of adjacent clusters having the same Einstein frequency is high, as all the heavier clusters have essentially the same frequencies. Therefore the Einstein modes from the heavier superconducting clusters hybridize forming extended low frequency modes with $\tilde{d} > 2$.

In 1D we cannot do simulations at $p_c = 1$ so we have worked at small $(1-p)$. For frequencies $\omega < \omega_{co}$ or equivalently for wavelengths $\lambda > \xi \sim (1-p)^{-1}$ which is the typical length of a rigid cluster, we expect phonons with a constant density of states

$$\rho(\omega) \sim C(p)^{-1}/f \quad . \quad (26)$$

Because the linear chain just involves adding springs in series in the static limit, we have

$$g(E) = \frac{1}{2\pi} \frac{1}{\sqrt{V(1-p)E}} \quad (27)$$

In Fig. 3.8 we have plotted $\rho(\omega)$ against ω [or equivalently $\sqrt{E} g(E)$ against \sqrt{E}] for $p = 0.9, 0.99$ and 0.999 . The results were obtained from chains of 20000 clusters ($Nf = 20000$) using a transfer matrix technique.¹⁹ The results have been rescaled by plotting $\sqrt{E(1-p)} g(E)$ against $\sqrt{E/(1-p)}$ to show the scaling behavior. In Fig. 3.9 we have plotted $\sqrt{E} g(E)$ against \sqrt{E} for $p = 0.999$ and the two limiting curves $\sqrt{E}g(E) = [2\pi\sqrt{V(1-p)}]^{-1}$ and $\sqrt{E}g(E) = 2V(1-p)/E^{3/2}$ for low and high energies respectively.



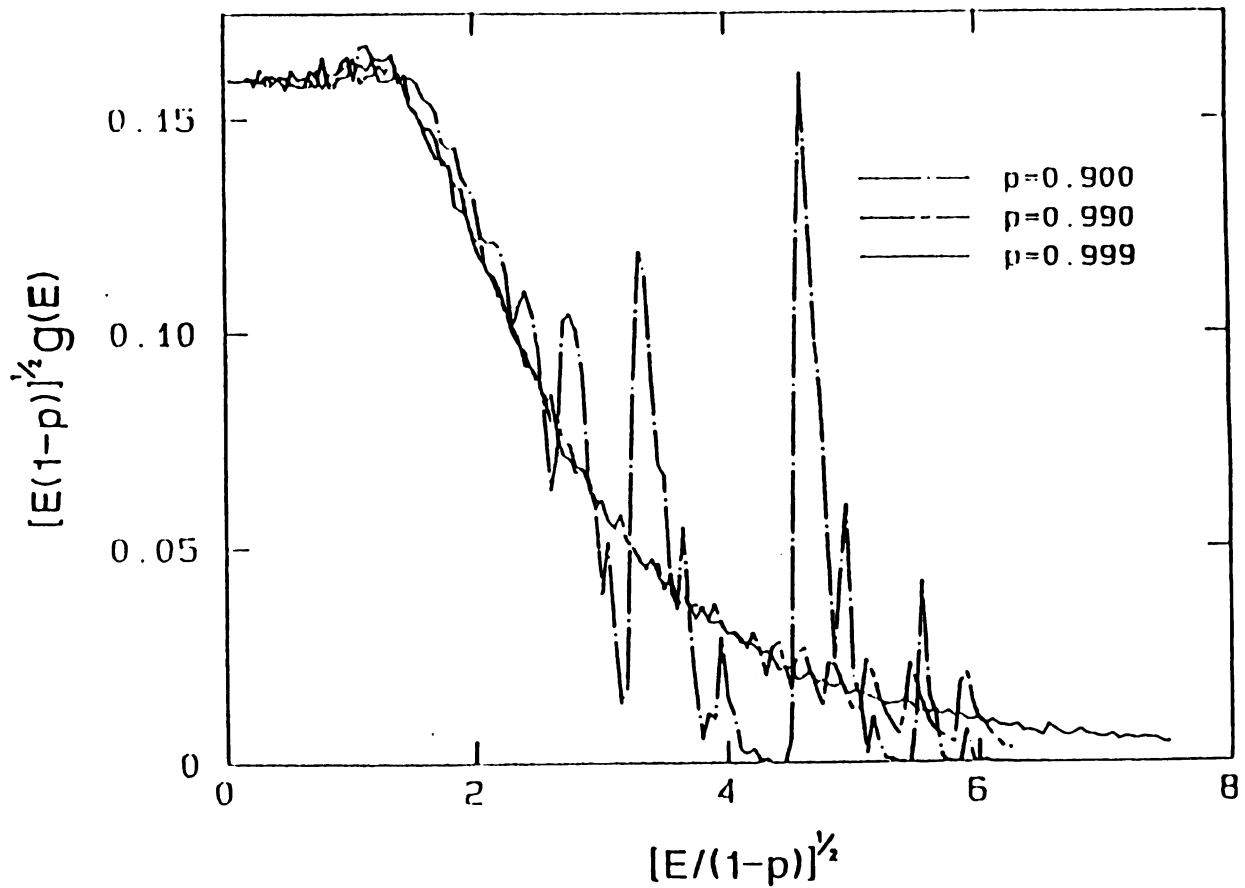


Fig. 3.8 The density of states for a random linear chain of superconducting and normal bonds of $p = 0.9, 0.99$ and 0.999 . The results are rescaled as indicated to show the scaling behavior. The energy is in units where $V = 1$.

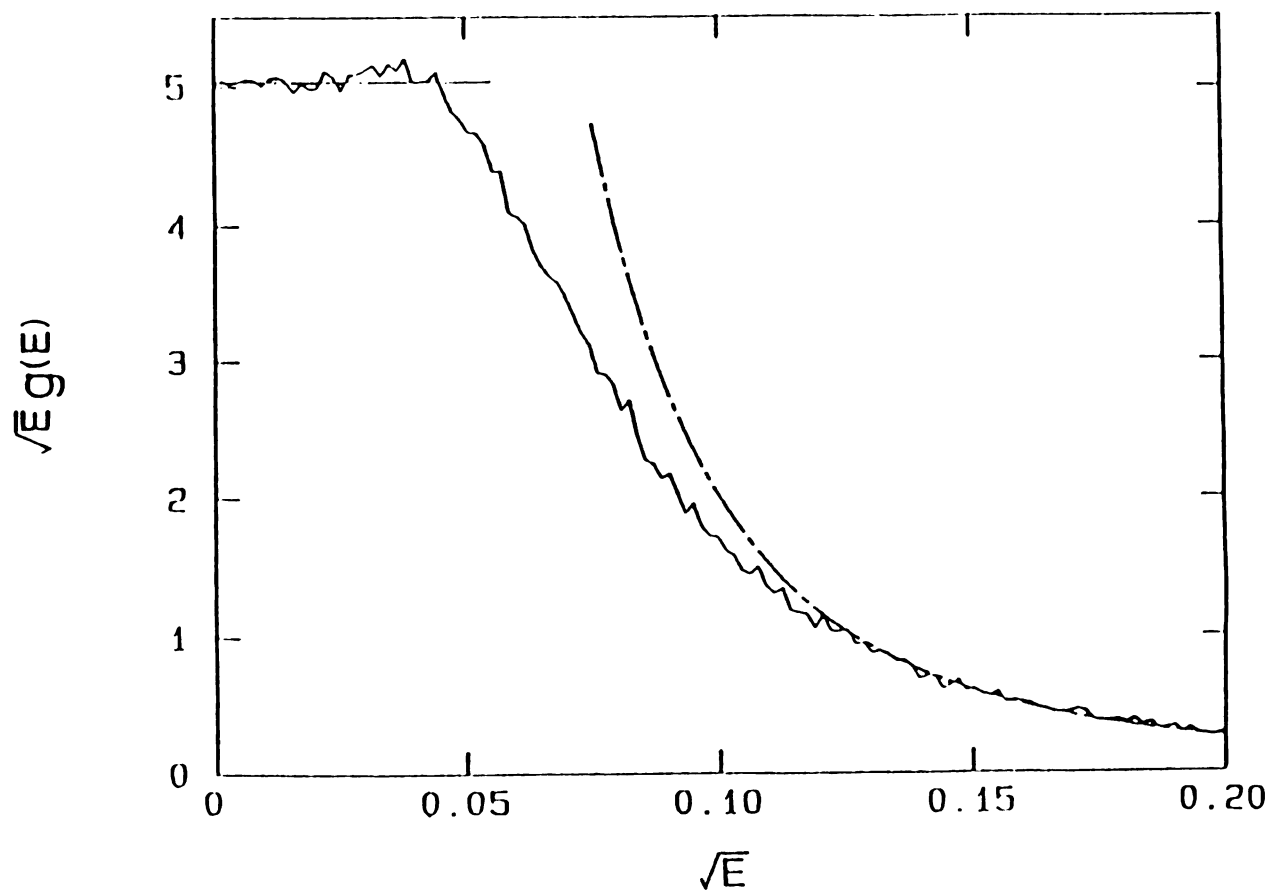


Fig. 3.9 The linear chain results for $p = 0.999$ and the two limiting forms Eqs. (24) and (27), are shown. The energy is in units where $v = 1$.

V Conclusions

We comment on our results compared to previous work on the "termite" diffusion problem. Alder et al.¹⁰ have predicted that $\langle r^2 \rangle \sim t^k$ with $k = 1+s/[2v+(t-8)]$ which, using $\tilde{d} = kd$ is at variance with our results. However it has been pointed out previously that this result is wrong¹² and Hong et al.¹¹ argue that there is no regime where $\langle r^2 \rangle \sim t^k$ because $\langle r^2 \rangle$ is dominated by diffusion on the superconducting clusters. Random walks on the superconducting clusters are related to eigenstates in the high frequency band which we are not considering. The low frequency states in which we are interested are related to random walks on the normal clusters and their dependance on the normal-superconducting interface. These walks were studied by Coniglio and Stanley²⁰ who used scaling arguments to find $\langle r^2 \rangle \sim t^k$ with $k = 2/(2-s/v)$. Using $\tilde{d} = dk$ this agrees with our equation (18). It is appropriate to use $\tilde{d} = \bar{d}k$ because the number of sites on normal clusters is not critical. Numerically, it would be very difficult to focus on these walks and exclude the random walks on the superconducting cluster.

In summary, we have evaluated the density of states of random superconducting normal networks at the percolation threshold and found the spectral dimension \tilde{d} which governs the low frequency density of states. Our values of \tilde{d} agree very well in 2D and reasonably well in 3D with our predictions for \tilde{d} using scaling theory. In this problem, as in the random resistor network problem, \tilde{d} is also related to anomalous diffusion but in contrast to the random resistor network problem, it cannot be obtained from numerical simulations of random walkers.

VI References

1. S. Alexander and R. Orbach, J. de Physique Letters 43, L625, (1982).
2. R. Rammal and G. Toulouse, J. de Physique Lettres, 44, L13 (1983).
3. S. J. Lewis and R. Stinchcombe, Phys. Rev. Lett. 52, 1021 (1984).
S. N. Evangelou, Phys. Rev. B 33, 3602 (1986).
4. Y. Gefen, A. Aharony and S. Alexander, Phys. Rev. Lett. 50, 77 (1983).
5. L. Puech and R. Rammal, J. Phys. C 35, L1197 (1983).
P. Argyrakis and R. Kopelman, Phys. Rev. B 29, 511 (1984).
6. S. Alexander, C. Laermans, R. Orbach and H.M. Rosenberg, Phys. Rev. B 28, 4615 (1983).
7. A. Aharony, S. Alexander, O. Entin-Wohlman and R. Orbach, Phys. Rev. B 31, 2565 (1985).
8. D. Stauffer, Introduction to Percolation Theory (Taylor and Francis, London and Philadelphia, 1985).
9. P.G. de Gennes, J. Phys. (Paris) Colloq. 41 C3-17 (1980).
10. J. Adler, A. Aharony and D. Stauffer, J. Phys. A 18, L129 (1985).
11. D. C. Hong, H. E. Stanley, A. Coniglio and A. Bunde, Phys. Rev B 33, 4564 (1986).
12. F. Leyvraz, J. Adler, A. Aharony, A. Bunde, A. Coniglio, D. C. Hong, H. E. Stanley and D. Stauffer, J. Phys. A 19, 3683 (1986).
13. R. Alben, M. Blume, H. Krakauer and L. Schwartz, Phys. Rev. B 15, 4090 (1975); M. F. Thorpe and R. Alben, J. Phys. C 9, 2555 (1976).

14. M. F. Thorpe, *J. Non-Cryst. Sol.* 57, 355 (1983).
15. M. F. Sykes, D. S. Gaunt and Maureen Glen, *J. Phys. A* 14, 287 (1981).
16. The quantity f can be evaluated exactly in 2D for bond percolation on the square net at p_c . The value of $f = 0.0981\dots$ can be obtained from H.N.V. Temperley and E. H. Lieb *Proc. Roy. Soc. A* 322, 251 (1977). This value was given incorrectly in Ref. 14. We have confirmed this value of f by directly counting the clusters in the samples studied in this work. A similar counting of clusters in 3D leads to the value of $f = 0.27$ for bond percolation on the simple cubic lattice at p_c .
17. S. E. Koonin, Computational Physics (Benjamin/Cummings Publishing Company, Inc., Menlo Park, CA, 1986).
18. H. J. Herrmann, B. Derrida and J. Vannimenus, *Phys. Rev. B* 30, 4080 (1984) and J. G. Zabolitzky, *Phys. Rev. B* 30, 4077 (1984).
19. M. A. Lemieux, P. Breton, A.-M. S. Tremblay, *J. Phys. (Paris) Lett* 46 L1 (1985).
20. A. Coniglio and H. E. Stanley, *Phys. Rev. Lett.* 52, 1068 (1984).

APPENDICES

APPENDIX I

Elasticity of Pure Honeycomb Lattice

The elastic moduli of model (8) in part II of this thesis is derived below. Without any dilution (i.e. perfect lattice case) $L_{ij} = L$, the lattice spacing, and $K_{ij} = K$. To avoid any confusion we change \vec{u}_{ij} to \vec{U}_{ij} to reserve the notation u for x component of \vec{U}_{ij} . The elastic energy can be written as

$$\begin{aligned}
 V = & \frac{1}{2} \sum_{\langle ij \rangle} K(L - L_0)^2 + \sum_{\langle ij \rangle} K(L - L_0) (\vec{U}_{ij} \cdot \hat{r}_{ij}) + \\
 & + \frac{1}{2} \sum_{\langle ij \rangle} K \{ (1 - L_0/L) U_{ij}^2 + L_0/L (\vec{U}_{ij} \cdot \hat{r}_{ij})^2 \} + \dots \quad (1)
 \end{aligned}$$

As mentioned in the thesis the strain energy can always be written as

$$V = \sum_{\alpha\beta} S_{\alpha\beta} \epsilon_{\alpha\beta} + \frac{1}{2} \sum_{\alpha\beta\gamma\tau} C_{\alpha\beta\gamma\tau} \epsilon_{\alpha\beta} \epsilon_{\gamma\tau} \quad (2)$$

where $S_{\alpha\beta}$ are the elements of the stress tensor and $C_{\alpha\beta\gamma\tau}$ are the second order elastic constants which are directly associated with the elastic moduli. The quantity $\epsilon_{\alpha\beta}$ is called the strain and defined by

$$\epsilon_{\alpha\beta} = \frac{\partial U_{\alpha}}{\partial x_{\beta}} \quad \alpha, \beta = x, y$$

where U_{α} and x_{β} are the components of small displacement \vec{U}_{ij} and position \vec{r} . In two dimensions

$$\epsilon_{xx} = \frac{\partial u}{\partial x} \quad \epsilon_{yx} = \frac{\partial u}{\partial y}$$

$$\epsilon_{xy} = \frac{\partial v}{\partial x} \quad \epsilon_{yy} = \frac{\partial v}{\partial y}$$

If x and y are the x and y components of the distance between site i and j then it is conventional [see Kittel] to define the uniform displacement \vec{U}_{ij} in two dimensions as

$$\begin{aligned} \vec{U}_{ij} &= u \hat{e}_x + v \hat{e}_y \\ &= (x\epsilon_{xx} + y\epsilon_{yx})\hat{e}_x + (x\epsilon_{xy} + y\epsilon_{yy})\hat{e}_y \end{aligned}$$

So

$$u = x\epsilon_{xx} + y\epsilon_{yx} \quad (3a)$$

$$v = x\epsilon_{xy} + y\epsilon_{yy} \quad (3b)$$

(3a) and (3b) are the uniform distortion on a Bravais lattice when a small force is applied.

Now let us put a small force on the frame which holds the springs of a honeycomb lattice. As discussed in the thesis the displacements (i.e. the distortions) between any two nearest neighbor sites of the sublattice A and sublattice B [see Fig.2.2] can always be written as

$$u = x\epsilon_{xx} + y\epsilon_{yx} + u' \quad (4a)$$

$$v = x\epsilon_{xy} + y\epsilon_{yy} + v' \quad (4b)$$

where x and y are the x and y components of the distance between two sites. Quantities u' and v' are the relative shift of the two sublattices in the x and y directions and can be determined by minimizing the elastic energy (1).

In Fig. 2.2 the three neighbors of site 0 are labeled by 1, 2 and 3. If the coordination of site 0 is chosen as $(0, 0)$ then the coordinates of 1, 2 and 3 will be

$$\begin{array}{ll} 0: (0, 0) & 1: \left(-\frac{\sqrt{3}}{2}a, -\frac{1}{2}a\right) \\ 2: \left(\frac{\sqrt{3}}{2}a, -\frac{1}{2}a\right) & 3: (0, a) \end{array}$$

where a is the lattice spacing. So the relative displacements of site 0 to site 1, 2 and 3 will be

$$\begin{aligned}
 u_{01} &= \frac{\sqrt{3}}{2} a \epsilon_{xx} + \frac{a}{2} \epsilon_{yx} + u' \\
 v_{01} &= \frac{\sqrt{3}}{2} a \epsilon_{xy} + \frac{a}{2} \epsilon_{yy} + v' \\
 u_{02} &= -\frac{\sqrt{3}}{2} a \epsilon_{xx} + \frac{a}{2} \epsilon_{yx} + u' \\
 v_{02} &= -\frac{\sqrt{3}}{2} a \epsilon_{xy} + \frac{a}{2} \epsilon_{yy} + v' \\
 u_{03} &= -a \epsilon_{yx} + u' \\
 v_{03} &= -a \epsilon_{yy} + v' \tag{5}
 \end{aligned}$$

If we take the parallelogram in Fig. 2.2 as a unit cell then the elastic energy per unit cell for perfect lattice can be written as

$$\begin{aligned}
 V' &= V_0 + 2N_d B \left\{ \frac{1}{2} (\sqrt{3} u_{01} + v_{01}) + \frac{1}{2} (-\sqrt{3} u_{02} + v_{02}) - v_{03} \right\} + \\
 &+ N_d \left[\frac{B}{2} (u_{01}^2 + u_{02}^2 + u_{03}^2 + v_{01}^2 + v_{02}^2 + v_{03}^2) \right. \\
 &+ \left. \frac{a}{2} \left[\frac{1}{4} (\sqrt{3} u_{01} + v_{01})^2 + \frac{1}{4} (-\sqrt{3} u_{02} + v_{02})^2 + v_{03}^2 \right] \right] \tag{6}
 \end{aligned}$$

where $B = K(1 - L_0/L)$ and $\alpha = L_0/L$. V_0 is just the static elastic energy independent of \vec{U}_{ij} . In (6) we have also used \hat{r}_{01} , \hat{r}_{02} and \hat{r}_{03} which can be easily calculated. N_d in (6) is a constant which is associated with the area of unit cell. Now we minimizing the elastic energy (6) with respect to u' and v' i.e.

$$\frac{\partial V}{\partial u'} = 0 \quad (7a)$$

and
$$\frac{\partial V}{\partial v'} = 0 \quad (7b)$$

Substituting all equations in (5) into (6) and solving (7a) and (7b) we obtain

$$u' = - \frac{\alpha(\epsilon_{yx} - \epsilon_{xy})}{2(2\alpha+B)} \quad (8a)$$

$$v' = - \frac{\alpha(\epsilon_{xx} - \epsilon_{yy})}{2(2\alpha+B)} \quad (8b)$$

Now substituting (8a) and (8b) back into (6) and compare (6) with (2) which can be written as

$$V = S_{xx}\epsilon_{xx} + S_{yy}\epsilon_{yy} + S_{xy}\epsilon_{xy} + S_{yx}\epsilon_{yx} + \\ + \frac{C_{xxxx}}{2}(\epsilon_{xx}^2 + \epsilon_{yy}^2) + C_{xxyy}\epsilon_{xx}\epsilon_{yy} + \frac{C_{xyxy}}{2}(\epsilon_{xy}^2 + \epsilon_{yx}^2) +$$

$$+ C_{xyyx} \epsilon_{xy} \epsilon_{yx} , \quad (2')$$

it is straight forward although a little bit lengthy to show that

$$T = S_{xx} = S_{yy} = \frac{B}{\sqrt{3}} = (1 - \eta) \frac{K}{\sqrt{3}}$$

$$S_{xy} = S_{yx} = 0$$

$$C_{xxxx} = C_{11} = \frac{a^2 + 5aB + 4B^2}{2\sqrt{3} (2B + a)} = \frac{4 - 3\eta}{2 - \eta} \frac{K}{2\sqrt{3}}$$

$$C_{xxyy} = C_{12} = \frac{a^2 + aB}{2\sqrt{3} (2B + a)} = \frac{\eta}{2 - \eta} \frac{K}{2\sqrt{3}}$$

$$C_{xyxy} = \tilde{C}_{44} = \frac{4B^2 + 3aB}{2\sqrt{3} (2B + a)} = \frac{\eta(1 - \eta)}{2 - \eta} \frac{K}{2\sqrt{3}}$$

$$C_{xyyx} = C_{44} = \frac{aB}{2\sqrt{3} (2B + a)} = \frac{(4 - \eta)(1 - \eta)}{2 - \eta} \frac{K}{2\sqrt{3}}$$

In the second column above we have used the conventional notation $C_{xxxx} = C_{11}$, $C_{xxyy} = C_{12}$, $C_{xyxy} = C_{44}$ and $C_{xyyx} = \tilde{C}_{44}$. In the fourth column we have used $a = K\eta$, $B = K(1 - \eta)$ and $\eta = L_0/L$. We have also considered the symmetries of the honeycomb lattice to reduce the number of independent elastic constants.

APPENDIX II

Percolation Thresholds of Stretched Spring Model
on Honeycomb Lattice

We give a derivation of the percolation thresholds p for the stretched spring model in part II of this thesis.

The method here is the same as that of Tang and Thorpe but it is generalized to the honeycomb lattice which is a non-Bravais lattice. A honeycomb lattice is composed of two interpenetrating triangular sublattices. We start by writing down the forces on the sublattice A and sublattice B. [see Fig. 2.2] Using the elastic energy (8) in part II of this thesis we have

$$\vec{F}_A = - \frac{\partial V}{\partial \vec{u}_A} = - B \sum_{\delta} (\vec{u}_A - \vec{u}_{\delta}) - \alpha \sum_{\delta} [(\vec{u}_A - \vec{u}_{\delta}) \cdot \hat{r}_{A\delta}] \hat{r}_{A\delta} \quad (1a)$$

$$\vec{F}_B = - \frac{\partial V}{\partial \vec{u}_B} = - B \sum_{\delta} (\vec{u}_B - \vec{u}_{\delta}) - \alpha \sum_{\delta} [(\vec{u}_B - \vec{u}_{\delta}) \cdot \hat{r}_{B\delta}] \hat{r}_{B\delta} \quad (1b)$$

Here the subscripts A and B are used to denote the quantities of sublattice A and B respectively and the symbol δ is used for nearest neighbors of A and B. Now substituting the Fourier transformations of displacements and forces

$$\vec{u}_A = \frac{1}{N} \sum_{\vec{k}} \vec{u}_{A\vec{k}} e^{i\vec{k} \cdot \vec{R}_A} \quad (2a)$$

$$\vec{u}_B = \frac{1}{N} \sum_{\vec{k}} \vec{u}_{B\vec{k}} e^{i\vec{k} \cdot \vec{R}_B} \quad (2b)$$

$$\vec{F}_A = \frac{1}{N} \sum_{\vec{k}} \vec{F}_{A\vec{k}} e^{i\vec{k} \cdot \vec{R}_A} \quad (3a)$$

$$\vec{F}_B = \frac{1}{N} \sum_{\vec{k}} \vec{F}_{B\vec{k}} e^{i\vec{k} \cdot \vec{R}_B} \quad (3b)$$

into (1a) and (1b) and writing the results in the matrix form we will have [for each \vec{k}]

$$F_{A\vec{k}} = -D_{AA}(\vec{k})u_{A\vec{k}} - D_{AB}(\vec{k})u_{B\vec{k}} \quad (4a)$$

$$F_{B\vec{k}} = -D_{BA}(\vec{k})u_{A\vec{k}} - D_{BB}(\vec{k})u_{B\vec{k}} \quad (4b)$$

where

$$u_{A\vec{k}} = \begin{pmatrix} u_{A\vec{k}}^x \\ u_{A\vec{k}}^y \end{pmatrix}$$

$$u_{B\vec{k}} = \begin{pmatrix} u_{B\vec{k}}^x \\ u_{B\vec{k}}^y \end{pmatrix}$$

$$F_{A\vec{k}} = \begin{pmatrix} F_{A\vec{k}}^x \\ F_{A\vec{k}}^y \end{pmatrix}$$

$$F_{B\vec{k}} = \begin{pmatrix} F_{B\vec{k}}^x \\ F_{B\vec{k}}^y \end{pmatrix}$$

Here the superscripts x and y denote the x and y components. Subscript k denotes the k th Fourier component. 2×2 Matrices D_{AA} , D_{AB} , D_{BA} and D_{BB} are the following.

$$D_{AA} = \begin{vmatrix} 3(\alpha + 2B)/2 & 0 \\ 0 & 3(\alpha + 2B)/2 \end{vmatrix} \quad D_{AB} = \begin{vmatrix} -a_1 & -a_2 \\ -a_2 & -a_3 \end{vmatrix}$$

$$D_{BA} = \begin{vmatrix} -a_1^* & -a_2^* \\ -a_2^* & -a_3^* \end{vmatrix} \quad D_{BB} = \begin{vmatrix} 3(\alpha + 2B)/2 & 0 \\ 0 & 3(\alpha + 2B)/2 \end{vmatrix}$$

$$\text{and } a_1 = B e^{ik_1 \sqrt{3}a} + (B + \frac{3}{4}\alpha) e^{ik_2 \sqrt{3}a} + (B + \frac{3}{4}\alpha) e^{ik_1 \sqrt{3}a + ik_2 \sqrt{3}a}$$

$$a_2 = \alpha \frac{\sqrt{3}}{4} e^{ik_2 \sqrt{3}a} (1 - e^{ik_1 \sqrt{3}a})$$

$$a_3 = (\alpha + B) e^{ik_1 \sqrt{3}a} + (B + \frac{\alpha}{4}) e^{ik_2 \sqrt{3}a} + (B + \frac{\alpha}{4}) e^{ik_1 \sqrt{3}a + ik_2 \sqrt{3}a}$$

where a^* is the complex conjugate of a and $\alpha = KL_0/L$, $B = K(1-L_0/L)$. k_1 and k_2 are the k 's components in the \vec{b}_1 and \vec{b}_2 directions. [see Fig. 2.2]

From (4a) and (4b) we can solve u_{Ak} and u_{Bk} in the following form

$$D_{AB}^{-1} F_{Ak} - D_{BB} F_{Bk} = (-D_{AB}^{-1} D_{AA} + D_{BB}^{-1} D_{BA}) u_{Ak} \quad (5a)$$

$$D_{AA}^{-1} F_{Ak} - D_{BA} F_{Bk} = (-D_{AA}^{-1} D_{AB} + D_{BA}^{-1} D_{BB}) u_{Bk} \quad (5b)$$

By defining

$$\begin{aligned}
 A &= D_{AB}^{-1} (-D_{AB}^{-1} D_{AA} + D_{BB}^{-1} D_{BA})^{-1} \\
 B &= D_{BB}^{-1} (-D_{AB}^{-1} D_{AA} + D_{BB}^{-1} D_{BA})^{-1} \\
 C &= D_{AA}^{-1} (-D_{AA}^{-1} D_{AB} + D_{BA}^{-1} D_{BB})^{-1} \\
 D &= D_{BA}^{-1} (-D_{AA}^{-1} D_{AB} + D_{BA}^{-1} D_{BB})^{-1},
 \end{aligned} \tag{6}$$

(5a) and (5b) can be written as

$$u_{Ak} = AF_{Ak} + BF_{Bk} \tag{7a}$$

$$u_{Bk} = CF_{Ak} + DF_{Bk} \tag{7b}$$

Here symbols for matrices A, B, C and D should not be confused with the subscripts.

After removing a spring the two sites move along the direction of the missing spring (see Fig. 2.4). In order to calculate the effective spring constant of the resulting network in this direction one needs to pull the two sites back along the same direction. So the net force is in the direction of unit vector \hat{r}_{AB} . Thus

$$\tilde{F}_{A\delta} = f \hat{r}_{AB} \delta_{A\delta} \quad (8a)$$

$$\tilde{F}_{B\delta} = f \hat{r}_{BA} \delta_{B\delta} = -f \hat{r}_{AB} \delta_{B\delta} \quad (8b)$$

The Fourier transformation of \tilde{F}_{Ak} and \tilde{F}_{Bk} are

$$\tilde{F}_{Ak} = \sum_{\delta} \tilde{F}_{A\delta} e^{i\vec{k} \cdot \vec{R}_{A\delta}} \quad (9a)$$

$$\tilde{F}_{Bk} = \sum_{\delta} \tilde{F}_{B\delta} e^{i\vec{k} \cdot \vec{R}_{B\delta}} \quad (9b)$$

Substituting (7a) and (7b) into (2a) and using (8a), (8b), (9a) and (9b) we have

$$\begin{aligned} \tilde{u}_A &= \frac{1}{\bar{N}} \sum_{\mathbf{k}} e^{i\vec{k} \cdot \vec{R}_A} \tilde{u}_{Ak} \\ &= \frac{f}{\bar{N}} \sum_{\mathbf{k}} \sum_{\delta} e^{i\vec{k} \cdot \vec{R}_A} (A e^{-i\vec{k} \cdot \vec{R}_A} - B e^{-i\vec{k} \cdot \vec{R}_B}) \hat{r}_{AB} \end{aligned} \quad (10a)$$

Similarly

$$\tilde{u}_B = \frac{f}{\bar{N}} \sum_{\mathbf{k}} \sum_{\delta} e^{i\vec{k} \cdot \vec{R}_B} (C e^{-i\vec{k} \cdot \vec{R}_A} - D e^{-i\vec{k} \cdot \vec{R}_B}) \hat{r}_{AB} \quad (10b)$$

So

$$\vec{u}_B - \vec{u}_A = \frac{f}{N} \sum_{\vec{k}} \sum_{\delta} [-(A + D) + Be^{i\vec{k} \cdot \vec{R}_{AB}} + Ce^{-i\vec{k} \cdot \vec{R}_{AB}}] \hat{r}_{AB}$$

$$\delta u_{AB} = \hat{r}_{AB} \cdot (\vec{u}_B - \vec{u}_A) = \frac{f}{N} \sum_{\vec{k}} \sum_{\delta} \hat{r}_{AB} [-(A + D) + Be^{i\vec{k} \cdot \vec{R}_{AB}} + Ce^{-i\vec{k} \cdot \vec{R}_{AB}}] \hat{r}_{AB}$$

In the summation

$$\vec{R}_{AB} = \vec{R}_{\delta} \quad \text{and} \quad \hat{r}_{AB} = \hat{\delta}$$

Therefore following Tang and Thorpe

$$p = a^* = \frac{K}{2Nz} \sum_{\vec{k}} \text{Tr} \{ \hat{\delta} \hat{\delta} [-(A + D) + Be^{i\vec{k} \cdot \vec{R}_{AB}} + Ce^{-i\vec{k} \cdot \vec{R}_{AB}}] \} \quad (12)$$

APPENDIX III

Published Paper

Spectral dimensionality of random superconducting networks

A. R. Day, W. Xia, and M. F. Thorpe

Department of Physics and Astronomy and Center for Fundamental Materials Research, Michigan State University, East Lansing, Michigan 48824

(Received 2 March 1987; revised manuscript received 2 July 1987)

We compute the spectral dimensionality \bar{d} of random superconducting-normal networks by directly examining the low-frequency density of states at the percolation threshold. We find that $\bar{d} = 4.1 \pm 0.2$ and 5.8 ± 0.3 in two and three dimensions, respectively, which confirms the scaling relation $\bar{d} = 2d/(2 - s/\nu)$, where s is the superconducting exponent and ν the correlation-length exponent for percolation. We also consider the one-dimensional problem where scaling arguments predict, and our numerical simulations confirm, that $\bar{d} = 0$. A simple argument provides an expression for the density of states of the localized high-frequency modes in this special case. We comment on the connection between our calculations and the "termite" problem of a random walker on a random superconducting-normal network and point out difficulties in inferring \bar{d} from simulations of the termite problem.

1. INTRODUCTION

The question of *dynamics* on dilute random systems at the percolation threshold has been the subject of considerable attention in the past five years.¹⁻⁴ The infinite cluster at percolation is a fractal, so that the excitations are qualitatively different to those on a regular Euclidean lattice and are governed by an additional dimension, the spectral dimension \bar{d} .^{1,2} Because of the similarities between the diffusion equation and the equations of motion for a system described by a tight-binding Hamiltonian (or an elastic Hamiltonian) it is clear that there are two approaches to evaluating \bar{d} .

One approach is to examine the *low-frequency dynamical response* of the system described by the Hamiltonian

$$H = \sum_{\langle i,j \rangle} V_{ij} (a_i^\dagger a_j - a_j^\dagger a_i), \quad (1)$$

where the V_{ij} are randomly distributed on the nearest-neighbor bonds according to the probability distribution

$$P(V_{ij}) = p\delta(V - V_{ij}) + (1-p)\delta(V_{ij}), \quad (2)$$

and we restrict the sum to sites on the infinite cluster. The a_i, a_i^\dagger are either Bose or Fermi operators (the results are the same when only one particle excitations are considered) and the diagonal term is present in (1) to preserve translational invariance. This dilute tight-binding Hamiltonian describes the physics of several different random systems; dilute magnetic systems, random resistor networks, and random scalar elastic networks. By scalar elasticity we mean for example displacements perpendicular to the elastic network. The low-frequency density of states at p_c is predicted to behave as

$$\rho(E) \sim E^{(d-\bar{d})/2}, \quad (3)$$

where \bar{d} is the spectral dimensionality that can be expressed as^{1,2}

$$\bar{d} = \frac{2\bar{d}}{2 + \frac{t-\beta}{\nu}}, \quad (4)$$

and t is the conductivity exponent. The quantities β and ν are the geometric exponents³ which govern the probability of being on the infinite cluster, and the correlation length, respectively. The fractal dimensionality is $\bar{d} = d - \beta/\nu$. Direct numerical evaluation of the density of states in two dimensions¹ on dilute spin systems has confirmed Eq. (4) and that \bar{d} is close to $\frac{1}{2}$ which Alexander and Orbach¹ have conjectured to be the value of \bar{d} in all dimensions except one dimension (1D).

An alternative approach is to study the anomalous diffusion of a random walker on the infinite percolation cluster. Scaling arguments^{1,2,4} suggest that the mean square displacement $\langle r^2 \rangle$ scales with time as

$$\langle r^2 \rangle \sim t^k \quad (5)$$

and

$$k = \frac{2}{2 + \frac{t-\beta}{\nu}},$$

where t, β , and ν were defined previously. By relating the probability of return to the origin with the density of states,¹ one obtains $\bar{d} = \bar{d}k$ in agreement with Eq. (4).

Numerical simulations of random walks on *dilute systems* are a good indirect way of obtaining the spectral dimensionality \bar{d} using Eq. (5) and the relation $\bar{d} = k\bar{d}$. Value of \bar{d} obtained in this way⁵ agree with direct simulations¹ of the low-frequency density of states at p_c .

The randomly dilute problem discussed above can be considered as a random system of strong bonds V_s and weak bonds V_w in the limit $V_s \rightarrow V, V_w \rightarrow 0$. The other limit, $V_s \rightarrow \infty, V_w \rightarrow V$, is also of considerable interest and is the subject of this article. It would describe a random superconducting network or the elastic properties of

a system with rigid grains weakly coupled by soft springs. In the general problem, the density of states is divided into bands: a high frequency band associated with internal modes of the clusters of strong bonds and a low-frequency band associated with vibrations of the soft regions. In the limit $V_w \rightarrow 0$, $V_s \rightarrow V$, the low-frequency band becomes a δ function at the origin and the spectral dimension describes the low-frequency edge of the high-frequency band. In the limit $V_w \rightarrow V$, $V_s \rightarrow \infty$, the high-frequency band is driven off to infinity and the δ function broadens. There will be a different spectral dimension associated with this low-frequency edge.

In diffusion language, the superconducting limit is the problem of termite diffusion⁹ which has been the subject of considerable work¹⁰⁻¹² and some controversy. In principle, it should provide information about the density of states and the spectral dimension d for the problem but in practice this is not the case because the random walk is completely dominated by the distances moved on the *superconducting clusters*. As has been pointed out by Hong *et al.*¹¹ there is no region where $\langle r^2 \rangle \sim t^k$ because even at time zero, $\langle r^2 \rangle \sim \xi^2 \sim t^{d/2}$, the average radius of the superconducting clusters. The low-frequency excitations we are interested in are associated with the small, time-dependent contribution to $\langle r^2 \rangle$ superimposed on the divergent $\xi^2 \sim t^{d/2}$. Clearly this is impossible to obtain numerically and we therefore believe that direct simulations of the low frequency response is the best way to evaluate the spectral dimension.

II. DENSITY OF STATES

In this paper we obtain the density of states, and hence the spectral dimension d for the *superconducting case*. The system is described by the Hamiltonian (1) but with the interaction strength distribution

$$P(V_{ij}) = p\delta(V_{ij} - V_w) + (1-p)\delta(V_{ij} - V_s), \quad (6)$$

where $V_s \rightarrow \infty$ in the superconducting limit. The equations of motion for the Hamiltonian (1) are

$$i\hbar \frac{\partial c_k}{\partial t} = \sum_l V_{kl}(c_k - c_l), \quad (7)$$

where the c_k are the amplitudes of the wave function on the k site.

Two sites k and l , connected by a bond $V_{kl} = \infty$, have the same amplitudes so that $c_k = c_l$ can be considered as a single site of mass 2. This process is repeated for all superconducting bonds so each superconducting cluster has one degree of freedom and a mass M equal to the number of sites in the cluster. We consider a site connected to no superconducting bonds to be a cluster of size 1. The equations of motion for the clusters so defined are

$$i\hbar M_k \frac{\partial c_k}{\partial t} = \sum_l V_{kl}(c_k - c_l), \quad (8)$$

where k, l are now cluster indices and n_{kl} is the total number of normal bonds between the k and the l cluster. By defining $(M_k)^{1/2} c_k = c'_k$, we have the Hermitian equation of motion

$$i\hbar \frac{\partial c'_k}{\partial t} = \sum_l V_{kl} \left[\frac{c'_k}{M_k} - \frac{c'_l}{\sqrt{M_k M_l}} \right], \quad (9)$$

which we solve numerically using the equation of motion technique.¹

If the original system has N sites, there are only Nf clusters¹¹ so we have reduced the number of degrees by a factor of f . For small p

$$f = 1 - \frac{zp}{2} + \dots, \quad (10)$$

where z is the number of nearest neighbors. Note that f decreases to a very small value at p_c . In the square net and simple cubic lattice we find it is 0.098 and 0.27, respectively.¹⁵ Thus setting V_w strictly equal to infinity reduces the effective size of the system, especially in 2D, although there is some initial time cost in identifying all the clusters. This advantage cannot be achieved by setting V_w large and taking a limiting process. Note also that f is finite at p_c for $d > 2$ but it is zero in 1D which affects the scaling arguments for d as we discuss later.

The equations of motion were integrated forward in time from $0 \rightarrow T$ using standard methods.¹¹ The first few points were obtained using a fourth-order Runge-Kutta algorithm and subsequently a fourth-order Adams integration scheme was used.¹⁶ The density of states $g(E)$ is obtained from Fourier transforming the result of the time integration,

$$g(E) = \frac{1}{2\pi} \sum_k M_k \int_{-\infty}^{+\infty} c_k(t)c_k^*(0)e^{iEt} dt. \quad (11)$$

This integral is converted to one over positive times only.¹¹ Random phases¹¹ are put on the clusters so that only the on-site terms required in (11) are retained in the limit of a large system. This is a standard way to obtain densities of states in the equation of motion technique.

In Fig. 1 we show results for the square lattice at $p_c = \frac{1}{2}$. The results are from averages over 25 samples of

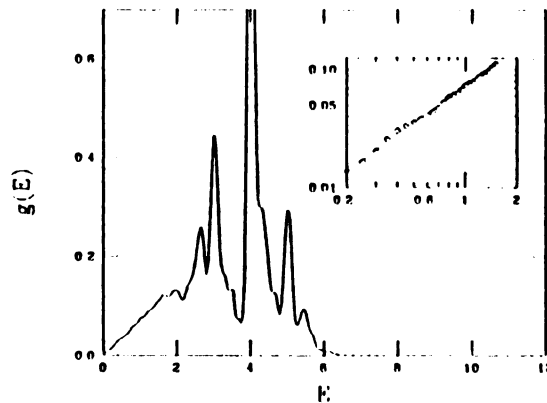


FIG. 1. The density of states for a random square lattice of superconducting and normal bonds at $p_c = \frac{1}{2}$. The inset shows the low-energy data on a log log base 10 plot. The straight line drawn is a least squares fit to the data points shown from which d is obtained via Eq. (3). The energy is in units with $V = 1$.

100 × 100 networks. Because of the reduction in size due to the f factor only ~ 1000 amplitudes had to be monitored. The inset shows a log-log plot at low frequencies which gives a slope of 1.05 ± 0.1 leading to $\bar{d} = 4.1 \pm 0.2$ from Eq. (3). In Fig. 2 we show similar results for the simple cubic lattice⁶ at $p_c = 0.2491$. The results are from average over 25 samples of 21 × 22 × 23 networks. Because of the reduction due to the f factor only ~ 2800 amplitudes had to be monitored. The inset shows a log-log plot at low frequencies which gives a slope of 1.9 ± 0.15 and hence $\bar{d} = 5.8 \pm 0.3$. We examined a single sample with about 16 times as many sites in both 2D and 3D and found no significant changes in the values of \bar{d} . The sharp features at higher energies in Figs. 1 and 2 will be discussed in a subsequent publication.¹⁷

III. SCALING ARGUMENTS

The scaling argument for \bar{d} is given below following the ideas developed for the dilute case.^{7,8} It is easiest to use the language of *phonons*, i.e., vibrations on a network of normal and infinitely rigid springs. The results apply equally well to any system described by the tight-binding Hamiltonian (1) with the probability distribution (6). Close to p_c and for systems of size L much greater than the correlation length $\xi \sim (p_c - p)^{-\nu}$ we expect the system to appear homogeneous with an effective elastic modulus $Y \sim (p_c - p)^{-s}$ where s is the superconducting exponent. Because the system is fully connected, *all sites contribute to the inertia* in the long-wavelength limit, the total mass $M \sim L^{-d}$ and thus the mass density ρ is *noncritical*, i.e., it is independent of ξ . The low-frequency excitations are phonons with a sound velocity

$$c^2(\xi) \sim Y/\rho \sim \xi^{s/\nu}. \quad (12)$$

For wavelengths $\lambda \sim \xi$ the fractal structure of the lattice becomes important. The excitations are no longer phonons and we have a fracton-phonon crossover. The crossover frequency is given by

$$\omega_{co} \sim \frac{c(\xi)}{\xi} \sim \xi^{-(2-s/\nu)/2}. \quad (13)$$

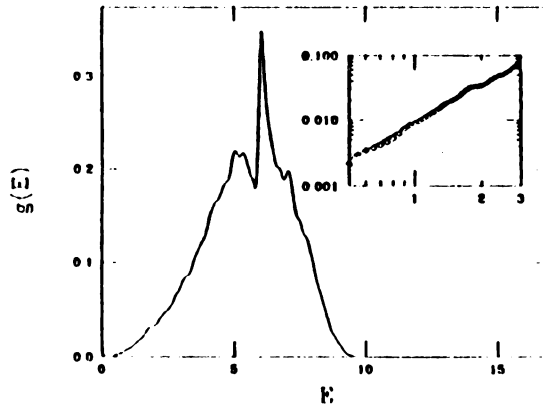


FIG. 2. Same as Fig. 1 except for a simple cubic lattice at $p_c = 0.2491$. The inset shows the low energy data on a log-log (three 10) plot. The energy is in units where $V = 1$.

Using a Debye-type theory we can write the normalized density of states for the phonons as

$$\rho(\omega) \sim C(\xi)^{-d} \left[\frac{L}{2\pi} \right]^d \omega^{d-1} / Nf. \quad (14)$$

To allow for the fracton-phonon crossover we introduce a scaling function $h(\omega/\omega_{co})$ into (14) and obtain

$$\rho(\omega) \sim C(\xi)^{-d} \left[\frac{L}{2\pi} \right]^d \omega^{d-1} h(\omega/\omega_{co}) / Nf. \quad (15)$$

For $d \geq 2$, f is noncritical and so the critical behavior of $\rho(\omega)$ is

$$\begin{aligned} \rho(\omega) &\sim \xi^{-d/(2\nu)} \omega^{d-1} h \left[\frac{\omega}{\omega_{co}} \right] \\ &\sim \omega_{co}^{d/(2\nu-1)} \omega^{d-1} h \left[\frac{\omega}{\omega_{co}} \right], \end{aligned} \quad (16)$$

where we have used (12) and (13). In the low-frequency (phonon) regime $x = \omega/\omega_{co} \ll 1$ and $h(x) \rightarrow \text{constant}$, so that $\rho(\omega) \sim \omega^{d-1}$ as expected. For $\omega > \omega_{co}$, the fracton regime, we rewrite (15) as

$$\begin{aligned} \rho(\omega) &\sim \omega^{(2d)/(2-s/\nu)-1} \left[\frac{\omega}{\omega_{co}} \right]^{-d/(2\nu-1)} h \left[\frac{\omega}{\omega_{co}} \right] \\ &\sim \omega^{d-1} r \left[\frac{\omega}{\omega_{co}} \right], \end{aligned} \quad (17)$$

where $r(x) = x^{-d/(2\nu-1)} h(x)$ is expected to tend to a constant for x large because $\rho(\omega)$ should be independent of ξ or equivalently of ω_{co} in this limit. Equation (17) defines the spectral dimension,

$$\bar{d} = \frac{2d}{2-s/\nu}. \quad (18)$$

We have discussed scaling relations for *vibrational modes*. Exactly parallel arguments can be made in all dimensions for *tight-binding Hamiltonians* where $E \sim \omega^2 \sim c^2 k^2$ leading to

$$g(E) \sim E^{(\bar{d}-2)/2}. \quad (19)$$

Comparing Eq. (18) with the result for dilute systems Eq. (4), we notice the following differences.

(a) The numerator involves d rather than \bar{d} . The excitations in the superconducting case can explore the whole system whereas in the dilute case, Eq. (4) is obtained for excitations on the infinite cluster. If the *finite clusters* are included in the dilute case,⁶ then \bar{d} is also replaced by d in Eq. (4).

(b) The conductivity exponent t in Eq. (4) is replaced by the superconducting exponent $-s$ in Eq. (18).

(c) The exponent β does not appear in Eq. (18). In the dilute system, the probability of being on the infinite cluster scales as $(p - p_c)^\beta$. In the low-frequency dynamical

TABLE I. Comparison of the spectral dimensionality \bar{d} obtained directly in this work with the scaling relation. Values of s/v are taken from Ref. 18.

d	\bar{d} (This work)	$\bar{d} = 2d/(2-s/v)$
2	4.1 ± 0.2	3.91 ± 0.04
3	5.8 ± 0.3	5.2 ± 0.2

response of the infinite cluster, this is the inertia term and appears in (4). In the superconducting system, all sites are connected and so contribute to the inertia which is independent of p .

Good estimates of s/v for 2D and 3D are given in Ref. 18. Using $s/v = 0.977 \pm 0.010$ and 0.85 ± 0.04 in 2D and 3D, respectively, gives $\bar{d} = 3.91 \pm 0.04$ in 2D and $\bar{d} = 5.2 \pm 0.2$ in 3D. We see from Table I that this is in good agreement with our results in 2D and reasonable agreement with our results in 3D where the numerical results are less accurate because the lattices had smaller linear dimensions.

IV. ONE DIMENSION: A SPECIAL CASE

The scaling in 1D is rather different because $f \sim (1-p) \sim \xi^{-1}$ is critical. We start with the Debye form for the integrated density of states [see Eq. (15)]

$$I(\omega) \sim \frac{1}{Nf} c(\xi)^{-d} \left[\frac{L}{2\pi} \right]^d \omega^d H \left[\frac{\omega}{\omega_{co}} \right]. \tag{20}$$

Setting $d = 1$ and keeping only the critical terms we have

$$\begin{aligned} I(\omega) &\sim \xi^{1-(s/2v)} \omega H \left[\frac{\omega}{\omega_{co}} \right] \\ &\sim \left[\frac{\omega}{\omega_{co}} \right] H \left[\frac{\omega}{\omega_{co}} \right] \\ &\sim R \left[\frac{\omega}{\omega_{co}} \right], \end{aligned} \tag{21}$$

where $R(x) = xH(x)$ is expected to tend to a constant for x large. In this limit we have $I(\omega) \sim \omega^d$ which leads to $\bar{d} = 0$ in 1D. This result is expected because in the limit $p \rightarrow p_c = 1$ we have a perfect superconducting chain which is completely rigid and thus has only one degree of freedom. This can be considered as a zero-dimensional object for which $\bar{d} = d = 0$.

In 1D there are still excitations associated with rigid clusters of lengthless than ξ . Because the probability of neighboring clusters having the same mass M is small, we can treat each cluster as an *Einstein oscillator* of frequency $\omega^2 = 2V/M$. The probability of a cluster having mass M is

$$P(M) = (1-p)^{M-1}, \tag{22}$$

where we have chosen the mass of a single site to be one, so M is an integer. The density of states

$$\rho(\omega) = P(M) \left| \frac{dM}{d\omega} \right|,$$

so

$$\begin{aligned} \rho(\omega) &= (1-p)^{M-1} \frac{\omega M^2}{V} \\ &= (1-p)^{(2V/\omega^2)-1} \frac{4V}{\omega^3}. \end{aligned} \tag{23}$$

For $(1-p)$ small, we can write $p \approx e^{-(1-p)}$ and thus

$$\rho(\omega) \approx \frac{1-p}{p} e^{-2V/(1-p)\omega^2} \frac{4V}{\omega^3},$$

which to leading order in $(1-p)$ gives

$$\rho(\omega) = 4V(1-p)/\omega^3,$$

or equivalently in tight-binding language

$$g(E) = 2V(1-p)/E^2. \tag{24}$$

The exponential can be replaced by unity as there are other terms $O(1-p)^2$ that we have neglected in deriving Eq. (24).

This result is *special* in 1D. In higher dimensions if we tried to consider the superconducting clusters as Einstein oscillators they would have a frequency

$$\omega_i^2 = \frac{n_i V}{M_i}, \tag{25}$$

where $n_i = \sum_{j \neq i} n_{ij}$ is the number of surface bonds connecting cluster i to other clusters bonds and M_i is the mass of the i cluster. However, for superconducting clusters we find numerically that $n_i/M_i \sim \text{const}$ of order 1, unlike in 1D where $n_i = 2$ always and M_i can take any value. In 1D the likelihood of having two adjacent clusters with the same mass, and hence the same frequency, is small. Therefore the modes do not hybridize and remain localized with $\bar{d} = 0$. However for $d \geq 2$, the likelihood of adjacent clusters having the same Einstein frequency is high, as all the heavier clusters have essentially the same frequencies. Therefore, the Einstein modes from the heavier superconducting clusters hybridize forming extended low-frequency modes with $\bar{d} > 2$.

In 1D we cannot do simulations at $p_c = 1$ so we have worked at small $(1-p)$. For frequencies $\omega < \omega_{co}$ or equivalently for wavelengths $\lambda > \xi \sim (1-p)^{-1/2}$ which is the typical length of a rigid cluster, we expect phonons with a constant density of states

$$\rho(\omega) \sim C(p)^{-1}/f. \tag{26}$$

Because the linear chain just involves adding springs in series in the static limit, we have

$$g(E) = \frac{1}{2\pi [V(1-p)E]^2}. \tag{27}$$

In Fig. 3 we have plotted $\rho(\omega)$ against ω [or equivalently $\sqrt{VE}g(E)$ against \sqrt{E}] for $p = 0.9, 0.99,$ and 0.999 . The results were obtained from chains of 20000 clusters

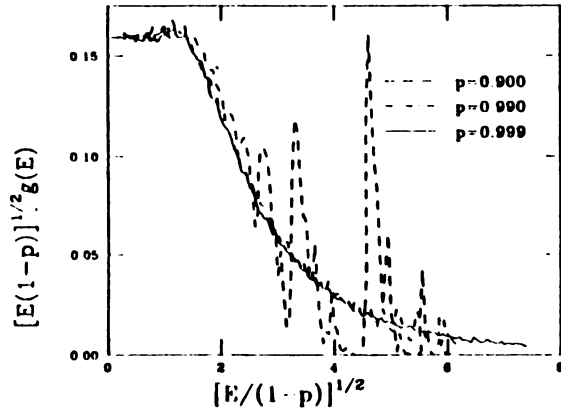


FIG. 3. The density of states for a random linear chain of superconducting and normal bonds of $p=0.9, 0.99, \text{ and } 0.999$. The results are rescaled as indicated to show the scaling behavior. The energy is in units where $V=1$.

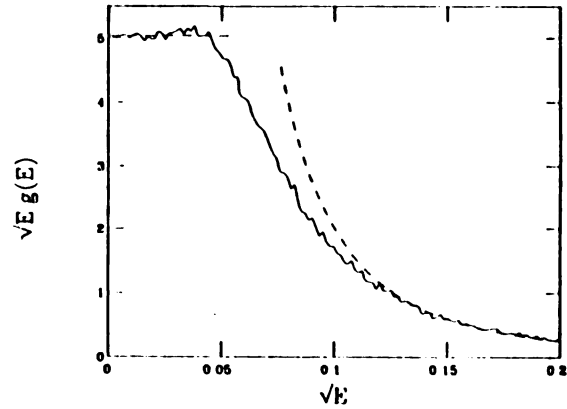


FIG. 4. The linear chain results for $p=0.999$ are shown as a solid line and the two limiting forms Eqs. (24) and (27) are shown as dashed lines. The energy is in units where $V=1$.

($Nf=20000$) using a *transfer matrix technique*.¹⁹ The results have been rescaled by plotting $\sqrt{E(1-p)}g(E)$ against $\sqrt{E/(1-p)}$ to show the scaling behavior. In Fig. 4 we have plotted $\sqrt{E}g(E)$ against \sqrt{E} for $p=0.999$ and the two limiting curves

$$\sqrt{E}g(E) = [2\pi\sqrt{V(1-p)}]^{-1}$$

and

$$\sqrt{E}g(E) = 2V(1-p)/E^{1/2}$$

for low and high energies, respectively.

V. CONCLUSIONS

We comment on our results compared to previous work on the "termite" diffusion problem. Alder *et al.*¹⁰ have predicted that $\langle r^2 \rangle \sim t^k$ with

$$k = 1 + s/[2v + (t - \beta)]$$

which, using $\bar{d} = dk$ is at variance with our results. However, it has been pointed out previously that this result is wrong¹² and Hong *et al.*¹¹ argue that there is no regime where $\langle r^2 \rangle \sim t^k$ because $\langle r^2 \rangle$ is dominated by diffusion on the superconducting clusters. Random walks on the superconducting clusters are related to eigenstates in the high-frequency band which we are not considering. The low-frequency states in which we are interested are relat-

ed to random walks on the normal clusters and their dependence on the normal-superconducting interface. These walks were studied by Coniglio and Stanley²⁰ who used scaling arguments to find $\langle r^2 \rangle \sim t^k$ with $k = 2/(2 - s/\nu)$. Using $\bar{d} = dk$ this agrees with our Eq. (18). It is appropriate to use $\bar{d} = dk$ rather than $\bar{d} = \bar{d}k$, because the number of sites on normal clusters is not critical. Numerically, it would be very difficult to focus on these walks and exclude the random walks on the superconducting cluster.

In summary, we have evaluated the density of states of random superconducting normal networks at the percolation threshold and found the spectral dimension \bar{d} which governs the low-frequency density of states. Our values of \bar{d} agree reasonably well with our predictions for \bar{d} using scaling theory. In this problem, as in the random resistor network problem, \bar{d} is also related to anomalous diffusion but in contrast to the random resistor network problem, it cannot be obtained easily from numerical simulations of random walkers.

ACKNOWLEDGMENTS

We would like to thank C. J. Lambert for useful discussions and D. C. Hong for bringing Refs. 11 and 12 to our attention. This work was supported by the National Science Foundation under Grant No. DMR8317610 and by the Center for Fundamental Materials Research at Michigan State University.

¹S. Alexander and R. Orbach, *J. Phys. (Paris) Lett.* **43**, L625 (1982).

²R. Rammal and G. Toulouse, *J. Phys. (Paris) Lett.* **44**, L13 (1983).

³S. J. Lewis and R. Stinchcombe, *Phys. Rev. Lett.* **52**, 1021 (1984); S. N. Evangelou, *Phys. Rev. B* **33**, 3602 (1986).

⁴Y. Gefen, A. Aharony, and S. Alexander, *Phys. Rev. Lett.* **50**, 77 (1983).

⁵L. Puech and R. Rammal, *J. Phys. C* **35**, L1197 (1983); P. Argyrakis and R. Kopelman, *Phys. Rev. B* **29**, 511 (1984).

⁶S. Alexander, C. Laermans, R. Orbach, and H. M. Rosenberg, *Phys. Rev. B* **28**, 4615 (1983).

⁷A. Aharony, S. Alexander, O. Entin-Wohlman, and R. Orbach, *Phys. Rev. B* **31**, 2565 (1985).

⁸D. Stauffer, *Introduction to Percolation Theory* (Taylor and Francis, London, 1985).

- ⁹P. G. de Gennes, *J. Phys. (Paris) Colloq.* **41**, C3-17 (1980).
- ¹⁰J. Adler, A. Aharony, and D. Stauffer, *J. Phys. A* **18**, L129 (1985).
- ¹¹D. C. Hong, H. E. Stanley, A. Coniglio, and A. Bunde, *Phys. Rev. B* **33**, 4564 (1986).
- ¹²F. Levstak, J. Adler, A. Aharony, A. Bunde, A. Coniglio, D. C. Hong, H. E. Stanley, and D. Stauffer, *J. Phys. A* **19**, 3683 (1986).
- ¹³R. Alben, M. Blume, H. Krakauer, and L. Schwartz, *Phys. Rev. B* **15**, 4090 (1975); M. F. Thorpe and R. Alben, *J. Phys. C* **9**, 2555 (1976).
- ¹⁴M. F. Thorpe, *J. Non-Cryst. Solids* **57**, 355 (1983).
- ¹⁵The quantity f can be evaluated exactly in 2D for bond percolation on the square net at p_c . The value of $f = 0.0981 \dots$ can be obtained from H. N. V. Temperley and E. H. Lieb, *Proc. R. Soc. London, Ser. A* **322**, 251 (1977). This value was given incorrectly in Ref. 14. We have confirmed this value of f by directly counting the clusters in the samples studied in this work. A similar counting of clusters in 3D leads to the value of $f = 0.27$ for bond percolation on the simple cubic lattice at p_c .
- ¹⁶S. E. Koonin, *Computational Physics* (Benjamin/Cummings, California, 1986).
- ¹⁷R. Burton, C. Lambert, A. R. Day, W. Xia, and M. F. Thorpe (unpublished).
- ¹⁸H. J. Herrmann, B. Derrida, and J. Vannimenus, *Phys. Rev. B* **30**, 4080 (1984); J. G. Zabolitzky, *ibid.* **30**, 4077 (1984).
- ¹⁹M. A. Lemieux, P. Breton, A.-M. S. Tremblay, *J. Phys. (Paris) Lett.* **46**, L1 (1985).
- ²⁰A. Coniglio and H. E. Stanley, *Phys. Rev. Lett.* **52**, 1068 (1984).

MICHIGAN STATE UNIV. LIBRARIES



31293005633239